

1997

## Discrete-time linear and nonlinear aerodynamic impulse responses for efficient CFD analyses

Walter A. Silva  
*College of William & Mary - Arts & Sciences*

Follow this and additional works at: <https://scholarworks.wm.edu/etd>



Part of the [Aerospace Engineering Commons](#), and the [Mathematics Commons](#)

---

### Recommended Citation

Silva, Walter A., "Discrete-time linear and nonlinear aerodynamic impulse responses for efficient CFD analyses" (1997). *Dissertations, Theses, and Masters Projects*. Paper 1539623917.  
<https://dx.doi.org/doi:10.21220/s2-cw4r-jc50>

This Dissertation is brought to you for free and open access by the Theses, Dissertations, & Master Projects at W&M ScholarWorks. It has been accepted for inclusion in Dissertations, Theses, and Masters Projects by an authorized administrator of W&M ScholarWorks. For more information, please contact [scholarworks@wm.edu](mailto:scholarworks@wm.edu).

## INFORMATION TO USERS

This manuscript has been reproduced from the microfilm master. UMI films the text directly from the original or copy submitted. Thus, some thesis and dissertation copies are in typewriter face, while others may be from any type of computer printer.

**The quality of this reproduction is dependent upon the quality of the copy submitted.** Broken or indistinct print, colored or poor quality illustrations and photographs, print bleedthrough, substandard margins, and improper alignment can adversely affect reproduction.

In the unlikely event that the author did not send UMI a complete manuscript and there are missing pages, these will be noted. Also, if unauthorized copyright material had to be removed, a note will indicate the deletion.

Oversize materials (e.g., maps, drawings, charts) are reproduced by sectioning the original, beginning at the upper left-hand corner and continuing from left to right in equal sections with small overlaps. Each original is also photographed in one exposure and is included in reduced form at the back of the book.

Photographs included in the original manuscript have been reproduced xerographically in this copy. Higher quality 6" x 9" black and white photographic prints are available for any photographs or illustrations appearing in this copy for an additional charge. Contact UMI directly to order.

# UMI

A Bell & Howell Information Company  
300 North Zeeb Road, Ann Arbor MI 48106-1346 USA  
313/761-4700 800/521-0600



DISCRETE-TIME LINEAR AND NONLINEAR AERODYNAMIC IMPULSE  
RESPONSES FOR EFFICIENT CFD ANALYSES

---

A Dissertation

Presented to

The Faculty of the Department of Applied Science  
The College of William and Mary in Virginia

In Partial Fulfillment

Of the Requirements for the Degree of  
Doctor of Philosophy

---

by

Walter A. Silva

1997

**UMI Number: 9820443**

---

**UMI Microform 9820443**  
**Copyright 1998, by UMI Company. All rights reserved.**

**This microform edition is protected against unauthorized  
copying under Title 17, United States Code.**


---

**UMI**  
**300 North Zeeb Road**  
**Ann Arbor, MI 48103**


APPROVAL SHEET


This dissertation is submitted in partial fulfillment of  
the requirements for the degree of


Doctor of Philosophy

  
Author

Approved October 1997

  
Dennis M. Manos

  
Mark K. Hinders

  
Oscar R. Gonzalez, ODU

  
Fereidoun Farassat, NASA

  
Thomas B. Gatski, NASA

## DEDICATION

It is with great pleasure that I dedicate this dissertation to my wife, Donna Marie Silva, for her tremendous amount of support and encouragement. She took on all the responsibilities associated with running a home and taking care of our wonderful children so that I could dedicate myself to the demands of a PhD program. Thank you, dear.

## TABLE OF CONTENTS

	Page
ACKNOWLEDGEMENTS	vii
LIST OF TABLES	viii
LIST OF FIGURES	ix
NOMENCLATURE	xiv
ABSTRACT	xvi
CHAPTER 1: INTRODUCTION	2
Motivation	2
Background	3
Outline of Dissertation	8
Contributions of Dissertation	10
Related Publications	11
CHAPTER 2 : LINEAR DISCRETE-TIME SYSTEMS	12
The Unit Sample Response	12
Discrete-Time Convolution	13
Unit Sample Response vs. Unit Step Response	14
Application to Classical Aerodynamic Functions	16
New Perspective of Computational Aerodynamics	21
CHAPTER 3: BRIEF DESCRIPTION OF AN AEROELASTIC SYSTEM	23
Linear Aeroelasticity	23
Nonlinear Aeroelasticity	26
Implications	29
CHAPTER 4: VOLTERRA THEORY	33



Introduction	33
Mathematical System Definitions	34
Kernel Definition	37
Weakly Nonlinear Systems	38
Kernel Identification	40
Example - Nonlinear Circuit	48
<b>CHAPTER 5: APPLICATION TO CFD MODELS</b>	<b>58</b>
Navier-Stokes Equations	58
Related Concepts	61
Computational Benefits	64
Example - Viscous Burger's Equation	65
Aerodynamic System Input Definition	78
<b>CHAPTER 6: RESULTS USING THE CAP-TSD CODE</b>	<b>87</b>
Linear CAP-TSD - Plunge	87
Linear CAP-TSD - Pitch	94
Summary fo Linear CAP-TSD Results	103
Nonlinear CAP-TSD	103
<b>CHAPTER 7: RESULTS USING THE CFL3D CODE</b>	<b>112</b>
Results for RAE Airfoil	112
Computational Efficiency	125
<b>CONCLUSIONS</b>	<b>127</b>
<b>FUTURE RESEARCH</b>	<b>129</b>
<b>APPENDIX: Fundamental Aspects of the Volterra Theory of Nonlinear Systems</b>	<b>131</b>
Mathematical Classification of Systems	131
Impulse Response, Convolution, and Memory	134
Functional Origins and Interpretation of the Volterra Kernels	138
Convergence Issues	142

Error Bound for a Truncated Volterra Series	145
BIBLIOGRAPHY	146
VITA	160

## ACKNOWLEDGEMENTS

As with any important achievement, there are always several people who have contributed to its success. First, I would like to acknowledge the support of my wife, Donna Marie, to whom I owe half of this degree. I would also like to acknowledge my children, Samantha Marie and Justen Peter Antonio, for putting up with and without me during this effort. I want to thank my mother, Cecilia, for her lifelong encouragement; my father, Antonio, for his love and memories; my sisters, Maria Consuelo and Gladys Amanda, for their love, friendship, and support; and my brother, Antonio, for promoting in me an interest in math at an early age.

Additional acknowledgements go to Prof. Luigi Morino and Dr. E. Carson Yates, Jr. for their excellent mentorship and to my dissertation committee for their guidance and critique: Prof. Dennis M. Manos (Applied Science, W&M), Prof. Mark K. Hinders (Applied Science, W&M), Prof. Oscar R. Gonzalez (Electrical and Computer Engineering, ODU), Prof. Fereidoun Farassat (NASA, Fluid Mechanics and Acoustics Division), and Prof. Thomas B. Gatski (NASA, Fluid Mechanics and Acoustics Division).

A word of thanks must go to Dr. Thomas E. Noll and Mr. Boyd Perry, III of the NASA Langley Research Center, who believed in my ideas when they were just ideas. And, finally, I would like to thank the NASA Langley Research Center for helping me to achieve this dream.

## LIST OF TABLES

Table		Page
1.	Computational Cost Comparisons: Linear Results	94
2.	Computational Cost Comparisons: First-Order Results	108

## LIST OF FIGURES

Figure	Page
1. W. P. Jones approximation to Wagner's function for an airfoil in incompressible flow (Reference 33).	17
2. Impulse response in angle of attack of an airfoil in incompressible flow (derivative of Figure 1).	18
3. R. T. Jones approximation to Kussner's function, the response of an airfoil to a sharp-edged (step) gust in incompressible flow (Reference 33).	19
4. Gust impulse response for an airfoil in incompressible flow (derivative of Figure 3).	20
5. Schematic showing relationship of aerodynamic impulse response to classical aerodynamic functions.	22
6a. Schematic of process for computing linear aeroelastic responses.	27
6b. Schematic showing a potential flutter situation not predicted by linear methods (symbols) and the various types of nonlinear aerodynamic methods available for flutter analysis.	28
6c. Schematic showing inclusion of nonlinear aerodynamics into aeroelastic analyses.	30
7. Equations that define the first- and second-order kernels for a second-order truncated Volterra approximation and a schematic of the required responses.	44
8. Schematic of the different components that comprise a symmetric second-order kernel.	47
9. Simple nonlinear circuit defined by the Riccati equation shown with $x(t)$ as the input to the system and $y(t)$ as the output of the system.	49
10. First-order kernel for the Riccati nonlinear circuit, Case 1, $\alpha=1.0$ , $\epsilon=0.0001$ , $DT=0.01$ .	50
11. Selected components of the second-order kernel for the Riccati nonlinear circuit, Case 1, $\alpha=1.0$ , $\epsilon=0.0001$ , $DT=0.01$ .	51
12. Comparison of Actual and First-Order responses due to three	

different step inputs for Riccati nonlinear circuit, Case 1, $\alpha=1.0$ , $\epsilon=0.0001$ , $DT=0.01$ .	52
13. First-order kernels for Case 1 and Case 2 for the Riccati nonlinear circuit.	55
14. Comparison of Actual and First-Order responses due to three step inputs for Riccati nonlinear circuit, Case 2 $\alpha=0.1$ , $\epsilon=0.001$ , $DT=0.01$ .	56
15. Selected components of the second-order kernel for the Riccati nonlinear circuit, Case 2 $\alpha=0.1$ , $\epsilon=0.001$ , $DT=0.01$ .	57
16. Equation hierarchy (from Reference 63).	59
17. Application of the discrete-time Volterra theory to the viscous Burger's equation consisting of identification and application phases.	66
18. First-order kernel for viscous Burger's equation problem.	67
19. Twenty components of the second-order kernel for the viscous Burger's equation problem.	68
20. Three-dimensional perspective of the twenty components of the symmetric second-order kernel for the viscous Burger's equation problem.	69
21. "Zoom-in" view of Figure 20.	70
22. Comparison of Actual, to step inputs at four different amplitudes (0.25, 0.50, 1.0, 2.0) for the viscous Burger's equation problem.	72
23. Comparison of Actual, First-Order only, and First-Plus-Second-Order responses due to a low-frequency (5 Hz) sinusoidal input for the viscous Burger's equation problem.	73
24. Comparison of Actual, First-Order only, and First-Plus-Second-Order responses due to a high-frequency (20 Hz) sinusoidal input for the viscous Burger's equation problem.	74
25. Comparison of low-amplitude, quasi-random responses including actual, first-order, and first- plus second-order responses for viscous Burger's equation problem.	76

26. Comparison of medium-amplitude, quasi-random responses including actual, first-order, and first- plus second-order responses for viscous Burger's equation problem.	77
27. Comparison of high-amplitude, quasi-random responses including actual, first-order, and first- plus second-order responses for viscous Burger's equation problem.	79
28. Example of an arbitrary plunge motion, $u(t)$ , and corresponding rate-of-change of motion, $u'(t)$ .	81
29. Example of a narrower arbitrary plunge motion, $u(t)$ , and corresponding rate-of-change of motion, $u'(t)$ .	83
30. Comparison of plunge unit sample response and plunge unit step response, linear CAP-TSD, $M=0.9$ , $DT= 0.001$ .	88
31. Step response computed via convolution of unit sample response with a unit step input, linear CAP-TSD, $M=0.9$ , $DT= 0.001$ .	90
32a. Comparison of Actual and Convolved Plunge Response, linear CAP-TSD, $M=0.9$ , $DT= 0.001$ .	91
32b. Comparison of Actual and Convolved Responses for lower frequency (longer timelength) arbitrary plunge motion, linear CAP-TSD, $M=0.9$ , $DT= 0.001$ .	92
33. Comparison of Actual and Unit Step Response convolved with $u''(t)$ , linear CAP-TSD, $M=0.9$ , $DT= 0.001$ .	93
34. Linear unit sample response due to unit pulse applied to the motion "input channel" of the downwash equation.	96
35. Linear unit sample response due to unit pulse applied to the rate-of-change of motion "input channel" of the downwash equation.	97
36. Arbitrary pitching motion, low frequency.	98
37. Comparison of actual and convolved plunge responses due to arbitrary	

pitch motion of Fig. 36, linear CAP-TSD, $M=0.8$ , $DT=0.001$ .	99
38. Arbitrary pitching motion, high frequency.	100
39. Comparison of actual and convolved plunge responses due to arbitrary pitch motion of Fig. 38, linear CAP-TSD, $M=0.8$ , $DT=0.001$ .	101
40. Comparison of actual and convolved plunge responses due to a sinusoidal pitch motion (1.5 degrees amplitude).	102
41. Enlarged view of initial portion of Figure 40.	103
42. First-order kernel in plunge, nonlinear CAP-TSD.	105
43. Comparison of actual nonlinear first-order convolved responses for three different plunge motions; linear response for first amplitude is also presented.	106
44. Four components of the plunge second-order kernel.	109
45. Combined pitch first-order kernel, nonlinear CAP-TSD.	110
46. Single pitching motion (deconvolution) and comparison of linear and nonlinear, actual and convolved responses.	111
47. Four selected components of the second-order kernel for the combined pitch motion.	113
48. RAE 2822 airfoil grid, from Ref. 71.	115
49. First-order kernel for RAE airfoil in plunge, first-order accurate in time, with and without diagonalization; $M=0.75$ , $\alpha=0.0$ .	117
50. First-order kernel for RAE airfoil in plunge, first-order accurate in time, with and without diagonalization, with and without multigrid; $M=0.75$ , $\alpha=0.0$ .	118
51. First-order kernel for RAE airfoil in plunge, non-diagonalized, no multigrid, $M=0.75$ , $\alpha=0.0$ .	119



52. First-order kernel for RAE airfoil in plunge, non-diagonalized, no multigrid, effect of ID amplitudes.	121
53. Comparison of actual nonlinear responses and first-order convolved responses (small amplitude, 1st-order in time) for three different plunge motions.	122
54. Comparison of actual nonlinear and first-order (2nd order accuracy, large amp.) responses for three different plunge motions and a linear response for the largest plunge motion.	123
55. First five components of the second-order kernel for the RAE airfoil in plunge, non-diagonalized, no multigrid, second-order accurate in time, largest ID amplitudes.	125
A1. Mathematical system classifications and some examples.	134
A2. Response characteristics of time-invariant and time-varying systems.	135
A3. Application of a continuous-time unit impulse function to a continuous-time, linear time-invariant system to yield the continuous-time unit impulse response function.	136
A4. Convolution as a three-part process: scaling, shifting, and summation of memory function (impulse response).	138
A5. Application of the discrete-time unit pulse to a discrete-time linear time-invariant (DT-LTI) system, yielding the system's unit sample response. The unit sample response is then used in the discrete-time convolution process.	139
A6. Interpretation of each of the terms of the Volterra series for a nonlinear time-invariant (NLTI) system with input $u(t)$ and output $y(t)$ .	143
A7. The various components that define the second-order memory function (kernel) and the resultant response ( $y_2(t)$ ) due to a second-order convolution of this second-order memory function with some arbitrary input.	144

## NOMENCLATURE

$D_0$	maximum amplitude of exponential pulse input (user defined)
$E_t$	total energy per unit volume (Navier-Stokes equations)
$U, E, F, G$	flux vectors for the Navier-Stokes equations
$h_0$	zeroth-order Volterra kernel, constant
$h(t)$	unit impulse response
$h[n]$ or $h[k]$	discrete-time unit sample response
$h_1(t, \text{amp})$	first-order Volterra kernel, function of time and amplitude
$h_1[k, \text{amp}]$	discrete-time, first-order Volterra kernel
$h_2(t_1, t_2, \text{amp})$	second-order Volterra kernel, two-dimensional function of time and function of amplitude
$h_2[k_1, k_2, \text{amp}]$	discrete-time, second-order Volterra kernel
$h_n(t_1, \dots, t_n, \text{amp})$	'nth'-order Volterra kernel, 'nth' dimensional function of time and function of amplitude
$h_n[k_1, \dots, k_n, \text{amp}]$	discrete-time, 'nth'-order Volterra kernel
$q_i$	heat transfer (Navier-Stokes equations)
$S[n]$ or $S[k]$	discrete-time unit step response
$u, v, w$	velocity components for x, y, and z directions, respectively (Navier-Stokes equations)
$u(t)$	arbitrary input
$w(x, y, t)$	downwash function that defines motion of a surface
$x, y, z$	position coordinates, (Navier-Stokes equations)
$x[n]$ or $u[n]$	arbitrary discrete-time input
$x'[n]$	temporal derivative of $x[n]$

$y(t)$	response to arbitrary input $u(t)$
$y[n]$	discrete-time response to arbitrary input $u[n]$ (or $x[n]$ )
$y_0(t)$	response to unit impulse at time $t$ , $\delta_0(t)$
$y_0(t+T)$	response to unit impulse at time $t+T$ , $\delta_0(t+T)$
$y_1(t)$	response to unit impulse at time $t$ , $\delta_0(t)$ , and unit impulse at time ( $t+T$ ), $\delta_0(t+T)$
$\alpha, \varepsilon$	parameters in nonlinear Riccati differential equation
$\delta_0(t)$	unit impulse function
$\delta_0[k]$	discrete-time unit pulse
$\rho$	fluid density (Navier-Stokes equations)
$\nu$	parameter in viscous Burger's equation
$\tau_{ij}$	viscous stress tensors (Navier-Stokes equations)
$\Phi(\tau)$	Approximation to Wagner's function
$\Psi(\tau)$	Approximation to Kussner's function
$\Phi(x,y)$	structural modeshape function
$\Phi'(x,y)$	slopes of structural modeshape function

## ABSTRACT

This dissertation discusses the mathematical existence and the numerical identification of linear and nonlinear aerodynamic impulse response functions. Differences between continuous-time and discrete-time system theories, which permit the identification and efficient use of these functions, will be detailed. Important input/output definitions and the concept of linear and nonlinear systems with memory will also be discussed. It will be shown that indicial (step or steady) responses (such as Wagner's function), forced harmonic responses (such as Theodorsen's function or those from doublet lattice theory), and responses to random inputs (such as gusts) can all be obtained from an aerodynamic impulse response function. This will establish the aerodynamic discrete-time impulse response function as the most fundamental and computationally efficient aerodynamic function that can be extracted from any given discrete-time, aerodynamic system. The results presented in this dissertation help to unify the understanding of classical two-dimensional continuous-time theories with modern three-dimensional, discrete-time theories.

Nonlinear aerodynamic impulse responses are identified using the Volterra theory of nonlinear systems. The theory is described and a discrete-time kernel identification technique is presented. The kernel identification technique is applied to a simple nonlinear circuit for illustrative purposes. The method is then applied to the nonlinear viscous Burger's equation as an example of an application to a simple CFD model. Finally, the method is applied to a three-dimensional aeroelastic model using the CAP-TSD (Computational Aeroelasticity Program - Transonic Small Disturbance) code and then to a two-dimensional model using the CFL3D Navier-Stokes code. Comparisons of accuracy and computational cost savings are presented. Because of its mathematical generality, an important attribute of this methodology is that it is applicable to a wide range of nonlinear, discrete-time systems.

**DISCRETE-TIME LINEAR AND NONLINEAR AERODYNAMIC IMPULSE  
RESPONSES FOR EFFICIENT CFD ANALYSES**

## INTRODUCTION

### *Motivation*

Nonlinear unsteady aerodynamics is of great interest in the aerospace community because these phenomena can have a significant effect on the performance and stability of a flight vehicle, particularly at transonic speeds where detrimental aeroelastic phenomena are most likely to occur. At transonic speeds, complex aerodynamic flows can develop. These complex flows can include shocks, boundary layer interactions, and separated flows. Typically, these nonlinear aerodynamic phenomena tend to induce complex aeroelastic behavior which can significantly destabilize the vehicle. This destabilization in turn can result in limited flight operations of the vehicle or added weight to reduce the aeroelastic response. In either case, an economic and/or performance penalty is incurred. It is important, therefore, to be able to accurately predict and understand nonlinear unsteady aerodynamic behavior.

The most powerful and sophisticated tools for predicting nonlinear unsteady aerodynamic characteristics are being developed in the field of computational fluid dynamics (CFD)<sup>1</sup>. The nature and detail of the nonlinear fluid flow predicted by a particular flow solver depends on the governing equations that are discretized in the solver. The order of the governing flow equations can vary from the transonic small disturbance (TSD) level to the full Navier-Stokes equations. As CFD methods improve, it is a natural and important step to investigate methods for controlling the response to unsteady nonlinear flows in order to improve the performance and/or stability of a flight vehicle.

Modern aeroservoelastic (ASE) analysis tools, such as ISAC<sup>2</sup> (Interaction of Structures, Aerodynamics, and Controls) and ADAM<sup>3</sup> (Analog and Digital Aeroservoelastic Method), are used routinely for predicting the interaction between the structural system, the

aerodynamic system, and the control system of a flexible aircraft so that control laws that account for and take advantage of this flexibility can be designed. Even though the goal of the control law design may be for flutter suppression (stability)<sup>4</sup> and/or for load alleviation (performance), the control system design in the past has been primarily limited to linear aerodynamic responses. This limitation inhibits the design and analysis of control systems that can account for nonlinear responses induced by flow nonlinearities such as shocks, boundary layer effects, and separated flows. Although nonlinear aerodynamics are eventually incorporated into the control system design via wind-tunnel studies and/or semi-empirical simulations, there is a need for including nonlinear aerodynamic behavior, such as that predicted by CFD codes, early in the design phase. Direct incorporation of a CFD code into the ASE process is currently not a practical consideration due to the high computational costs and turnaround time required by CFD codes. As computational speeds improve and as new algorithms are developed to address this problem, the practicality of this approach may improve. At the moment, however, the efficient incorporation of the information provided by a CFD code into related disciplines, such as aeroelasticity and aeroservoelasticity, remains a problem. This is described in more detail in a subsequent section of this dissertation.

### *Background*

Although some work has been done in directly incorporating simple control laws into CFD codes<sup>5,6</sup>, these approaches do not generate a mathematical model of the nonlinear aerodynamic system. Instead, the control law gains are varied, in an expensive manner (multiple linearized models or trial-and-error, for example) as flight conditions are varied, to achieve a desired response. A significantly more efficient approach is to develop mathematical models that completely characterize the aerodynamic system of interest and then use these models in various analyses without costly re-execution of the CFD code. A new method for generating these mathematical models is presented in this dissertation.

During the early development of mathematical models of unsteady aerodynamic responses, the efficiency and power of superposition of scaled and shifted fundamental responses, or convolution, was quickly recognized. This led to the classical Wagner's function<sup>7</sup>, which is the response of a two-dimensional airfoil, in incompressible flow, to a unit step variation in angle of attack. Similar functions such as Kussner's function, which is the response of a two-dimensional airfoil to a sharp-edged gust in incompressible flow, were developed as well<sup>7</sup>. Theodorsen's function is the frequency response function due to sinusoidal motion for a two-dimensional airfoil in incompressible flow. Sear's function is the frequency response function due to a sinusoidal gust for a two-dimensional airfoil in incompressible flow. These are classical, analytically-derived unsteady aerodynamic responses that are studied in a modern course in unsteady aerodynamics or aeroelasticity. It is surprising to the author, however, that given these step and frequency responses, no mention is ever made of aerodynamic impulse responses, the origin of all these functions. The results presented in this dissertation are, therefore, a contribution to classical (continuous time) unsteady aerodynamic theory because of the new and fundamental perspective that is presented. Application of these concepts to numerical (discrete time) methods results in significant computational efficiencies.

As geometric complexity increased, the analytical derivation of these time-domain functions became impractical. Ultimately, for three-dimensional configurations, the computation of linear unsteady aerodynamic responses<sup>8</sup> in the frequency domain became the method of choice. For the case where geometry- and/or flow-induced nonlinearities are significant in the aerodynamic response, time integration of the nonlinear equations is necessary. This requirement for time integration imposes severe computational costs when analyzing complex configurations using CFD codes. This is particularly true for CFD aeroelastic analyses where the nonlinear aerodynamic system is coupled to a linear structural system. Post-processing of the resulting time transients provides information on the stability of the coupled system. When this method is applied at several flight



conditions, the computational costs become prohibitively expensive, both in terms of CPU costs and turnaround time. The turnaround time is the time it takes for a solution to be obtained from the moment it is submitted to the computer for execution to the moment it completes execution. This can be on the order of days, depending on the user demand for a particular computer.

Attempts to address this problem include the development of transonic indicial responses<sup>9,10,11</sup>. Transonic indicial (step) responses are responses due to a step excitation of a particular input, such as angle of attack, about a transonic (or nonlinear) steady state condition. However, as will be discussed, if these step inputs are not identified and used correctly, errors will be introduced into the analysis.

Reference 12 develops models of nonlinear aerodynamic maneuvers from an experimental database using neural networks. Since neural networks and Volterra series involve the characterization of a system via an input-output mapping, it is not surprising to realize that similarities exist between these two methods<sup>13</sup>. The direct relationship between the weights of a neural network and the kernels of a Volterra series representation for a particular system is discussed in Ref. 14. Reference 15 applies neural networks and genetic algorithms to the development of nonlinear unsteady aerodynamic models while recognizing the similarity with Volterra models. There is, clearly, valuable work that needs to be done in this area.

A potential difficulty with neural networks, however, is the effort required for training<sup>12</sup>. A benefit of the present method is that there is no training period required nor is there a need for curve fitting of any kind. Also, the Volterra kernels provide a direct means for physical interpretation of the system's response characteristics, both in the time and frequency domains. Potential disadvantages of the Volterra theory approach include input amplitude limitations related to convergence issues and the need for higher order kernels. These issues will be discussed in subsequent sections of this dissertation.

Another approach to reduce the computational cost of CFD codes is to linearize the response about a nonlinear steady-state condition, obtain a linear state-space representation of the system at that condition and then reduce the order of the state-space model using various techniques<sup>16,17</sup>. If a linearized, frequency-domain aerodynamic model from a CFD model is preferred, the method of the exponential pulse input can be applied<sup>18</sup>. Issues regarding the application of this input are discussed in detail later in this dissertation.

However, in order to develop robust, mathematically-correct and efficient *nonlinear* models of the CFD response, a mathematically-formal method is required that is well defined in the time and frequency domains and that is well defined for continuous- and discrete-time systems. The Volterra theory of nonlinear systems fulfills these requirements and has been applied in the present research. In particular, this theory has found wide application in the field of nonlinear discrete-time systems<sup>19</sup> and nonlinear digital filters for telecommunications and image processing<sup>20</sup>. Additional references, for continuous- and discrete-time formulations of the Volterra theory, are discussed in detail in Chapter 4 of this dissertation and the Appendix.

Application of nonlinear system theories, including the Volterra theory, to the problem of modeling nonlinear unsteady aerodynamic responses has not been extensive. Ueda and Dowell's<sup>21</sup> application of the concept of describing functions to unsteady transonic aerodynamic responses is one approach. The work by Tobak and Pearson<sup>22</sup> involved the application of the continuous-time Volterra concept of functionals to indicial (step) aerodynamic responses for the analytical derivation and experimental determination of nonlinear stability derivatives. The work by Jenkins<sup>23</sup> is also an investigation into the determination of nonlinear aerodynamic indicial responses and nonlinear stability derivatives. Stalford, Bauman, Garrett, and Herdman<sup>24</sup> successfully developed Volterra models for simulating the behavior of a simplified nonlinear stall/post-stall aircraft model and the limit cycle oscillations of a simplified model of wing rock.

In Ref. 24, the nonlinear aerodynamic response is analytically defined a priori so that derivation of the Volterra kernels is a straightforward analytical procedure. The output from a CFD code provides information regarding the nonlinear aerodynamic response of a complex configuration to a selected input at a particular flight condition. It does not, however, provide general information regarding the nonlinear aerodynamic response of the configuration to a variation of the input, or the flight condition or both. As a result, repeated use of the CFD code is necessary as input parameters and flight conditions are varied. Characterization of the nonlinear aerodynamic response of a configuration to an arbitrary input, via the Volterra theory, requires identification of the nonlinear Volterra kernels for the particular configuration and at a particular flight condition.

The problem of Volterra kernel identification has been addressed by Rugh<sup>25</sup>, Clancy and Rugh<sup>26</sup>, Schetzen<sup>27</sup>, and more recently by Boyd, Tang, and Chua<sup>28</sup>. There are several ways of identifying the Volterra kernels in the time and frequency domains. The methods can be applied to continuous-time or discrete-time systems. Tromp and Jenkins<sup>29</sup> used aerodynamic indicial (step) responses from a Navier-Stokes flow solver and a Laplace domain scheme to identify the first-order kernel of a two-dimensional airfoil undergoing pitching motions. The second-order kernel was identified for a sample problem and the method of Boyd, Tang, and Chua<sup>28</sup> was suggested for identification of the second-order nonlinear kernel of the airfoil response. Rodriguez<sup>30</sup> performed realizations of state-affine systems for aeroelastic analyses. These state-affine systems are related to discrete-time Volterra kernels. Silva<sup>31</sup> introduced the concept of discrete-time, linear and nonlinear aerodynamic impulse responses, or kernels, for a rectangular wing under linear (subsonic) and nonlinear (transonic) conditions. These early results, however, were limited to high-frequency responses. Silva<sup>32</sup> improved upon these results and extended the methodology to arbitrary frequencies, resulting in discrete-time, linear and nonlinear aerodynamic impulse responses valid for arbitrary inputs. The identification technique, which involved separation of the input terms, had limited applicability for the identification of the nonlinear

kernels. This problem is addressed and treated in a mathematically correct fashion in a subsequent section of this dissertation. Reference 32 represents the first time that discrete-time, aerodynamic impulse responses were identified. This is significant because of the prevailing misconception that aerodynamic impulse responses are difficult, if not impossible, to compute. Reference 33 states this directly while Ref. 34 has the step response (Wagner's function) mislabeled as an impulse response in a section of the text. Reference 35, on the other hand, discusses aerodynamic step responses but aerodynamic impulse responses are not mentioned. It is interesting to note that Refs. 33-35 discuss the definition and application of the aerodynamic step (or indicial) response but do not mention the aerodynamic impulse response explicitly. Clearly, if a step response can be computed for a linear system, then the system's impulse response, which is the derivative of the step response, can be computed as well. As will be shown, the misconception that the impulse response is difficult to obtain is the result of fundamental differences in continuous-time and discrete-time theories. Whereas computational aerodynamic methods have, in the past, been dominated by continuous-time concepts, this dissertation presents a new perspective on computational aerodynamics based on a discrete-time approach. The implications of this research to linear and nonlinear, steady and unsteady aerodynamics, as well as to related fields that depend on computational aerodynamic models, such as aeroelasticity and aeroservoelasticity, will be discussed.

### *Outline of Dissertation*

This dissertation begins with a description of the fundamentals of linear, discrete-time systems. The differences between continuous-time and discrete-time system theories and the impact of these differences on the historical development of linear aerodynamic models is discussed. An analytically-derived aerodynamic impulse response function is derived from an approximation to the classical Wagner's function. A similar derivation is presented for Kussner's function. Although these are simple and straightforward derivations, they

are presented here for the first time. As previously mentioned, the concept of an aerodynamic impulse response function is not addressed consistently in any of the standard texts on unsteady aerodynamics and aeroelasticity. Therefore, this dissertation provides a new perspective of classical linear unsteady aerodynamic theory. Since an aerodynamic impulse response also can be used for computing steady-state results, this perspective applies to steady aerodynamic theory as well.

Continuous-time and discrete-time versions of the Volterra theory of nonlinear systems are then presented. The concept of memory of a linear and nonlinear system will be discussed. A time-domain kernel identification technique, using discrete-time impulse inputs, is described and then applied to a simple nonlinear circuit as an example. This example will demonstrate the relationship between the parameters of a nonlinear differential equation and the corresponding Volterra kernels for that system.

Application of the kernel identification technique to CFD models begins with a discussion of the functional nature of the Navier-Stokes equations. The important realization that the discrete-time, Navier-Stokes equations belong to the set of discrete-time, nonlinear, time-invariant systems, is discussed. This realization, presented here for the first time, allows the formal application of the time-invariant version of the Volterra theory to Navier-Stokes computational models.

The first- and second-order kernels of a simple CFD model governed by the nonlinear viscous Burger's equation are then generated. The kernels are used to predict the response of the system to arbitrary inputs ranging from step (steady) to quasi-random inputs. These results demonstrate the applicability and efficiency of the Volterra theory when applied to simple nonlinear, discrete-time fluid dynamics models.

Application of the Volterra method to more complex CFD models is introduced by the discussion a conceptually new perspective on input definitions for discrete-time, aerodynamic systems. This perspective enables the numerically-correct identification of Volterra kernels for CFD models of arbitrary complexity using any CFD code.

The kernel identification technique is applied, via appropriate inputs, to a three-dimensional aeroelastic model using the CAP-TSD<sup>36</sup> (Computational Aeroelasticity Program - Transonic Small Disturbance) code and to a two-dimensional model using the CFL3D<sup>37</sup> Navier-Stokes code. Comparisons of accuracy and computational cost savings will be presented. Finally, the Appendix discusses some of the fundamentals of the Volterra series.

The results presented in this dissertation represent a new approach and a new perspective on linear and nonlinear, steady and unsteady computational aerodynamic systems in general. Because of its mathematical generality, an important attribute of this methodology is that it is applicable to a wide range of nonlinear, time-invariant, discrete-time systems.

### *Contributions of Dissertation*

The contributions of this dissertation can be grouped into three categories: Linear Computational Aerodynamics, Nonlinear Computational Aerodynamics, and Nonlinear Systems.

#### Linear Computational Aerodynamics:

- Practical identification and application of aerodynamic impulse responses
- New perspective on classical and modern indicial (step) response methods
- New perspective of computational aerodynamic system inputs and outputs
- Digital convolution of impulse response (unit sample response) with arbitrary inputs (step, sinusoidal, and random) yields steady, harmonic, and random responses
- Method may offer new approach to simulation, optimization, and control

#### Nonlinear Computational Aerodynamics:

- Existence of nonlinear aerodynamic unit impulse (sample) responses (first- and second-order kernels)

- First- and second-order kernels can be used to efficiently compute the nonlinear response due to arbitrary inputs without costly re-execution of the CFD code
- May provide new insights into nonlinear aerodynamic behavior
- Potential for CFD diagnostic tool to separate physical from numerical effects
- Method may offer new approach to simulation, optimization, and control with nonlinear aerodynamics
- Classification of Navier-Stokes equations as time-invariant system

#### Nonlinear Systems

- Expansion of Volterra system identification techniques to aerodynamic systems
- Enhanced knowledge regarding amplitude-dependence of Volterra kernels

#### *Related Publications*

Silva, W.A., "Application of Nonlinear Systems Theory to Transonic Unsteady Aerodynamic Responses," *Journal of Aircraft*, Volume 30, Number 5, September-October 1993, pp. 660-668.

Silva, W.A., "Extension of a Nonlinear Systems Theory to General-Frequency Unsteady Transonic Aerodynamic Responses," AIAA Paper No. 93-1590, Presented at the 34th Structures, Structural Dynamics, and Materials Conference, La Jolla, California, April 19-21, 1993.

Silva, W.A., "Identification of Linear and Nonlinear Aerodynamic Impulse Responses Using Digital Filter Techniques," AIAA Paper No. 97-3712, Presented at the AIAA Atmospheric Flight Mechanics Conference, August 11-13, 1997, New Orleans, LA.

## CHAPTER 2

### LINEAR DISCRETE-TIME SYSTEMS

#### *The Unit Sample Response*

The modern field of discrete-time signal processing<sup>38</sup> is a mathematical systems field that addresses more concepts than just the sampling of a continuous-time signal. For example, main topics in this field are digital filter design and digital signal processing. In digital filter design, there exist mathematical concepts that are quite different from their continuous-time counterparts. One of these concepts is the unit impulse function, or the Dirac delta function. The continuous-time unit impulse is typically considered a generalized function, impractical for numerical applications<sup>33</sup>. On the other hand, the discrete-time equivalent, known as the unit sample function, is well-defined and easy to apply. Digital filters are designed using this function and its resultant output known as the unit sample response. The unit sample function is defined as

$$\mathbf{u[n]} = \begin{cases} 1.0 & \text{for } \mathbf{n} = \mathbf{n}_0 \\ 0.0 & \text{for } \mathbf{n} \neq \mathbf{n}_0 \end{cases} \quad (1)$$

where 'n' is the discrete-time variable. The application of this input to a linear, discrete-time system will yield the system's unit sample response, the discrete-time equivalent of the unit impulse response. The properties of the unit sample response are similar to those of the unit impulse response (see Appendix). Both responses completely define a linear system and, through convolution, the response of the system to *any* arbitrary input can be predicted exactly without actually processing the arbitrary input through the system. This is because the unit sample response captures the system's entire frequency content.



A linear system's frequency characteristics can be determined by applying multiple sinusoids of varying frequency, applying band-limited white noise, or by computing the fast Fourier transform (FFT) of the unit sample response. The application of multiple sinusoids is how linear, unsteady aerodynamics are currently generated. The band-limited, white-noise technique implies exploration of different segments of the system's bandwidth in a piecewise, overlapping fashion. The most efficient approach is to compute the FFT of the unit sample response, yielding the system's frequency response. This efficiency is the result of the fundamental properties of the unit sample response.

Additional evidence of this efficiency is the fact that the response of the system to multiple sinusoidal inputs and the band-limited white noise can be computed via convolution of these inputs with the unit sample response. Therefore, from the single computation of the unit sample response, all system responses, from steady (step) to random, can be generated as well. This concept is well understood and routinely applied in the design of digital filters yet appears to be uncommon in fields dominated by continuous-time concepts, such as aerodynamics. In aerodynamics research, the application of convolution techniques has, in the past, been limited to the convolution of step (indicial) responses.

### *Discrete-Time Convolution*

The concept of convolution is another idea that is routinely used in digital filter design but that has found only limited applications in the continuous-time community. This is due to the fact that the definition of the continuous-time unit impulse function is different (though related) from that of the discrete-time unit sample response. This leads to different interpretations of how the continuous-time unit impulse can be applied to a particular system or if it can be applied at all. This vagueness disappears in the context of discrete-time systems.

Convolution, in discrete-time, is defined as

$$y[n] = \sum_{k=0}^N h[n-k] x[k] \quad (2)$$

where  $h[n-k]$  is the unit sample response and  $x[k]$  is the arbitrary input. It is important to understand that this is not the discrete-time version of Duhamel's integral<sup>39</sup>, which is the convolution of a unit step response with the derivative of an arbitrary input. The unit step (indicial) response is not the same as the unit sample (impulse) response. As discussed in the introduction to this dissertation, all research involving convolution of aerodynamic responses by other researchers has been limited to the convolution of step responses. Convolution using the unit impulse response (or unit sample response), however, is more efficient, as will be seen. In fact, convolution using the unit sample response is the method of choice in the fields of digital signal processing and digital filter design.

#### *Unit Sample Response vs. the Unit Step Response*

Consider three methods to compute the response of a linear system to an arbitrary function of time,  $x[k]$ . The first, or trivial method, is to process the input through the system itself. If the system is complex and computationally intensive, significant computational costs, including turnaround time, will be incurred. The second method is to identify the system's unit step response and then, via convolution with the *derivative* of the arbitrary input, obtain the response of the system using

$$y[n] = x[0] S[n] + \sum_{k=0}^{\infty} S[n-k] x'[k] \Delta t \quad (3)$$

where  $S[n]$  is the unit step response and  $x'[k]$  is the derivative of the arbitrary input. Equation (3) is the discrete-time equivalent of Duhamel's integral. The first term in Eq.(3)

must, of course, be included whenever  $x[0]$  is nonzero or else a static (DC offset) error will result. Equation (3) is the correct discrete-time implementation for indicial (or step) aerodynamics. It is mathematically valid if and only if the step response is correctly identified and applied in Equation (3). The application of step functions has typically been a problem in computational unsteady aerodynamics because of the downwash (input) equation and the perceived problem with the derivative of a step input. This issue is addressed and clarified in a subsequent section of this dissertation.

The third method is to identify the system's unit sample response and, via convolution with the arbitrary input,  $x[k]$ , (Eq. (2)), obtain the response of the system. Again, proper identification of the unit sample response is a requirement for the successful application of this method.

Clearly, for complex and computationally-intensive linear systems, the second and third methods provide the most efficient method for computing responses because repeated execution of the system is not required. The unit sample response and the unit step response contain all the necessary information regarding the system's behavior in a concise form. In addition, the derivative of the unit step response is the unit sample response so that only one response, the step or the unit sample response, is needed to compute the other.

In the present research, the identification and use of linear and nonlinear aerodynamic unit sample responses is favored over that of the unit step responses for the following reasons: (1) Identification of the unit sample response is computationally more efficient than identification of the unit step response; (2) The unit step response can be computed via convolution of the unit sample response with a step input, yielding the steady-state solution; and (3) Convolution using the unit sample response involves the actual input (Eq. (2)) whereas convolution using the unit step response involves the derivative of the input (Eq. (3)), requiring additional, unnecessary computational effort. The unit sample response is the most concise representation of a linear system from which all other steady

and unsteady responses can be generated. Extension of this concept to nonlinear systems, via the Volterra theory, enables the efficient computation of nonlinear steady and unsteady responses due to arbitrary inputs.

### *Application to Classical Aerodynamic Functions*

These concepts can be applied directly to classical, unsteady aerodynamic theory. Wagner's function is the response of a two-dimensional airfoil in incompressible flow to a unit step variation in angle of attack; an approximation to this response<sup>33</sup> is

$$\Phi(\tau) = 1. - 0.165e^{-0.041\tau} - 0.335e^{-0.32\tau}$$

This function is plotted in Figure 1. The derivative of this approximation to Wagner's function yields an approximation to the incompressible, aerodynamic impulse response due to plunge for a two-dimensional airfoil, shown in Figure 2. Kussner's function<sup>33</sup> is the response of a two-dimensional airfoil in incompressible flow to a step change in gust velocity. An approximation to Kussner's function<sup>33</sup> is

$$\Psi(\tau) = 1. - 0.500e^{-0.130\tau} - 0.500e^{-\tau}$$

This function is plotted in Figure 3. The derivative of this approximation to Kussner's function yields an approximation to the incompressible, aerodynamic impulse response due to a gust for a two-dimensional airfoil. This function is shown in Figure 4. Surprisingly, these simply-defined aerodynamic impulse response functions are not presented in any of the classical textbooks on aeroelasticity. Figures 1-4 clearly demonstrate that identification of the impulse response requires less computational time than the identification of the unit step response, with no loss of information.

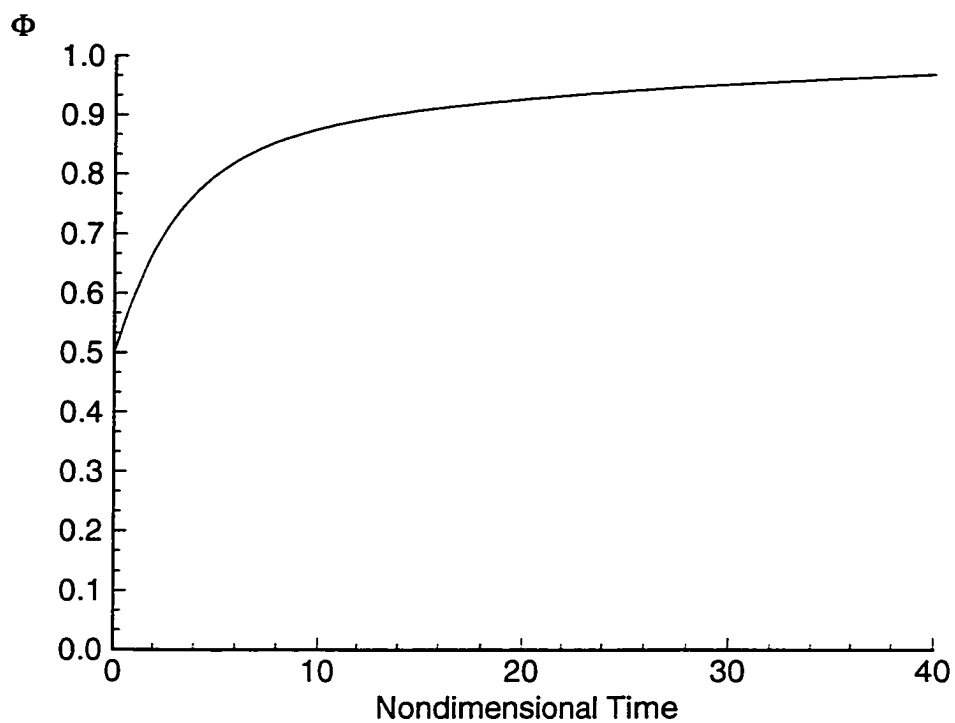


Figure 1 W. P. Jones' approximation to Wagner's function for an airfoil in incompressible flow (Reference 33).

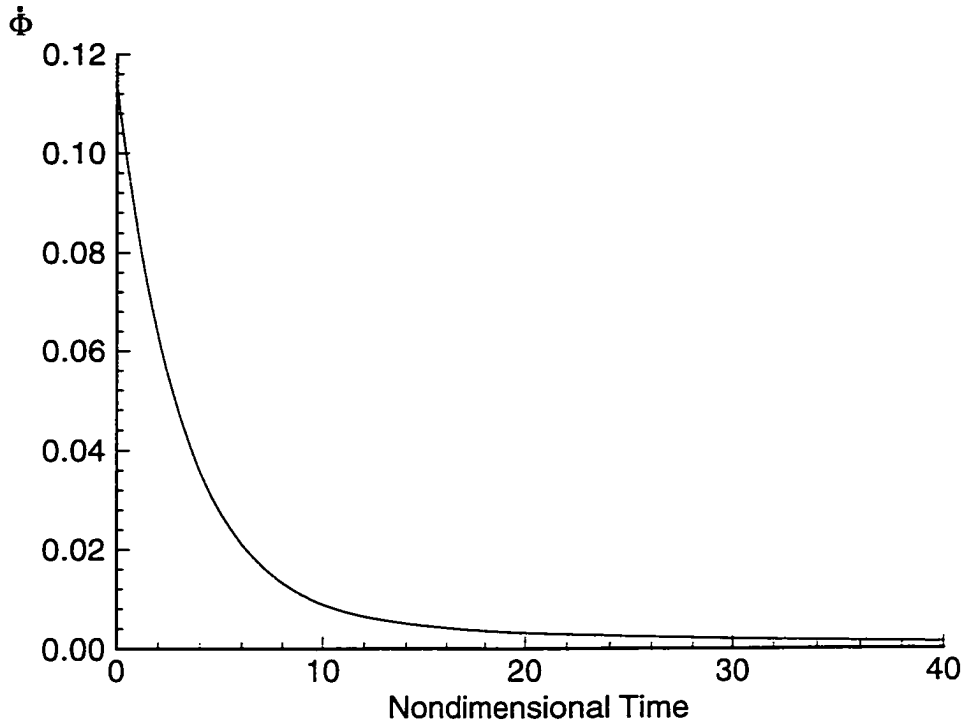


Figure 2 Impulse response in angle of attack of an airfoil in incompressible flow (derivative of Figure 1).

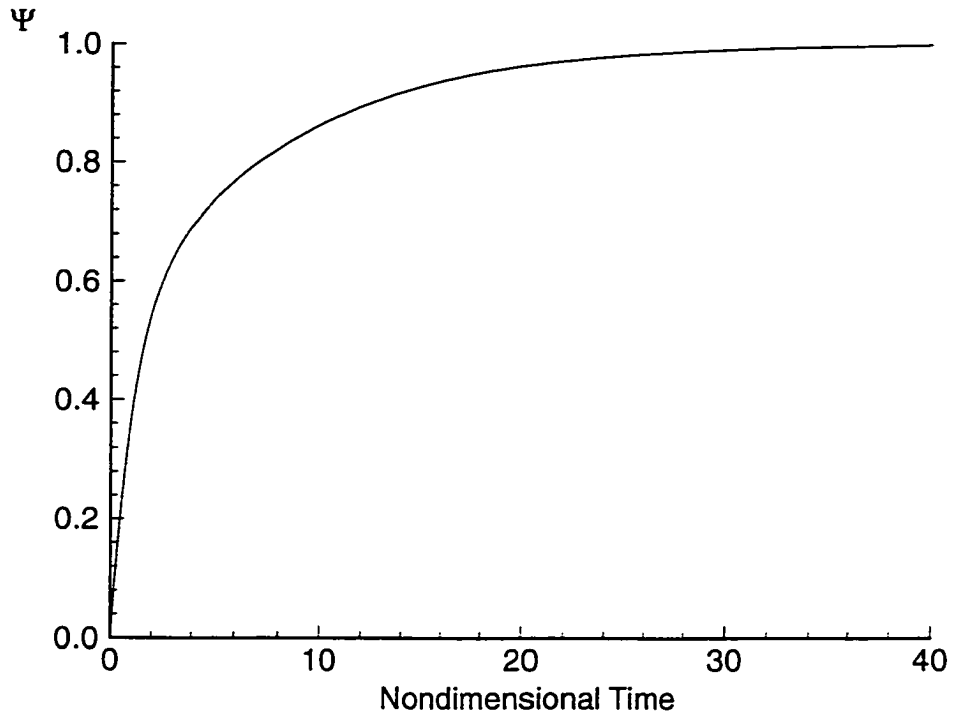


Figure 3 R. T. Jones approximation to Kussner's function, the response of an airfoil to a sharp-edged (step) gust in incompressible flow. (from Reference 33)

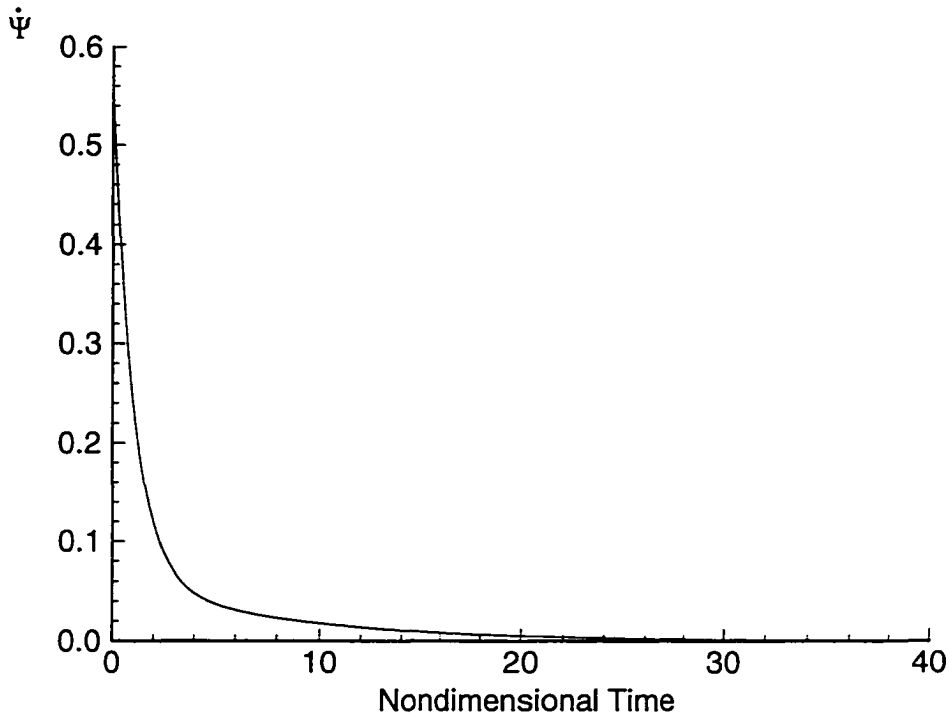


Figure 4 Gust impulse response for an airfoil in incompressible flow (derivative of Figure 3).



*New Perspective of Computational Aerodynamics*

The results from this dissertation may hopefully provide a unique and important perspective of unsteady aerodynamics and aeroelasticity. A schematic presenting this new perspective for linear computational aerodynamics is presented in Figure 5. This figure shows the relationship between the aerodynamic impulse responses presented in this dissertation and the classical methods for linear unsteady aerodynamics. Whereas classical methods begin with discussion of the indicial (or step) response or the forced harmonic response (Theodorsen's function, doublet lattice), the present research expands this view by introducing the aerodynamic impulse response. As has been mentioned previously, the aerodynamic impulse response can be used to compute the indicial response, the forced harmonic response, and the response of the aerodynamic system to any other arbitrary input. Proper use of the impulse response function (of any system, including aerodynamic systems) can yield significant computational efficiencies due to the fundamental nature of this function. This dissertation presents and demonstrates these concepts for linear and nonlinear aerodynamic systems.

# LINEAR AERODYNAMIC DISCRETE-TIME SYSTEMS

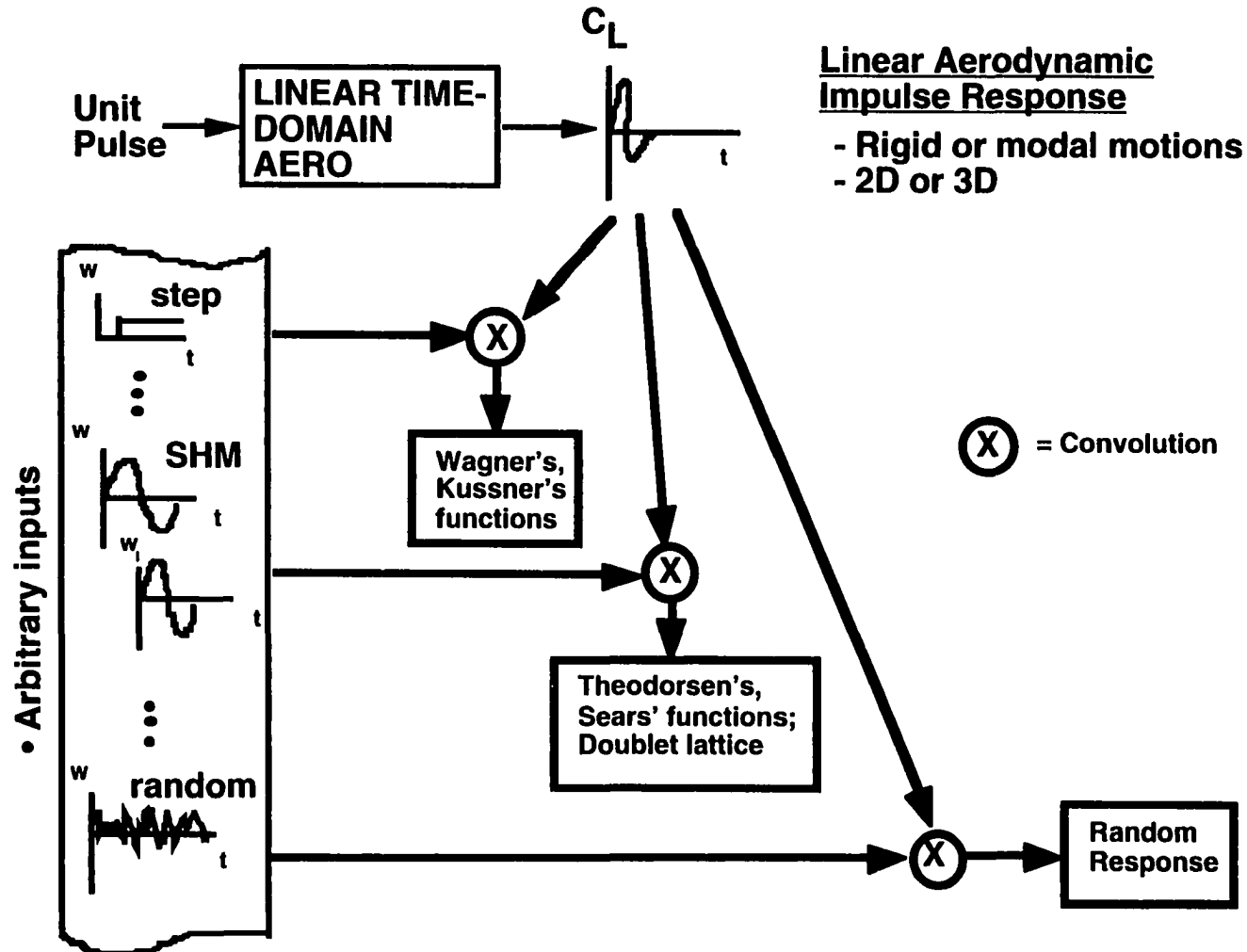


Figure 5 Schematic showing relationship of aerodynamic impulse response to classical aerodynamic functions.

## CHAPTER 3

### BRIEF DESCRIPTION OF AN AEROELASTIC SYSTEM

Excellent detailed descriptions of the theory of aeroelasticity can be found in Refs. 33-35 and the references therein. The purpose of this chapter is not to reproduce any of the information available in those references but rather to provide a global perspective of the various systems involved in the simulation of linear and nonlinear aeroelastic responses.

Aeroelasticity is the coupling and resultant interaction of two systems: a structural system and an aerodynamic system. Linear aeroelasticity is the interaction of a linear structural system with a linear aerodynamic system. Due to the linearity of both systems, and, therefore, the linearity of the combined aeroelastic system, several efficient methods exist for solving the governing equations. In nonlinear aeroelasticity, either the structural system or the aerodynamic system, or both, are nonlinear.

#### *Linear Aeroelasticity*

In linear aeroelasticity, the linear structure is typically modeled in state-space form. The states of this system are the structural modes of vibration. A structural mode is a vibratory shape of the structure. The solution of a linear vibration, or modal, problem for a given structure yields an orthogonal set of eigenvectors (modes, or modeshapes) and a corresponding set of eigenvalues (frequencies of vibration). Every structure exhibits some type of vibratory characteristics, although the spectrum can range from the very flexible to the very rigid.

The first step in an aeroelastic analysis is to obtain the vibratory characteristics of the structure of interest in terms of its modes of vibration (eigenvectors) and the corresponding vibratory frequencies (eigenvalues). The development of a state-space model for this

system is a well-known process that includes the generalized mass, damping, and stiffness of the structure (see Ref. 2, for example). The input to the structural system consists of forces and the output is the structural response, or motion, of the structure due to these forces.

Characterization of the linear aerodynamic system consists of determining the aerodynamic loads due to each of the structural modes. Because the systems are coupled, excitation of one of the structural modes induces an aerodynamic response in all of the modes. If the structure under investigation consists of four modes, the aerodynamic system will consist of a four-by-four matrix. The first value of the diagonal of this matrix (the (1,1) term) would consist of the aerodynamic response in mode 1 due to a motion of mode 1. The second diagonal value, the (2,2) term, would be the aerodynamic response in mode 2 due to a motion of mode 2, and so on. The off-diagonal terms are a measure of the aeroelastic coupling between modes and the matrix is typically not symmetric. Due to the historical developments mentioned in the Introduction, the majority of linear unsteady aerodynamic analyses define this matrix in the frequency domain, composed of aerodynamic frequency responses. This complex matrix is obtained by applying a simple harmonic perturbation to each of the modes at discrete frequencies, computing the resultant frequency responses, and populating the corresponding elements of the matrix. This aerodynamic matrix is the frequency-domain equivalent of an impulse response matrix. The input to the aerodynamic system is motion of the structure and the output is the force due to that motion.

The governing aerodynamic equations require that this analysis be repeated for every Mach number of interest. The resultant aerodynamic system consists of tabular information defining aerodynamic frequency responses due to structural motions at a specified set of input frequencies for each Mach number of interest. Several methods can be used to couple the aerodynamic and structural systems to obtain the flutter solution. The flutter solution is the condition at which this coupled, or aeroelastic, system achieves neutral stability. The

parameter that is varied is dynamic pressure, which can be considered to be a “closed-loop gain”. It is the value of this “gain” that helps determine the flight condition at which the aeroelastic system becomes neutrally stable.

A time-domain approach for defining the linear aerodynamic system<sup>10</sup> consists of using step responses that are converted into state-space form. This method has not received much attention but recent results from other researchers<sup>16</sup> are clearly related. In this technique, the linear state-space structural system is connected to the state-space aerodynamic system in a closed-loop sense. Again, with dynamic pressure as the gain, the time transients output from this closed-loop system are studied for signs of convergence (stable) or divergence (unstable).

Yet another important technique to mention is that of rational function approximations (RFAs)<sup>40</sup>. Since the frequency-domain aerodynamic matrix is not amenable for use with modern control theory (i.e., time-domain methods), RFAs were developed. Simply put, RFAs are s-plane approximations of the aerodynamic frequency responses. Since the frequency-domain aerodynamic matrix is valid only along the imaginary axis, due to the fact that it was generated using simple harmonic motion, the s-plane approximations extend the applicability of the aerodynamic system to the complex plane. The s-plane approximation is then defined in state-space form and the result is an approximate, time-domain representation of the aerodynamic system. A stability analysis is performed by augmenting the structural state-space matrix with the aerodynamic state-space matrices. An eigenvalue analysis of the resultant system, as dynamic pressure is varied, provides stability information.

One of the difficulties associated with RFAs, however, is that a tradeoff must be made between accuracy and model order. If the approximation is to include the entire bandwidth of a given aerodynamic frequency response, then the order of the resultant state-space system increases significantly. In order to keep state-space model order low, a particular

frequency range of interest is usually selected where the approximation (curve fit) is desired and optimized.

A classical, or typical, flutter mechanism that is often described is that of a simple, two-degree-of-freedom system. An airfoil is given plunge (vertical translation) and pitch (rotation about a point on the airfoil) degrees of freedom. The plunge structural frequency of vibration is lower than the pitch frequency of vibration. As the velocity of the flow (or dynamic pressure) is increased, the loading induced by the aerodynamic system is such that the two degrees of freedom (plunge and pitch) approach each other in frequency. Eventually, the modes coalesce, or combine into a single motion at a single frequency. This frequency is typically somewhere between the plunge (lower) frequency and the pitch (higher) frequency. This is the neutrally-stable condition known as flutter and it can result in damage to or destruction of the structure. More complex structures will exhibit different, more complex mechanisms, but the fundamental principles are basically the same. For this reason, two-degree-of-freedom systems (plunge and pitch) are studied often. A schematic of this process for linear aeroelasticity is presented in Figure 6a.

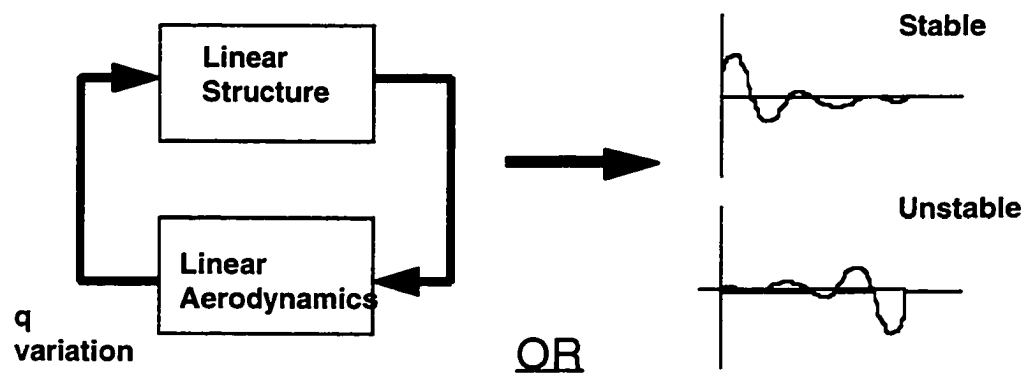
### *Nonlinear Aeroelasticity*

In nonlinear aeroelasticity, the efficiency of linear analysis techniques are not directly applicable. In the present dissertation, the nonlinearity is limited to the aerodynamic system. The present method might be useful in characterizing the response of a nonlinear structure but the development of such a system is beyond the scope of this dissertation. An obvious difficulty with a nonlinear structure is that the concept of eigenmodes and eigenvalues, valid for linear structures undergoing small perturbations, may no longer apply.

Nonlinear aerodynamic responses are computed using CFD models, as mentioned in the introduction (Figure 6b). Because these codes solve nonlinear equations in a time-marching sense, the nonlinear flutter (stability) analyses are, inevitably, performed in the

# AEROELASTICITY

## Linear Structure / Linear Aerodynamics



$$\dot{\mathbf{x}} = \mathbf{A}\mathbf{x} + \mathbf{B}u \quad \text{where}$$

$\mathbf{A}$  is structure augmented with aero; eigenvalues indicate system stability

Figure 6a Schematic of process for computing linear aeroelastic responses.

# AEROELASTICITY

## Nonlinear Aerodynamics

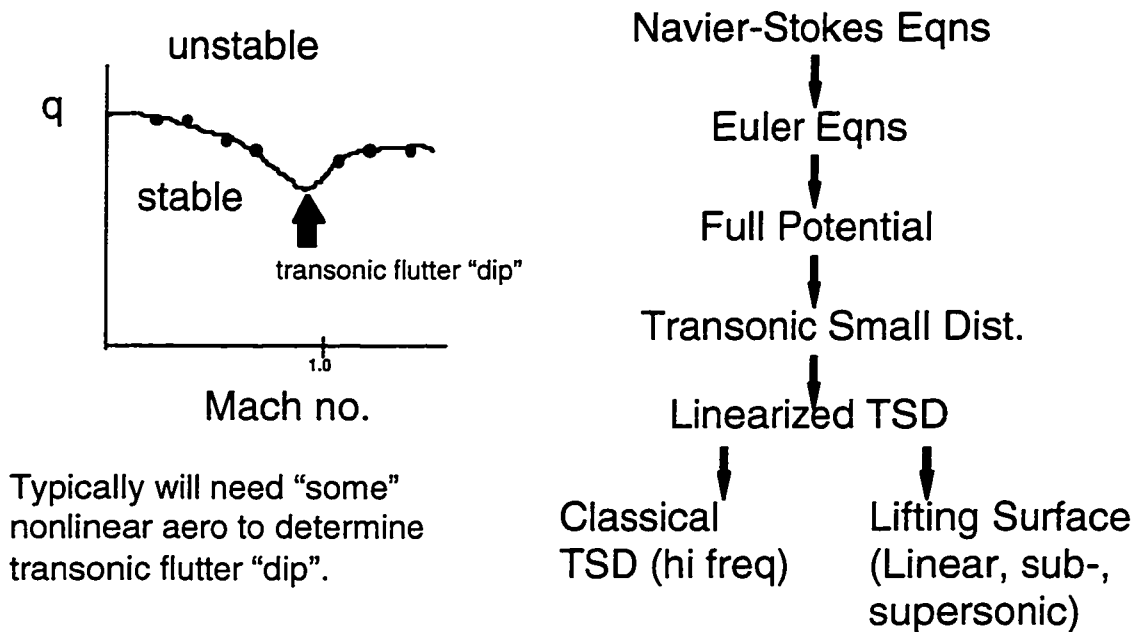


Figure 6b Schematic showing a potential flutter situation not predicted by linear methods (symbols) and the various types of nonlinear aerodynamic methods available for flutter analysis.



time domain as well. The approach is to transmit the nonlinear aerodynamic responses from the CFD model into the linear structural system. The structure then responds to these forces with a structural deformation, or motion. This motion is then passed back to the CFD model for the computation of a new, nonlinear aerodynamic load due to this new structural deformation. This closed-loop iteration continues and the resultant time histories are analyzed for stability (convergence vs. divergence) information (Figure 6c). These analyses are performed at each Mach number of interest. At each Mach number, the gain, or dynamic pressure, is varied until an unstable transient is encountered. The flutter dynamic pressure is therefore between the unstable dynamic pressure and the last stable dynamic pressure prior to the instability. It is this repetitive execution of the costly and time-consuming CFD code that causes a computational bottleneck in nonlinear aeroelastic analyses and all other analyses that involve the nonlinear aeroelastic system (aeroservoelasticity, optimization). If the problem of having to re-execute the CFD code can be alleviated, then the impact on all CFD-related analyses would be significant. This is a primary goal of this dissertation.

### *Implications*

Identification of linear aerodynamic unit sample responses<sup>32</sup> has interesting implications. First, it provides an alternative to the forced harmonic method for computing unsteady aerodynamic forces. Computing the unit sample responses for each structural mode and then performing the convolutions with sinusoidal inputs of varying frequency yields the aerodynamic frequency response functions. This could be done more directly by performing a Fourier transform of each of the modal unit sample responses.

The generation of aerodynamic frequency response functions may be avoided altogether by performing the aeroelastic analyses directly in the time domain<sup>31</sup>. This is done by coupling the aerodynamic unit sample responses with the linear, state-space structural model in a closed-loop sense and obtaining the aeroelastic transients. Since the

# AEROELASTICITY

## Nonlinear Aerodynamics (cont'd)

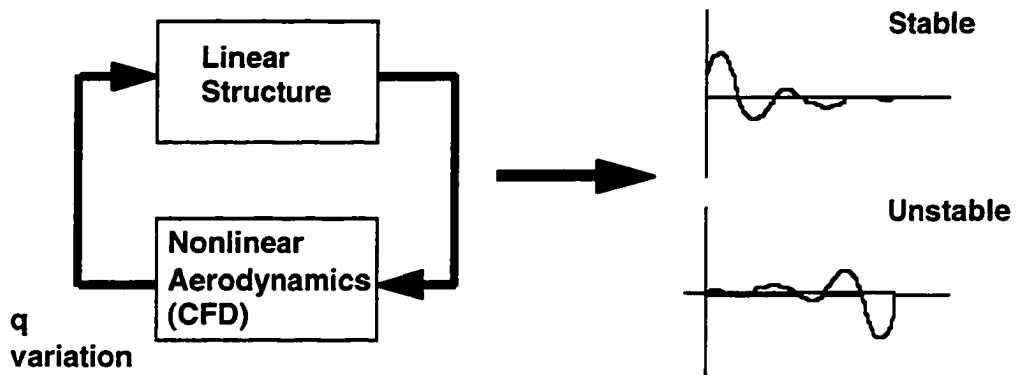


Figure 6c Schematic showing inclusion of nonlinear aerodynamics into aeroelastic analyses.

aerodynamic unit sample response is valid in the complex plane, there is no need for rational function approximations (RFAs). As mentioned above, RFAs are s-plane approximations of the linear aerodynamic system obtained from the linear aerodynamic frequency response functions (FRFs). The aerodynamic FRFs are also referred to as the generalized aerodynamic forces (GAFs) computed at discrete values of frequency and stored in tabular form.

Current methods for generating RFAs, limited by a specified frequency range of interest to generate a low-order, state-space model, are actually modeling that portion of the unit sample response that contains the particular frequency range of interest<sup>31</sup>. Recall that RFAs were developed in order to approximate the aerodynamic FRFs with an s-plane approximation amenable for use with modern control theory, i.e., time domain. Since the aerodynamic unit sample response function is already in the time domain, there is no need to generate the unsteady aerodynamic responses in the frequency domain only to transform them back to the time domain. Therefore, RFAs would not be necessary.

Instead, the aerodynamic unit sample response can be used to directly realize a linear, discrete-time, state-space system<sup>41</sup>. This approach has been investigated by the author on a preliminary basis, although it certainly merits further investigation. A fundamental problem with this technique, however, is that in order to capture the complete frequency response of the system, a high-order state-space system will need to be realized. Therefore, in order to obtain a reduced-order model, filtering of the unit sample response will be necessary prior to application of the realization technique. This filtering in the time domain is consistent with the selection of a frequency range within the FRFs when applying the RFA technique.

Linear frequency-domain and RFA methods are not directly applicable to nonlinear aerodynamics and, consequently, the generation of time-domain, aeroelastic responses is necessary. The discrete-time Volterra theory of nonlinear systems, along with new aerodynamic system input definitions presented in this dissertation, will provide a formal method for the identification of nonlinear aerodynamic unit sample responses. The

application of these nonlinear aerodynamic unit sample responses will result in significant CFD computational efficiency.

CHAPTER 4  
VOLterra THEORY

*Introduction*

The Volterra<sup>42</sup> theory was developed in 1930. The theory is based on functionals, or functions of other functions, and subsequently became a generalization of the linear convolution integral approach that is applied to linear, time-invariant (LTI) systems. The Appendix of this dissertation reviews some of the fundamental aspects of the theory.

The basic premise of the Volterra theory of nonlinear systems<sup>25,43</sup> is that any nonlinear system can be modeled as an infinite sum of multidimensional convolution integrals of increasing order. This infinite sum, presented here in continuous-time form, is known as the Volterra series and it has the form

$$\begin{aligned}
 y(t) = & \mathbf{h}_0 + \int_0^{\infty} \mathbf{h}_1(t - \tau) \mathbf{u}(\tau) \, d\tau + \\
 & \int_0^{\infty} \int_0^{\infty} \mathbf{h}_2(t - \tau_1, t - \tau_2) \mathbf{u}(\tau_1) \mathbf{u}(\tau_2) \, d\tau_1 \, d\tau_2 + \dots \\
 & + \int_0^{\infty} \dots \int_0^{\infty} \mathbf{h}_n(t - \tau_1, \dots, t - \tau_n) \mathbf{u}(\tau_1) \dots \mathbf{u}(\tau_n) \, d\tau_1 \dots d\tau_n + \dots
 \end{aligned} \tag{4}$$

where  $y(t)$  is the response of the nonlinear system to  $u(t)$ , an arbitrary input;  $h_0$  is a steady value about which the response is computed;  $h_1$  is the first-order kernel or the linear unit

impulse response;  $h_2$  is the second-order kernel, and  $h_n$  is the  $n$ th order kernel. It is assumed that:

1) the kernels, input function, and subsequently, the output function are real-valued functions defined for

$$t_i \in (-\infty, +\infty) \text{ for } i = 1, \dots, n, \dots$$

2) the system is causal so that  $h_n(t_1, \dots, t_n) = 0$  if any  $t_i < 0$

3) the system is time invariant

### *Mathematical System Definitions*

A time-invariant system, also referred to as a stationary or autonomous system, is a system whose fundamental properties do not change with time. That is,

$$f = f(x, \dot{x}, \ddot{x}, \dots)$$

An example of a simple, time-invariant, nonlinear system is a pendulum. Although the full nonlinear equation of a pendulum is certainly a function of time which can exhibit nonlinear, unsteady responses if an unsteady excitation is applied, neither the length of the pendulum nor the mass at the end of the pendulum are functions of time<sup>44</sup>. Simply stated, the equations defining a time-invariant system are not explicit functions of time.

In the case of a differential equation, for example, time-invariance refers to constant coefficients as opposed to coefficients that are explicit functions of time. Time-invariance is sometimes mistakenly interpreted as implying functions that are independent of time<sup>45</sup>. Even a classical, fundamental text such as Ref. 35 misinterprets nonlinear, time-invariant systems as systems that do not accept time-dependent forcing functions. This is clearly not

correct since the time-invariance of a system refers to the system itself and not to the characterization of the inputs or outputs (i.e., steady or unsteady) of the system.

A time-varying system, also referred to as a non-stationary or non-autonomous system, is a system whose fundamental properties do change with time. That is

$$f = f(x, \dot{x}, \ddot{x}, \dots, t)$$

An example of a time-varying system is a rocket during launch. The mass of the rocket, mostly fuel, is spent very quickly. The mass of the rocket, and therefore the rocket's dynamics, are changing with time. The identification of impulse responses for a time-varying system is typically more complicated than for a time-invariant system. Reference 46 addresses the problem of Volterra kernel identification for time-varying, nonlinear systems.

Fortunately, for many of the problems in aircraft unsteady aerodynamics, aeroelasticity, and aeroservoelasticity, the governing nonlinear equations are time-invariant. Although an airplane's fuel quantity, or mass, is certainly not constant, present-day analyses treat an airplane's fuel loading as separate, constant mass cases (full fuel to near empty, for example) as opposed to a continuously-varying quantity. The linearization of these time-invariant, nonlinear equations about an operating point yields the familiar time-invariant, linear equations that comprise the majority of modern-day, linear analysis techniques in these fields.

The impulse response of a linear system is a temporal representation of how long a unit perturbation remains active in the response of the system. This is referred to as the memory of the system. Convolution then allows exact prediction of the response of the system to an arbitrary input because all responses of the system are scaled and shifted superpositions of this memory function (see Appendix). It is important to understand that the set of arbitrary inputs includes any and all possible inputs, from steady (step) inputs to random inputs,

thus the term “arbitrary”. For the linear case, the arbitrary input has no amplitude or frequency limitations.

For a nonlinear system approximated by a Volterra series, the higher-order kernels are a measure of the nonlinear memory of the system. Unlike the linear system, however, the arbitrary nature of the input does have some limitations due to the fact that the series is usually truncated. As Boyd<sup>47</sup> has shown, the convergence of the Volterra series is limited by the infinity norm of the input (maximum value). If this norm exceeds a particular value, then convergence of the series, and, therefore, the predictive ability of the series, is not guaranteed (see Appendix). The critical norm of the input is, of course, system dependent and will not usually be known a priori. Similarly, the convergence of the series is a function of the number of components that are identified for a particular kernel. In an example to be presented subsequently, this relationship between number of components of a kernel and the predictive accuracy of the series will be discussed. Rugh<sup>25</sup> and Boyd<sup>47</sup> discuss Volterra’s (and Frechet’s) extension of the Weierstrass theorem to nonlinear systems with finite (or fading) memory, and its relationship to the Volterra series. This is presented in greater detail in the Appendix.

Wiener<sup>48</sup> contributed significantly to the development of the Volterra theory and, as a result, the theory is sometimes referred to as the Volterra-Wiener theory of nonlinear systems. Reference 49 presents a kernel identification technique based on auto- and cross-correlation functions. References 50-57 are additional, excellent sources of information regarding the Volterra theory of nonlinear systems.

This research focuses on the time-domain Volterra theory because CFD analyses are typically performed in the time domain. There exists, however, a great deal of information on the frequency-domain Volterra theory<sup>25,43,58</sup>. The frequency-domain Volterra theory deals with the multidimensional Fourier transforms of the time-domain kernels. The resultant functions are referred to as higher-order spectra<sup>59</sup>. A double Fourier transform of a second-order kernel is referred to as a bispectrum. An excellent textbook on the subject is



Ref. 60. Whereas time-domain Volterra kernels may be better suited for computational methods, the frequency-domain methods appear to be better suited for experimental identification techniques. Boyd et al<sup>28</sup> describe a frequency-domain technique that was successfully applied to the experimental identification of the second-order kernel of a nonlinear electroacoustic transducer (speaker) system. The theory also has some very interesting applications in the fields of general turbulence<sup>61</sup> and low-frequency drift oscillations (LFDO) experienced by moored vessels in turbulent seas<sup>62</sup>. As mentioned previously, a time-domain kernel identification technique and the time-domain Volterra theory are applied to the systems investigated in this dissertation.

### *Kernel Definition*

Inspection of Equation (4) reveals some very interesting and characteristic features of the Volterra series. The value of  $h_0$  is known based on the steady-state value of the system at a particular condition. It does not require any special identification technique. This will be discussed in more detail when applied to an aerodynamic system. Also, if the kernels of order two and above are zero, then the response of the system is linear and is completely described by the unit impulse response  $h_1(t)$ , and the first-order convolution integral. The assumption underlying the first-order, or linear, convolution integral is that the response of the system at a given time,  $t$ , is the result of superposition of scaled and shifted impulse responses.

The higher order kernels,  $h_n$ , are the responses of the nonlinear system to multiple unit impulses, with the number of impulses applied to the system equal to the order of the kernel of interest : e.g.,  $h_2$  is the response of the nonlinear system to two unit impulses applied at two points in time,  $t_1$  and  $t_2$ . The variation of the time difference between these two times characterizes the second-order memory of the system. Therefore, the second-order kernel is a two-dimensional function of time:  $t$  and the time difference  $T = t_1 - t_2$ . This mathematical definition follows directly for the 'nth' order kernel, although visualization of these

functions can become difficult for orders greater than three. As will be shown, these kernels are also a function of the amplitude of the input used for identification, which can be used to improve the accuracy of the kernels. The Appendix provides a more detailed interpretation of Volterra kernels.

The higher-order (nonlinear) kernels presented in Equation (4) are defined as 'symmetric' since  $h_2(t_1, t_2) = h_2(t_2, t_1)$ . Although, depending on the domain of integration that is chosen, the kernels can be defined in 'triangular' or 'regular' form, any kernel can be symmetrized without affecting the input/output relation. This is done by realizing that

$$h_{sym}(t_1, \dots, t_n) = (1/n!) \sum h(t_{p(1)}, \dots, t_{p(n)}) \quad (5)$$

where the indicated summation is over all  $n!$  permutations of the integers 1 through  $n$ . For the present study, only symmetric kernels will be investigated since these are mathematically easier to interpret and intuitively easier to visualize. Additional details regarding this issue can be found in Refs. 25 and 43.

### *Weakly Nonlinear Systems*

One approach for obtaining Volterra series representations of physical systems is to assume that the system is a 'weakly' nonlinear system. A system that is weakly nonlinear is a system that is well defined by the first few kernels of the Volterra series so that the kernels greater than third order and above are negligible. Boyd, Tang, and Chua<sup>28</sup> mention some physical systems that are accurately modeled as weakly nonlinear systems including electromechanical and electroacoustic transducers and some biological systems. In this study, it is assumed that the nonlinear aerodynamic systems that are identified from the transonic small-disturbance (TSD) potential equation and the Navier-Stokes equations are weakly nonlinear, second-order systems. It is important to develop expertise with the

application of Volterra methods to nonlinear aerodynamic models in a gradual manner and a weakly-nonlinear model provides this type of gradual approach to the problem.

Although this truncation might exacerbate known convergence and amplitude restrictions of the Volterra series, it is of interest to investigate the effectiveness of this truncated model to practical applications. Results are therefore, limited to the identification of the second-order kernel, or  $h_2$ . The discrete-time Volterra series for a truncated, second-order, time-invariant, system has the form

$$y[n] = h_0 + \sum_{k=0}^N h_1[n-k] u[k] + \sum_{k_1=0}^N \sum_{k_2=0}^N h_2[n-k_1, n-k_2] u[k_1] u[k_2] \quad (6)$$

For the applications considered in this dissertation, kernel identification will consist of the identification of  $h_1$  and  $h_2$ , with  $h_0$  clearly stated as appropriate.

It should also be noted that the kernels, linear and nonlinear, are input dependent. For example, for a linear system, if the response of the system to an arbitrary input is desired, the unit impulse response of the system due to that particular type of input must first be defined. For a single-input-single-output (SISO) system, there is only one unit impulse response. For a multiple-input-multiple-output (MIMO) system, there are  $n \times m$  unit impulse responses where  $n$  is the number of inputs and  $m$  is the number of outputs. These unit impulse responses are then combined to form the unit impulse response matrix.

The advantage of the Volterra series approach for modeling nonlinear systems is that once the kernels are identified, the response of the nonlinear system to an arbitrary input can be predicted. The problem of kernel identification, therefore, is central to the successful generation of an accurate Volterra series representation of a nonlinear system.

The most obvious approach for identifying the kernels is to derive analytical expressions for the kernels from the governing nonlinear equations of the system of interest<sup>48,50,51</sup>. Although this approach is theoretically applicable to any set of nonlinear equations, including the nonlinear fluid flow equations such as TSD, Euler, and Navier-Stokes equations, it would require a significant amount of effort to analytically compute the kernels for different configurations and for various inputs. Instead, a kernel identification technique is desired that uses the output of a CFD model directly for quick and efficient kernel identification, regardless of the CFD code being used and the particular model geometry.

In what follows, the kernel identification technique using unit impulse responses from Ref. 25, is presented. The technique is then applied to a simple problem in order to illustrate the discrete-time application of the technique and the nature of the second-order kernel that is identified.

### *Kernel Identification*

Consider a weakly nonlinear, second-order system described by

$$y(t) = \int_0^t \mathbf{h}_1(t-\tau) \mathbf{u}(\tau) d\tau + \int_0^t \int_0^t \mathbf{h}_2(t-\tau_1, t-\tau_2) \mathbf{u}(\tau_1) \mathbf{u}(\tau_2) d\tau_1 d\tau_2 \quad (7)$$

with  $\mathbf{h}_0$  assumed to be zero. Inputs consisting of single and double impulse functions can be defined as

$$\mathbf{u}_0(t) = \delta_0(t)$$

$$\mathbf{u}_1(t) = \delta_0(t) + \delta_0(t + T)$$

where  $T$  is a positive number. The responses of the system (Eq. (7)) to these two inputs are

$$y_0(t) = \int_0^t h_1(t - \tau) \delta_0(t) d\tau +$$

$$\int_0^t \int_0^t h_2(t - \tau_1, t - \tau_2) \delta_0(t) \delta_0(t) d\tau_1 d\tau_2$$

and

$$y_1(t) = \int_0^t h_1(t - \tau) (\delta_0(t) + \delta_0(t + T)) d\tau +$$

$$\int_0^t \int_0^t h_2(t - \tau_1, t - \tau_2) (\delta_0(t) + \delta_0(t + T)) (\delta_0(t) + \delta_0(t + T)) d\tau_1 d\tau_2$$

Applying the sifting property of the impulse function to the first-order integral of the first response is straightforward. Application of the sifting property to the second-order integral yields the components of the second-order kernel that correspond to the times for which the impulse functions are defined. Therefore, for the first response,

$$y_0(t) = h_1(t) + h_2(t, t)$$

The second response can be expanded as follows,

$$y_1(t) = \int_0^t h_1(t-\tau) \delta_0(t) d\tau + \int_0^t h_1(t-\tau) \delta_0(t+T) d\tau +$$

$$\int_0^t \int_0^t h_2(t-\tau_1, t-\tau_2) (\delta_0^2(t) + 2\delta_0(t+T)\delta_0(t) + \delta_0^2(t+T)) d\tau_1 d\tau_2$$

or

$$y_1(t) = \int_0^t h_1(t-\tau) \delta_0(t) d\tau + \int_0^t h_1(t-\tau) \delta_0(t+T) d\tau +$$

$$\int_0^t \int_0^t h_2(t-\tau_1, t-\tau_2) \delta_0^2(t) d\tau_1 d\tau_2 + \int_0^t \int_0^t h_2(t-\tau_1, t-\tau_2) (2\delta_0(t+T)\delta_0(t)) d\tau_1 d\tau_2$$

$$+ \int_0^t \int_0^t h_2(t-\tau_1, t-\tau_2) (\delta_0^2(t+T)) d\tau_1 d\tau_2$$

This yields

$$y_1(t) = h_1(t) + h_1(t+T) + h_2(t,t) + 2h_2(t, t+T) + h_2(t+T, t+T)$$

The  $2h_2(t, t+T)$  term is a result of the symmetry of the kernel since

$$h_2(t, t+T) = h_2(t+T, t)$$

Then

$$y_1(t) = y_0(t) + h_1(t+T) + 2h_2(t, t+T) + h_2(t+T, t+T)$$

and noticing that

$$y_0(t + T) = h_1(t + T) + h_2(t + T, t + T)$$

results in

$$y_1(t) = y_0(t) + y_0(t + T) + 2h_2(t, t + T)$$

Solving for the second-order kernel

$$h_2(t, t+T) = (1/2) (y_1(t) - y_0(t) - y_0(t+T)) \quad (8)$$

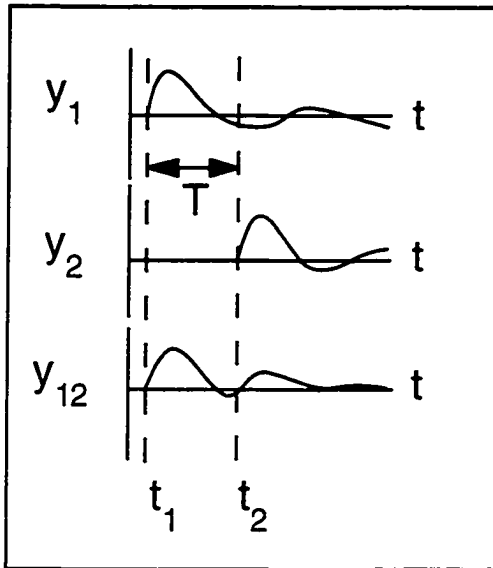
which is the value of the second-order kernel for any value of T.

The procedure for computing  $h_2$  is presented in Figure 7. First,  $y_0(t)$ , which is the response of the system to a unit impulse applied at time  $t$ , is generated. Then, since the system is time invariant,  $y_0$  is shifted in time to a new time  $(t + T)$ , which becomes  $y_0(t + T)$ . Then the response of the system to two unit impulses, one at time  $t$  and one at time  $t + T$  is generated. This is the  $y_1(t)$  response. All three responses are then substituted into equation (8) to yield one component of the second-order kernel. As can be seen, the second-order kernel,  $h_2$ , is a two-dimensional function of time. It is a function of time  $t$  and a function of time lag  $T$  so that for every value of  $T$  that is used, a new function of time  $t$  is defined. These functions of time are referred to as "components" of the second-order kernel. These components are sometimes referred to as "terms" but that phrasing is avoided here in order to avoid confusion with other uses of that phrase.

The first component of  $h_2$  is defined when  $T = 0$ , or when both unit impulse inputs are applied at the same point in time. When  $T=0$ , equation (8) reduces to

$$h_2(t, t) = (1/2)(y_1(t) - y_0(t) - y_0(t))$$

## KERNEL DEFINITION AND IDENTIFICATION



Linear system:  $h = y_1$   
higher order = 0.0

Nonlinear system:

$$h_1 = 2y_1 - .5 y_{11} \neq h$$

$y_{11}$  is double input

$h_1$  is  $f(t, \text{amplitude})$

$$h_2 = (1/2) (y_{12} - y_2 - y_1)$$

$h_2$  is  $f(t, T, \text{amplitude})$

Figure 7 Equations that define the first- and second-order kernels for a second-order truncated Volterra approximation and a schematic of the required responses.



$$= (1/2)y_1(t) - y_0(t) \quad (9)$$

The second component of the kernel depends on the next value of T selected. The number of components needed to accurately define a second-order kernel depends on the nonlinear system under investigation. As will be shown, the greater the nonlinearity, the greater the number of components required. Recall that these components are measures of the second-order memory of the system

In addition, the linear portion of the nonlinear response can be identified when  $T = 0$ . It is important to realize that the linear portion of the nonlinear response is not, in general, equivalent to the purely linear response. For example, for an aerodynamic system, the linear response computed using the linear equations (an airfoil represented by a flat plate) is not identical to the linear portion of the response computed using the nonlinear equations (an airfoil with thickness). One is a linear solution while the other is a linearized solution about a nonlinear condition. This difference will be demonstrated with the CFD applications later in this dissertation.

The linear portion of the nonlinear response is defined as follows. The response of the system represented by equation (7) to  $2u_0(t)$  is

$$y_2(t) = 2h_1(t) + 4h_2(t,t)$$

Then, solving simultaneously with  $y_0(t)$  results in

$$h_1(t) = 2y_0(t) - (1/2)y_2(t) \quad (10)$$

which is the unit impulse response of the linear portion of the nonlinear response.

The equations derived above for  $h_1$  and  $h_2$  are measures of deviation from linearity which implies nonlinearity. For a linear system,  $h_1$  (Eq. (10)) defaults to the value of the linear impulse response and  $h_2$  (Eq. (8)) is identically zero by the principle of superposition. For a nonlinear system,  $h_1$  captures some level of amplitude dependence and will therefore be different from the purely linear impulse response. The second-order kernel will be non-zero and the particular characteristics of this kernel provide some information regarding the level of nonlinearity of the system. Therefore, an additional benefit of the second-order kernel is that it can be used to establish boundaries beyond which the assumptions of linearity begin to fail. Definitions of higher-order kernels can be derived in the same way as for  $h_2$  by applying the appropriate number of unit impulses to the system.

Once  $h_2$  is identified, the nonlinear response of the weakly nonlinear, second-order system to an arbitrary input can be determined, keeping in mind convergence issues associated with this type of modeling. Figure 8 is a general representation of what the components of a second-order kernel might look like, how it is viewed in three dimensions, and its symmetric nature. It is worth mentioning that most kernel identification techniques applied in the literature are frequency-domain techniques with inherent complexity. The time-domain kernel identification technique presented, developed, and applied in this dissertation (Ref. 25) is computationally efficient and is directly applicable to many discrete-time, nonlinear, time-invariant systems. This kernel identification technique is now applied to a nonlinear circuit for illustrative purposes.

### Second-order kernel (Symmetric)

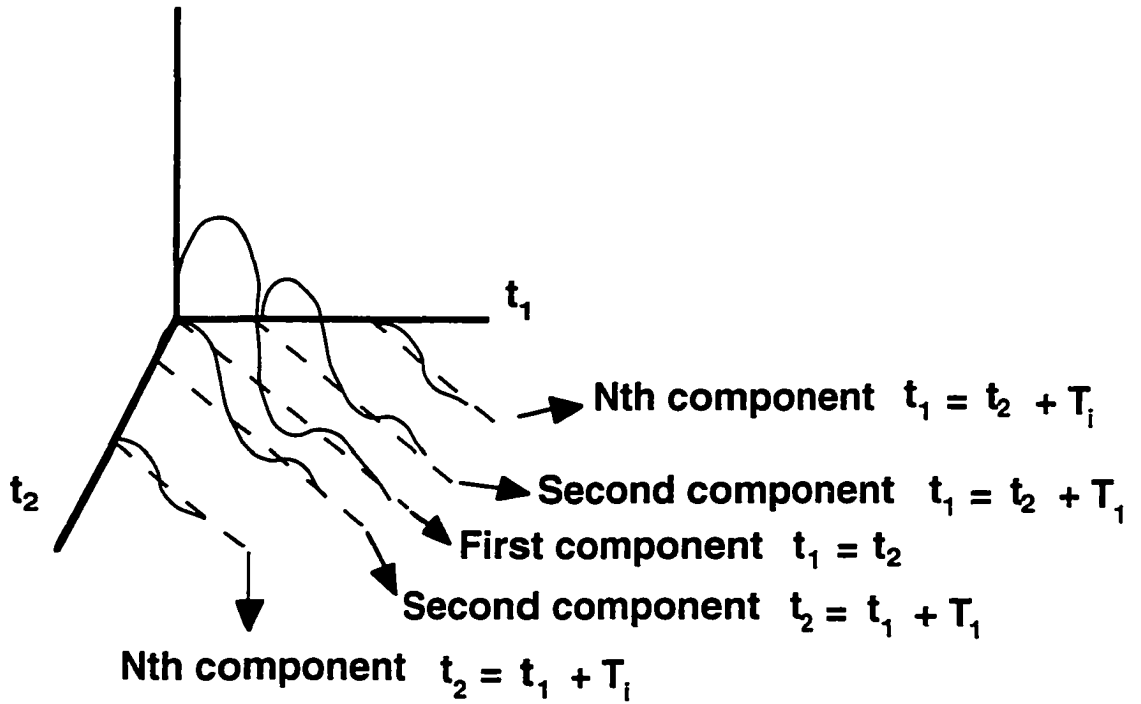


Figure 8 Schematic of the different components that comprise a symmetric second-order kernel.

### *Example - Nonlinear Circuit*

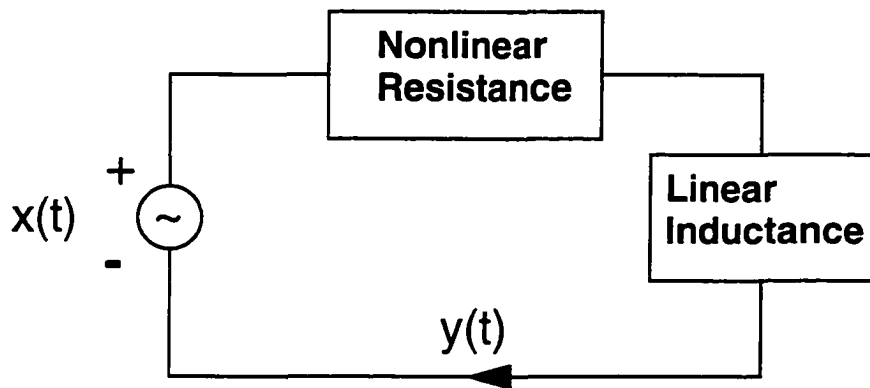
A simple nonlinear system that can be used to illustrate the kernel identification technique is a series circuit consisting of a linear inductance, a nonlinear resistance, and a voltage source<sup>54</sup>, shown in Figure 9. The governing equation for this circuit is the Riccati equation

$$\frac{dy}{dt} + \alpha y + \epsilon y^2 = x(t)$$

with  $y(t)$  the current around the circuit,  $x(t)$  the input voltage, and  $\alpha$  and  $\epsilon$  parameters from the nonlinear resistance. After discretization of the Riccati equation, Equation (8) is used to compute the various components of the second-order kernel for this system. The first-order kernel is computed using Equation (10). The system is discretized using a finite-difference approximation and the responses are obtained using a time step of 0.01.

#### Case 1: $\alpha = 1.0$ , $\epsilon = 0.0001$

The first-order kernel for this case is presented in Figure 10 for 5000 time steps. This kernel goes to zero very quickly, in less than 1000 time steps. Selected components for the corresponding second-order kernel are presented in Figure 11. Shown in Figure 11 are the first (1) component, the one-hundred-and-first (101) component, and so on. As can be seen, the largest component of the second-order kernel (the first) is quite small in magnitude as compared to the first-order kernel (Fig. 10) and goes to zero very quickly as well. Figures 10 and 11 indicate that nonlinear effects for this case are quite small, as would be expected with  $\epsilon = 0.0001$ . Verification of this is presented in Figure 12, a comparison of various step responses obtained directly from the model of the circuit and those obtained from the convolution of the step inputs with the first-order kernel of Fig.



$$\text{Riccati Equation: } (dy/dt) + \alpha y + \epsilon y^2 = x(t)$$

Figure 9 Simple nonlinear circuit defined by the Riccati equation shown with  $x(t)$  as the input to the system and  $y(t)$  as the output of the system.

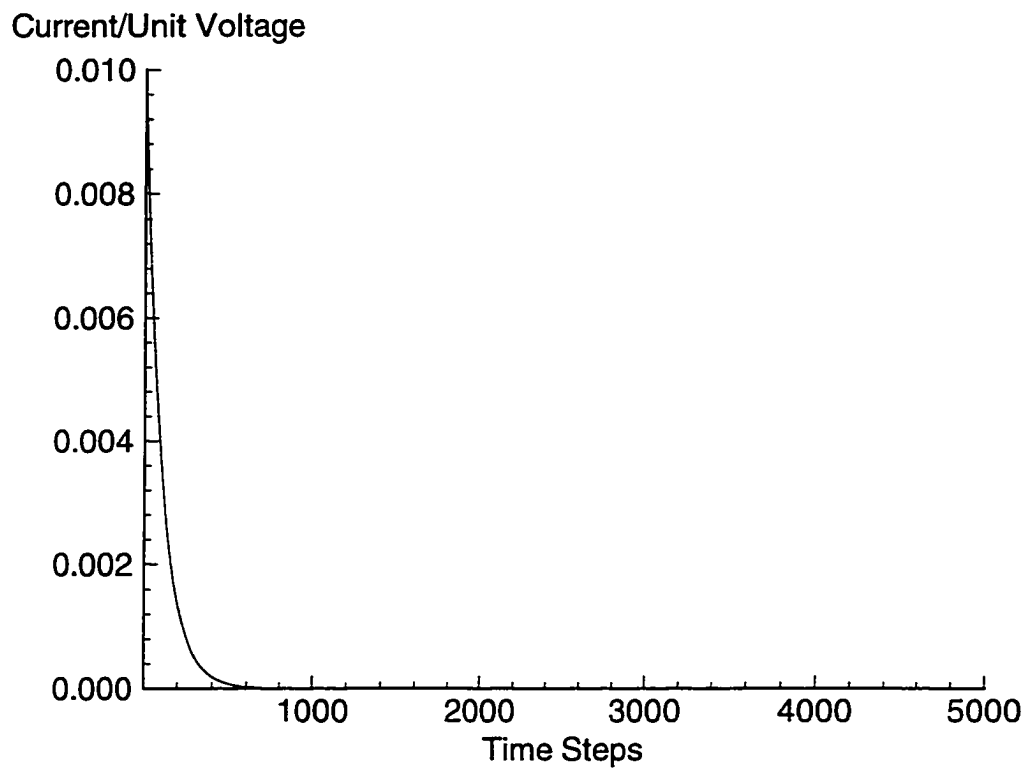


Figure 10 First-order kernel for the Riccati nonlinear circuit, Case 1,  $\alpha=1.0$ ,  $\epsilon=0.0001$ ,  $DT=0.01$ .

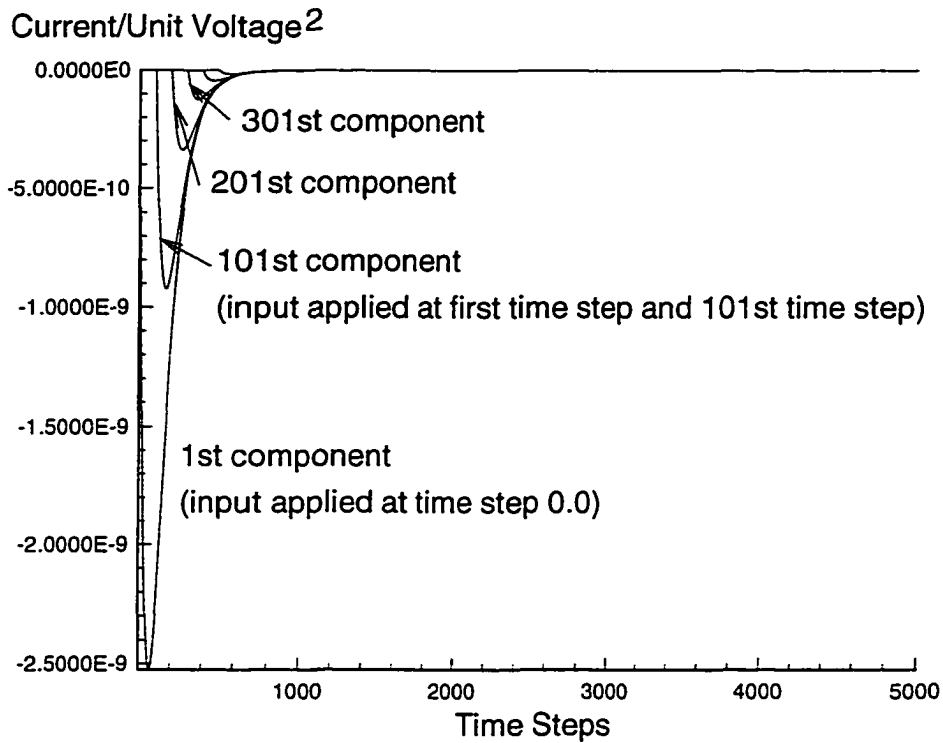


Figure 11 Selected components of the second-order kernel for the Riccati nonlinear circuit, Case 1,  $\alpha=1.0$ ,  $\epsilon=0.0001$ ,  $DT=0.01$ .

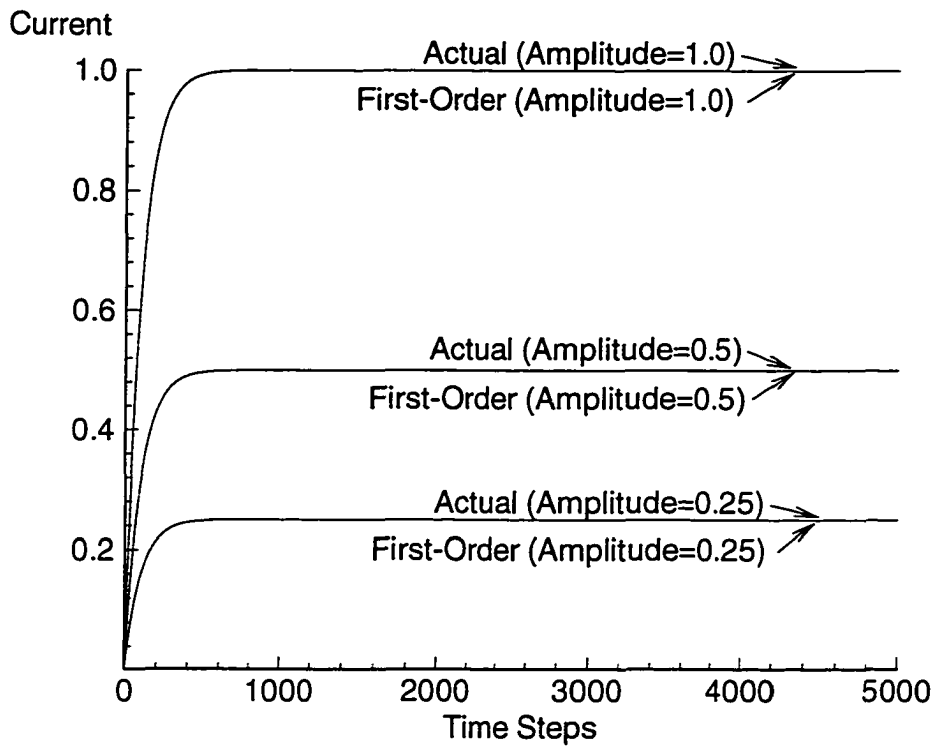


Figure 12 Comparison of Actual and First-Order responses due to three different step inputs for Riccati nonlinear circuit, Case 1,  $\alpha=1.0$ ,  $\epsilon=0.0001$ ,  $DT=0.01$ .



10. These identical results indicate that the first-order kernel is sufficient to capture the response of this system for the range of amplitudes investigated.

Case 2:  $\alpha = 0.1$ ,  $\epsilon = 0.001$

The first-order kernel for this case is presented in Figure 13, along with the first-order kernel from Case 1 (Fig. 10) for comparison purposes. The net effect of the change in the two parameters results in an increased effect of the nonlinearity of the Riccati equation. This is evidenced by the increased memory of the first-order kernel (slower approach to zero) as compared with the first-order kernel of Case 1. Figure 14 is a comparison of step responses obtained directly from the circuit and those obtained via convolution of the step inputs with the first-order kernel of Figure 13. Increased deviation between comparisons, as step amplitude is increased, indicates the effect of increased nonlinearity in the system and the need for the second-order kernel. Selected components from the second-order kernel for this case are presented in Figure 15, revealing a kernel larger in magnitude and memory than the second-order kernel of Case 1 (Fig. 11).

The dominant sign of the second-order kernel is actually quite important since it is an indication of the effect of the second-order nonlinearity on the total response of the system. That is, since the second-order kernel of Fig. 15 is negative, then the effect of the second-order convolution, which provides the effect of the second-order kernel, is to decrease the magnitude of the total response of the system from that obtained from the first-order convolution alone. This is clear in Figure 14 which shows that the response due to the first-order term “overshoots” the actual response. Addition of the negative second-order response would then approach the actual response. The second-order kernel can therefore provide an indication of the additive effect of the second-order nonlinearity with respect to the first-order term.

This example demonstrates the identification of first- and second-order kernels of a simple nonlinear system. Inspection of the kernels can provide very useful information

regarding the level of nonlinearity as well as the net effect of the nonlinearity of a particular system. These techniques will now be applied to CFD models.

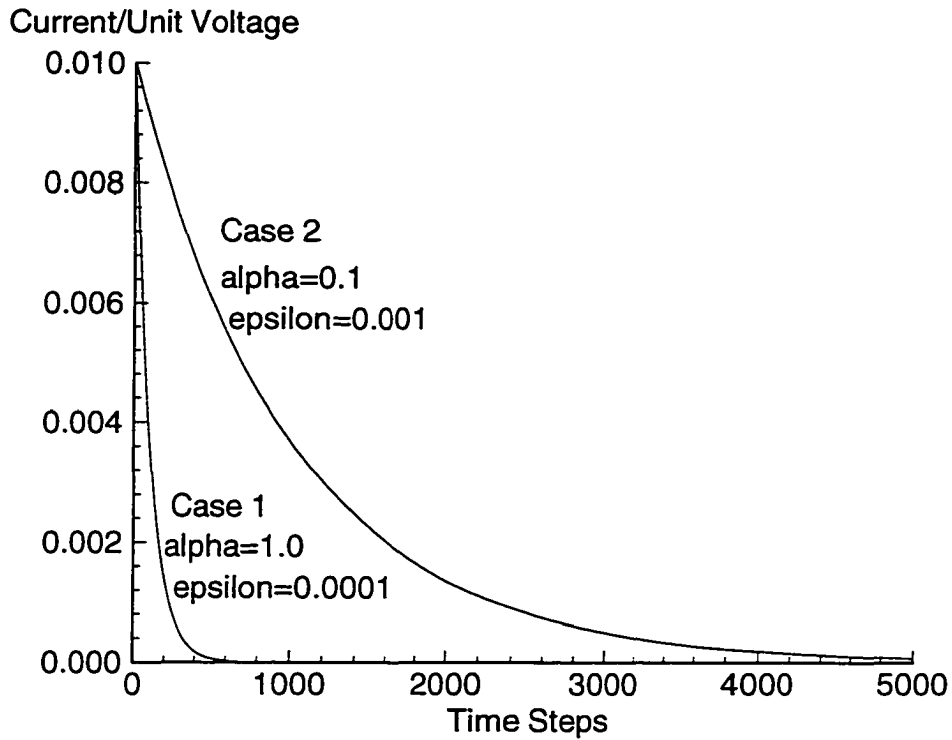


Figure 13 First-order kernels for Case 1 and Case 2 for the Riccati nonlinear circuit.

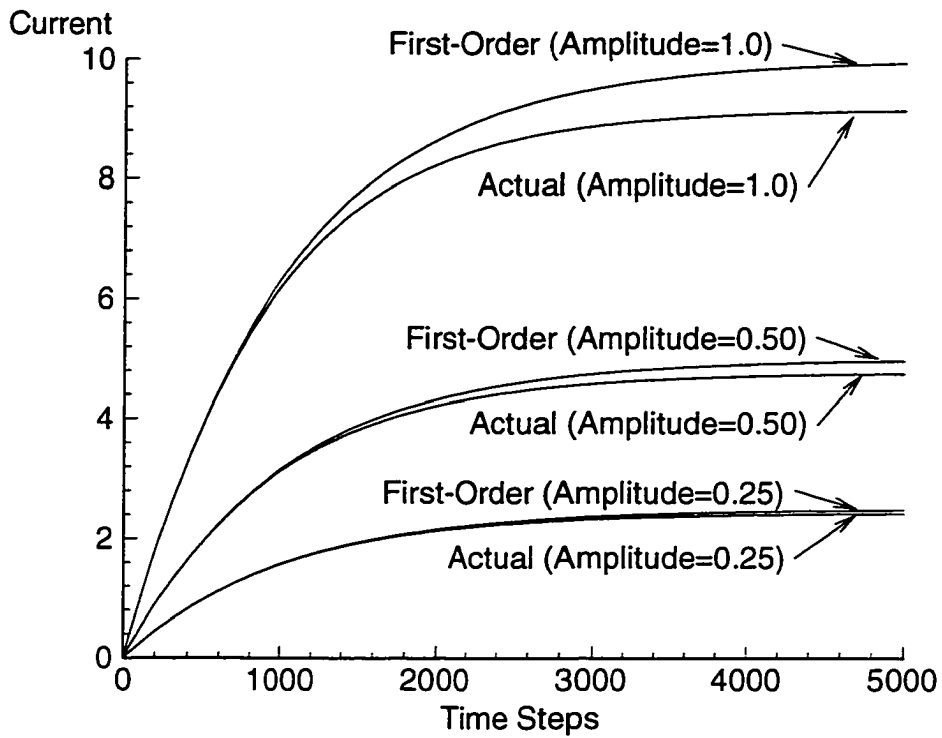


Figure 14 Comparison of Actual and First-Order responses due to three step inputs for the Riccati nonlinear circuit, Case 2,  $\alpha=0.1$ ,  $\epsilon=0.001$ ,  $DT=0.01$ .

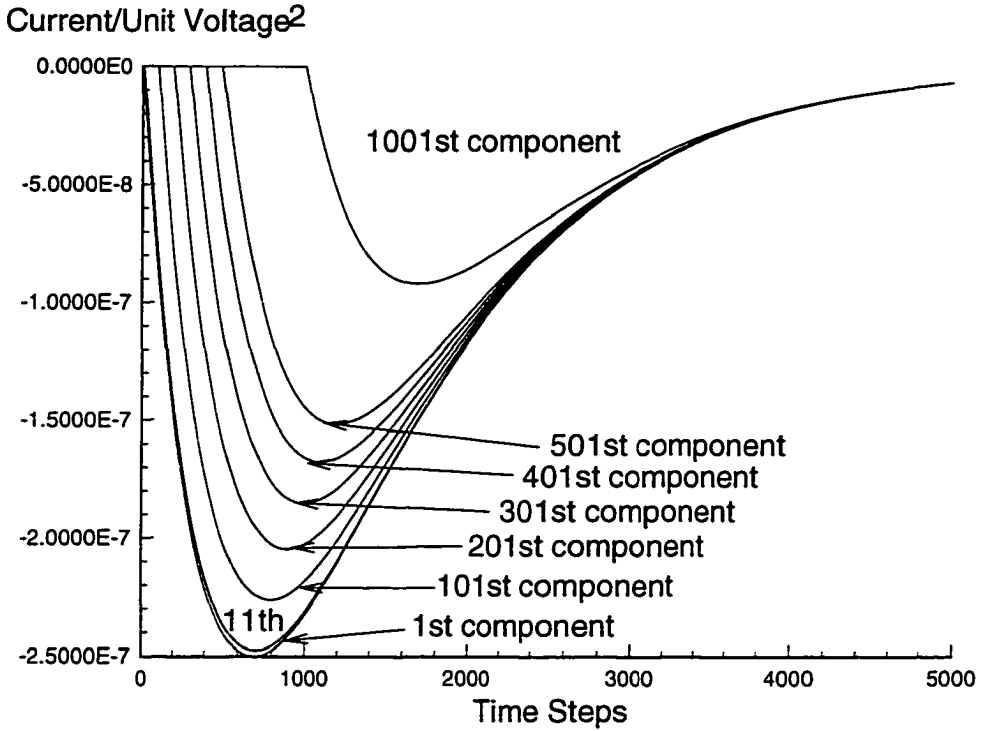


Figure 15 Selected components of the second-order kernel for the Riccati nonlinear circuit, Case 2, alpha=0.1, epsilon=0.001, DT=0.01.

CHAPTER 5  
APPLICATION TO CFD MODELS

*Navier-Stokes Equations*

The application of CFD codes involves, in general, the application of the discretized Navier-Stokes (NS) equations. This is true for the entire spectrum of equation levels, from the linear equations to the full Navier-Stokes equations, including transonic small-disturbance (TSD) and Euler equations. The only difference between the different equations is the number and type of simplifying assumptions used to derive the resultant governing equations. A flowchart of this process, from Ref. 63, is presented as Figure 16. It is important, therefore, to understand the functional nature of the NS equations<sup>64</sup>.

The compressible Navier-Stokes equations without body forces or external heat addition, in Cartesian coordinates, can be written

$$\frac{\partial \mathbf{U}}{\partial t} + \frac{\partial \mathbf{E}}{\partial x} + \frac{\partial \mathbf{F}}{\partial y} + \frac{\partial \mathbf{G}}{\partial z} = \mathbf{0}$$

with

$$\mathbf{U} = \begin{bmatrix} \rho \\ \rho u \\ \rho v \\ \rho w \\ E_t \end{bmatrix}$$

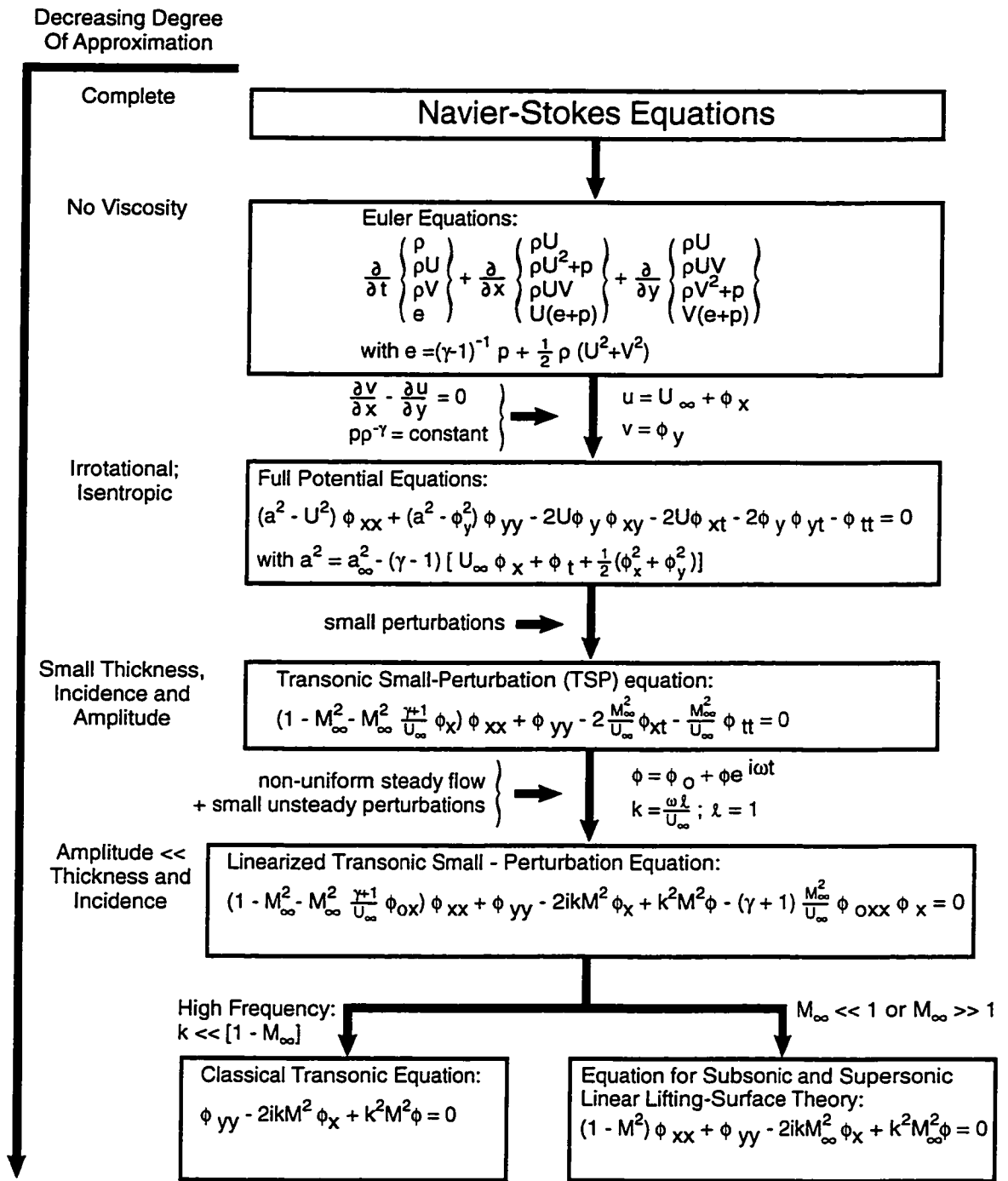


Figure 16 Equation hierarchy (from Reference 63).

$$\mathbf{E} = \begin{bmatrix} \rho u \\ \rho u^2 + p - \tau_{xx} \\ \rho uv - \tau_{xy} \\ \rho uw - \tau_{xz} \\ (\mathbf{E}_t + p)u - u\tau_{xx} - v\tau_{xy} - w\tau_{xz} + q_x \end{bmatrix}$$

$$\mathbf{F} = \begin{bmatrix} \rho v \\ \rho uv - \tau_{xy} \\ \rho v^2 + p - \tau_{yy} \\ \rho vw - \tau_{yz} \\ (\mathbf{E}_t + p)v - u\tau_{xy} - v\tau_{yy} - w\tau_{yz} + q_y \end{bmatrix}$$

$$\mathbf{G} = \begin{bmatrix} \rho w \\ \rho uw - \tau_{xz} \\ \rho vw - \tau_{yz} \\ \rho w^2 + p - \tau_{zz} \\ (\mathbf{E}_t + p)w - u\tau_{xz} - v\tau_{yz} - w\tau_{zz} + q_z \end{bmatrix}$$

The  $\rho$  is the density;  $u, v$ , and  $w$  are flow velocities in the  $x$ ,  $y$ , and  $z$  directions respectively; the  $\tau$  are the components of the viscous stress tensor;  $E_t$  is the total energy per unit volume;  $p$  is the pressure and  $q$  is the heat transfer. By inspection, it is clear that this system of equations is time invariant since there are no terms that are *explicit* functions of time. Discretization of these equations, however, can alter this condition, but only temporarily due to the residual of the numerical solution.

The rapid and often large variation of the numerical residual during the initial time stepping of a solution creates a time-varying numerical system. A converged, steady-state



solution is therefore required to drive the residual down to a level where the resultant numerical system is time invariant. Upon convergence of an initial, steady-state solution, the discretized NS equations form a discrete-time, nonlinear, time-invariant system. Reynold's averaging of the NS equations and inclusion of turbulence models to provide closure does not alter this aspect of the equations. Inspection of turbulence model equations reveals their time-invariant characterization as well. The realization that the discretized NS equations are a discrete-time, nonlinear, time-invariant system of equations allows the application of techniques routinely used in the modeling and design of nonlinear, discrete-time filters. In particular, Ref. 65 proves that discrete-time, nonlinear, time-invariant systems with memory can be modeled arbitrarily well using Volterra models, neural networks, or radial basis functions. The identification of impulse responses and their subsequent use in a convolution scheme requires knowledge of the classification of the system under investigation (time-varying vs. time-invariant). Because aerodynamic impulse responses were previously not identified (until Ref. 32), the classification of the Navier-Stokes (NS) equations regarding their shift (time) invariance was not addressed. The author has not been able to find references that discuss this simple yet powerful property of the NS equations.

### *Related Concepts*

Numerical approximations to ordinary and partial differential equations, such as finite-difference techniques, are defined by the dependence of the response on previous values of input and output. This applies to auto-regressive (AR), moving average (MA), and auto-regressive moving average (ARMA) systems as well. The similarity between finite-difference techniques and ARMA-type systems is obvious. Clearly then, time-accurate, discretized models, such as finite-difference models, are systems with memory, by definition. A discretized version of the NS equations (after steady-state convergence) is, therefore, a time-invariant, nonlinear, discrete-time system with memory and the

application of the discrete-time Volterra theory to this system of equations is a valid mathematical approach as proved by Ref. 65.

An intuitive explanation of the application of the Volterra theory to a CFD model (or any nonlinear system) can be described as follows. It is a well-established procedure to linearize a time-invariant, nonlinear system by expanding the nonlinear terms in a Taylor series about an operating point. The resultant Taylor series, if expanded to sufficient terms, is an excellent approximation to the actual nonlinearity. That is, there are no restrictions on the range of applicability regarding input amplitudes. As the series is truncated by gradual elimination of the higher-order terms, starting from highest to lowest, limitations on the range of applicability of the series approximation become more restrictive until the only term left is the linear term, the most severely restricted term of all. If higher-order terms are gradually added back to the series approximation, one at a time, the accuracy of the approximation is improved and the range of applicability is increased as well. The present method is, therefore, a method that re-instates higher-order terms that were, in a sense, removed during the linearization of the equations. This will yield improved accuracy over the purely linear solution and will increase the range of applicability as well. The relationship between the Volterra series and the Taylor series is discussed by Boyd<sup>47</sup> and others as well.

Also, when a “small” (or “linear”) input is applied to a time-invariant, nonlinear system, there is an implicit assumption of the equivalence between the nonlinear system and its series expansion. This is evident because it is in the presence of a series expansion formulation that a “small” input will, in fact, yield the “linear” portion of the response since the higher-order terms (second-order and above) are much smaller and, therefore, negligible. The accepted practice of using a “small” amplitude exponential pulse response within a CFD code, for example, to excite only the “linear” portion of the response about a nonlinear, steady-state solution implies a series approximation of the nonlinear response. As a result, this “small” input approach offers additional validation to the present

application of the discrete-time Volterra theory, which seeks to identify the next term of the Volterra series. The exponential pulse method is described later in this dissertation.

Furthermore, the first-order term is more accurate than the purely linear term because the first-order term is derived with knowledge of the second-order, or higher-order, terms. This is clear from the derivation of Equation (10). Therefore, for a second-order nonlinearity, the first-order term is the proper and correct linearization. The first-order term can be considered to represent a “mean” value of the response with the second-order term representing a higher-order variation about that mean.

The successful application of linearized aerodynamic methods, under certain geometrical and flow conditions, does not mean that rotational, viscous, and turbulent effects disappear from the flow at these conditions. What it does mean is that these effects are so small and/or so localized that they do not contribute significantly to the overall response. If one considers an aerodynamic response as a series expansion consisting of a linear term plus higher-order terms, then linearized aerodynamic methods are those methods where the response is dominated by the first (linear) term. As the flow- and/or geometry-induced nonlinearities begin to grow and the linear term is no longer adequate, it makes sense to expand our model to include the effects of the higher-order terms.

It is also important to realize that the level of aerodynamic nonlinearity, as measured by the series expansion, for example, depends on the macroscopic level being investigated. That is, it seems rather intuitive that the series expansion for the nonlinear response of a pressure sensing device (mounted somewhere on a wing) located in the vicinity of a shock will be different from that of the lift response of the wing. The response of the pressure sensing device will be dominated by the highly nonlinear effect of the shock and may require several higher-order terms to fully capture the nonlinear response. The lift of the wing, on the other hand, is the result of integration of pressures over the entire wing. The effect of this integration may be to reduce the effect of the localized shock on the global (lift) response of the wing. The series expansion for the lift response of the wing may

require less higher-order terms (if any) than the series expansion for the response of the pressure sensing device. Since loads are of primary importance in the preliminary design phase of a vehicle, it is quite reasonable to investigate the feasibility of a weakly-nonlinear model for the global (load) responses, even for conditions where highly nonlinear, but localized, flow phenomenon may exist.

### *Computational Benefits*

As will be shown, the computational efficiency of the present technique for CFD analyses is due to the following features of the method: 1) Identification of the first- and second-order kernels eliminates the need to re-execute the code. 2) The kernels can be coupled with a structure in a closed-loop sense “outside” of the CFD code, on a workstation for example, to generate aeroelastic responses thus sidestepping the current, very expensive method of solving the aeroelastic equations of motion within the CFD code. 3) The identification of the kernels is geometry independent. The first- and second-order kernels of a three-dimensional configuration are, topologically, the same as the kernels of a two-dimensional configuration. The only difference between the kernels of the two geometries is the initial cost of identification that requires the use of the CFD code. The complex CFD model, consisting of three spatial variables and one temporal variable, is mapped onto the unit sample response, a concise function of time only. The modal approach and the definition of boundary conditions within a CFD code make this mapping possible. 4) This technique permits a unified approach for the generation of concise mathematical models that can be used to compute linearized and nonlinear, steady and unsteady responses from a single, arbitrarily complex CFD model (complete configuration, finest grid, most detail).

The kernel identification technique is now applied to the viscous Burger’s equation as an example of the application of this technique to a simplified model of the Navier-Stokes equations.

*Example - Viscous Burger's Equation*

The 1-D viscous Burger's equation is defined as

$$\frac{\partial \mathbf{u}}{\partial t} + \mathbf{u} \frac{\partial \mathbf{u}}{\partial x} = \nu \frac{\partial^2 \mathbf{u}}{\partial x^2} \quad (11)$$

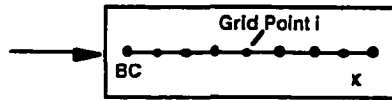
and is typically used as a simplified model of the Navier-Stokes equations for evaluating the effectiveness of numerical methods<sup>66</sup>. It is used here to demonstrate the effectiveness of the discrete-time Volterra technique when applied to a simple CFD model. Note that Equation (11) is clearly a time-invariant, nonlinear equation since it is not an explicit function of time. The numerical solution is implemented via a simple forward-in-time, central-in-space (FTCS) method with 40 grid points and a time step of 0.01. Figure 17 is a sketch that summarizes the application of the discrete-time Volterra theory to this example. The boundary condition (BC) grid point (grid point #1) is perturbed and the response to this perturbation is recorded at the fifth grid point, chosen arbitrarily.

The identification part of the process (Figure 17) consists of the generation of the first- and second-order kernels of the fifth grid point due to perturbation of the end-point boundary condition (BC) grid point. Shown in Figure 18 is the first-order kernel of the system, revealing a well-behaved, first-order memory function that goes to zero quickly. Shown in Figure 19 are the first twenty components of the second-order kernel. These components indicate a second-order nonlinear memory that goes to zero fairly quickly as well. Figure 20 is a three-dimensional visualization of the twenty components of this second-order kernel. The dominance of the first component is clear. Zooming in, in Fig. 21, the additional components are more visible.

It is helpful to consider the second-order kernel of a nonlinear system as a matrix. The

**IDENTIFICATION**

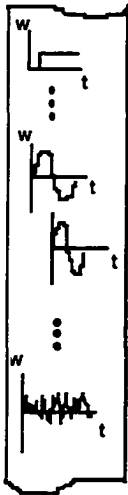
Multiple delayed perturbations of boundary condition (BC)



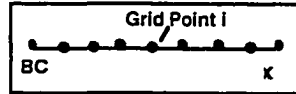
Output at Grid Point i

First-order kernel,  $h_1$   
 Second-order kernel,  $h_2$   
 (20 components)

**APPLICATION**



Numerical ("Actual") Solution



Digital Convolution

$$u(i) = \sum h_1(k) w(n-k) + \sum \sum h_2(k_1, k_2) w(n-k_1) w(n-k_2)$$

Compare results for Actual solution, First-order convolution, and First- plus Second-Order convolutions

Figure 17 Application of the discrete-time Volterra theory to the viscous Burger's equation consisting of identification and application phases.

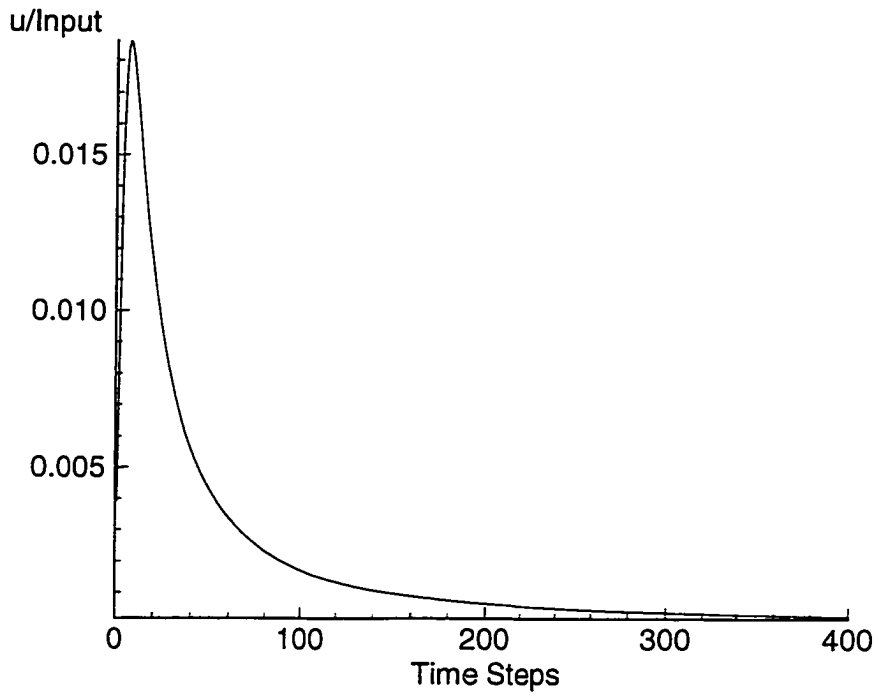


Figure 18 First-order kernel for viscous Burger's equation problem.

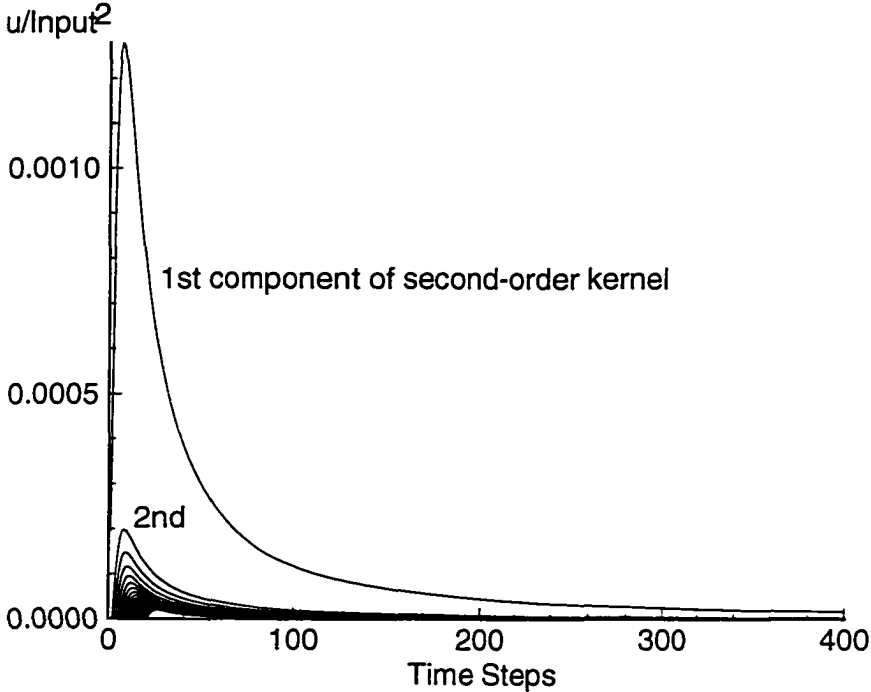


Figure 19 Twenty components of the second-order kernel for the viscous Burger's equation problem.



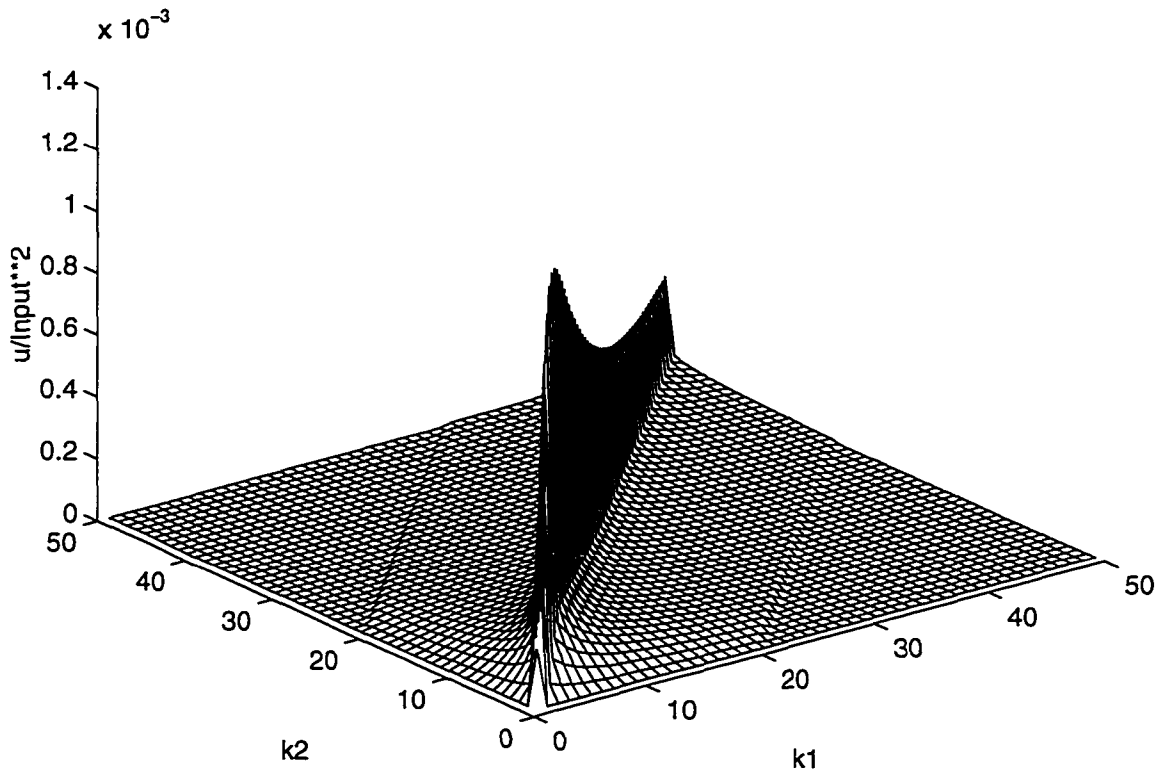


Figure 20 Three-dimensional perspective of the first twenty components of the symmetric second-order kernel for the viscous Burger's equation problem.

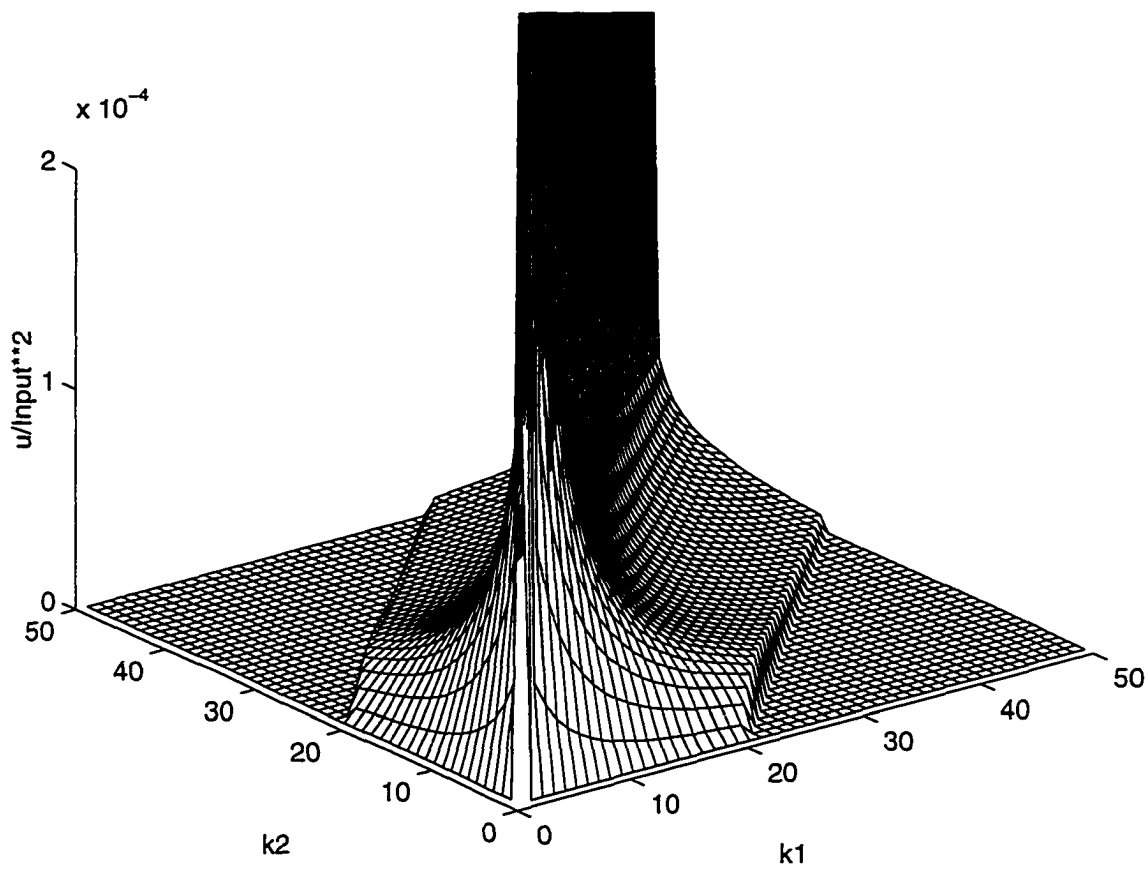


Figure 21 "Zoom-in" view of Figure 20.

diagonal of this symmetric matrix would be the first component of the second-order kernel. The lower (or upper since it is symmetric) diagonals are the additional components, with the second component of the kernel being the lower diagonal closest to the main diagonal and so on. This is typically the form used in nonlinear digital filtering techniques.

The application/validation part of the process (Figure 17) can now be carried out. Shown in Figure 22 is a comparison of several responses due to step inputs of increasing amplitude for the actual numerical solution, the convolution of the first-order kernel with each of the inputs, and the convolution of first- and second-order kernels with each of the inputs. As the amplitude is increased, the error between the actual ("true") response and the first-order response increases, indicating an increasing effect of the nonlinearity with amplitude. Addition of the second-order convolution shows a significant improvement in accuracy. The crossing over of the convolved response for the largest step response could be an indication of a convergence limit or the need for additional components of the second-order kernel. The improvement in response with the addition of the second-order term is, nonetheless, evident.

Using only the first- and second-order kernels, steady-state responses of the nonlinear system can be computed without re-execution of the actual numerical system. It is interesting to note that, for a certain range of amplitudes, the first-order response may be sufficient, depending on the level of accuracy desired. This is consistent with the well-established concept of linearization of a nonlinear system for small amplitudes.

Actual and convolved responses, using the same first- and second-order kernels, due to sinusoidal inputs were generated. Shown in Figures 23 and 24 is the comparison for a low-frequency input and a high-frequency input, respectively. Again, the comparisons were excellent with the combined first- and second-order response showing the best agreement with the actual responses. For the case of a purely linear system, these responses could be used to generate the frequency response function of the system, as is currently done for linear aerodynamic systems. Therefore, whereas the unit sample

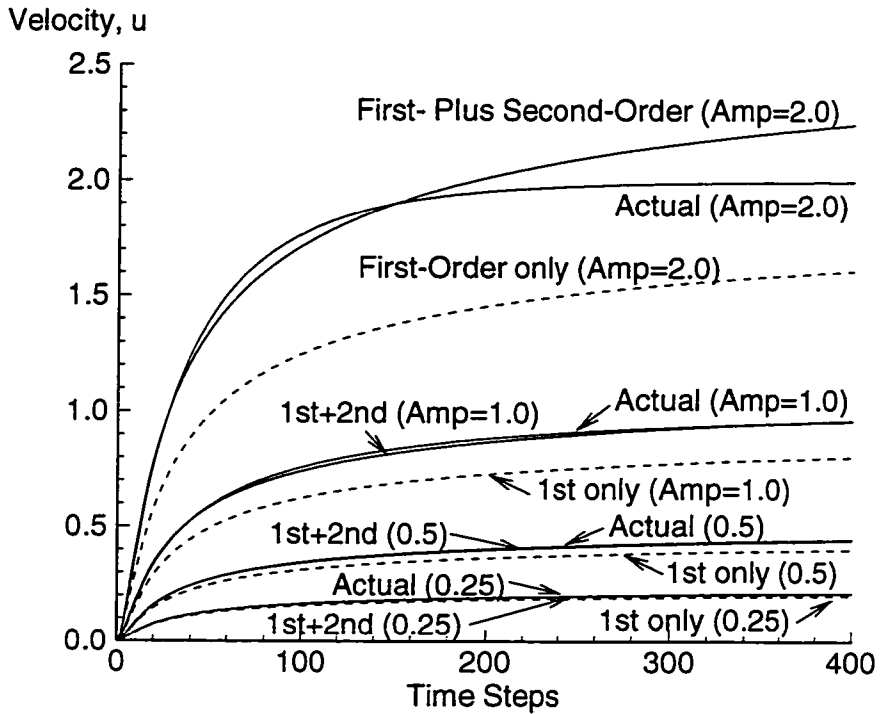


Figure 22 Comparison of Actual, First-Order only (1st only), and First- Plus Second-Order (1st+2nd) responses due to step inputs at four different amplitudes (0.25, 0.50, 1.0, 2.0) for the viscous Burger's equation problem.

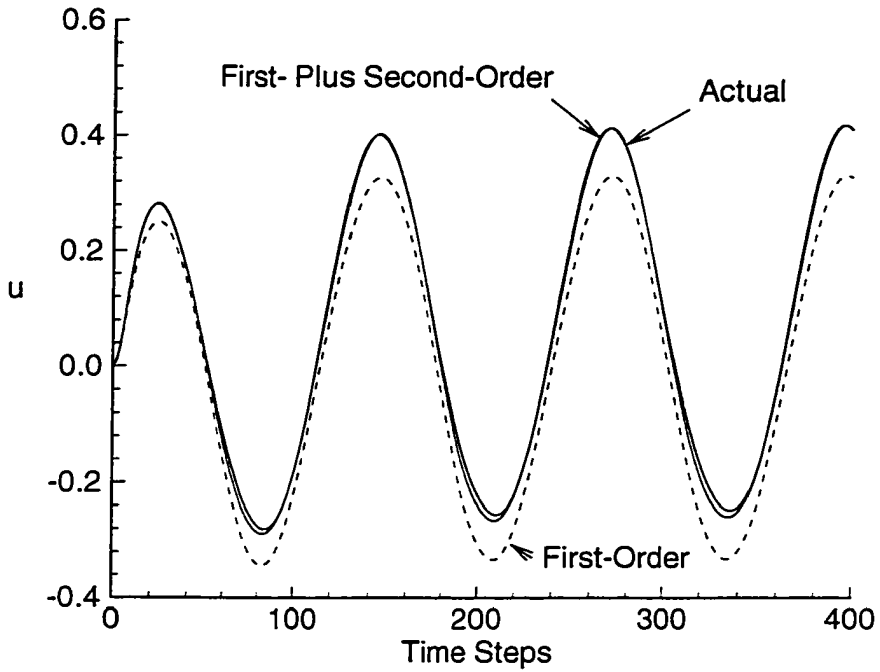


Figure 23 Comparison of Actual, First-Order only, and First-Plus Second-Order responses due to a low-frequency (5 Hz) sinusoidal input for the viscous Burger's equation problem.

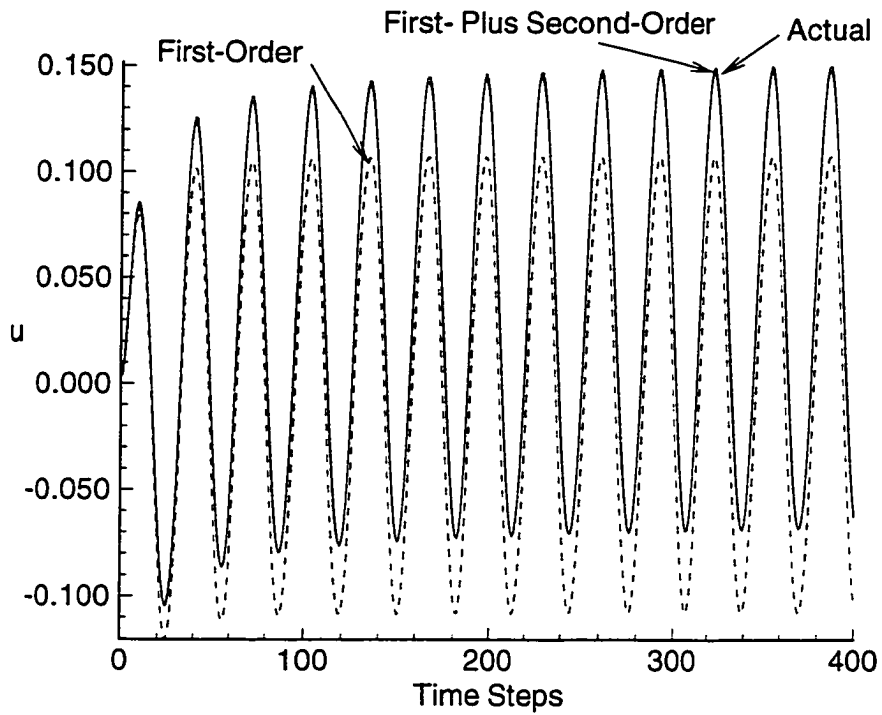


Figure 24 Comparison of Actual, First-Order only, and First-Plus Second-Order responses due to a high-frequency (20Hz) sinusoidal input for the viscous Burger's equation problem.

responses are valid in the complex plane, the forced harmonic response, which can be generated from the unit sample response, is valid only along the imaginary axis. The unit sample responses (linear) and first- and second-order kernels (nonlinear) do not have any such limitation. The only limitation of the nonlinear kernels is that the radius of convergence of the series is limited by the infinity norm of the input, which depends on the system being investigated. These kernels are therefore more powerful and, at the same time, more efficient than any other responses that can be obtained from a given system. This is because all other system responses are the result of a convolution of the system's unit sample response with some arbitrary input.

Shown in Figure 25 is a comparison of the actual, first-order, and first- plus second-order responses due to a low-amplitude (0.5) quasi-random input from a uniform probability distribution. The comparison is reasonable for the first-order only and excellent for the first- plus second-order response. It is interesting to note that the first-order only response captures the phasing very well while it is clearly deficient in amplitude. The addition of the second-order convolution yields a response identical to the actual response. The actual response and the first- plus second-order response are indistinguishable in Figure 25.

Shown in Figure 26 is a comparison of the actual, first-order, and first- plus second-order responses due to a medium-amplitude (1.0) quasi-random input from a uniform probability distribution. The first-order only response again captures the phasing accurately but the difference in amplitude with the actual response has increased. Addition of the second-order convolution to the first-order only response yields significant improvement over the first-order only response. Although improved, the comparison between the actual response and the first- plus second-order response is not as good as that of Figure 25 since slight differences between the two responses are visible in some portions of the responses.

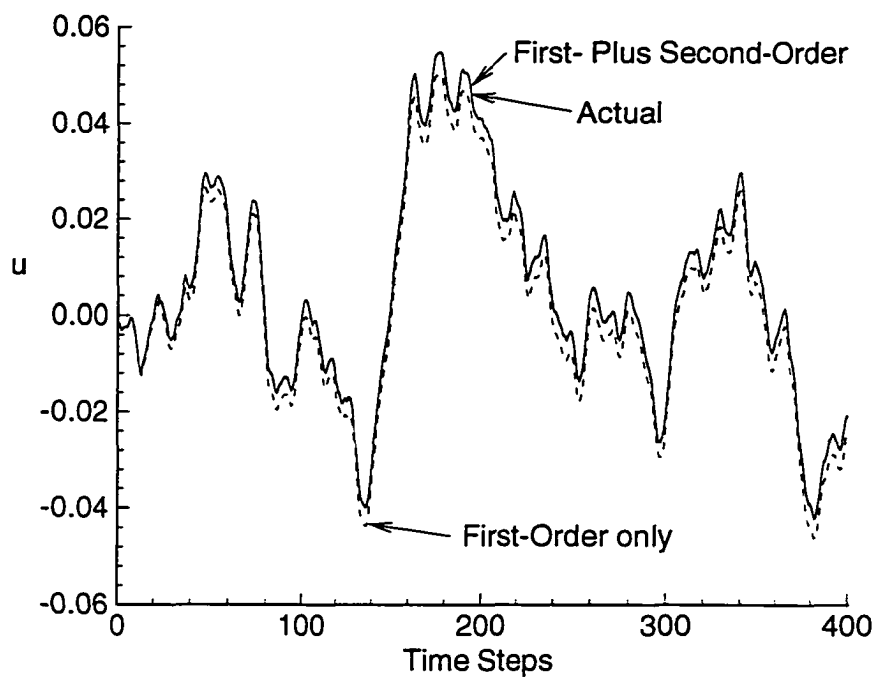


Figure 25 Comparison of low-amplitude, quasi-random responses including actual, first-order, and first- plus second-order responses for viscous Burger's equation problem.



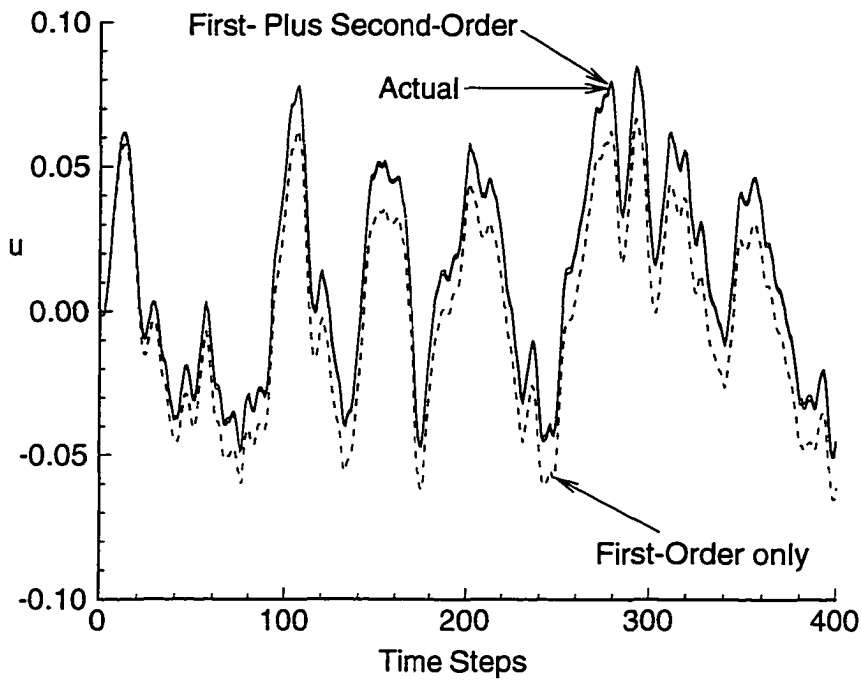


Figure 26 Comparison of medium-amplitude, quasi-random responses including actual, first-order, and first- plus second-order responses for viscous Burger's equation problem.

Shown in Figure 27 is a comparison of the actual, first-order, and first- plus second-order responses due to a large-amplitude (2.0) quasi-random input from a uniform probability distribution. The accuracy of the first-order only response continues to diminish with increasing input amplitude. Although the first- plus second-order response is still significantly better than the first-order only response, differences between the actual response and the first- plus second-order response are more noticeable.

The effect of input amplitude on the predictive accuracy of the first- and second-order kernels for this example is again revealed in Figures 25-27 as it was for the step responses. However, for a particular amplitude range, the first- and second-order kernels can be used to predict the response of the nonlinear system to *any arbitrary* input.

Application of the discrete-time Volterra kernel identification technique to more complex CFD models requires an understanding of the process by which the boundary conditions can be perturbed. The next section addresses this topic.

#### *Aerodynamic System Input Definition*

An important conceptual development of Ref. 32 was the mathematically-correct definition of the input to a discrete-time, unsteady aerodynamic system. The input for the excitation of a given structural mode (motion), known as the downwash function, is written as

$$w(x,y,t) = \Phi'(x,y) \cdot u(t) + \Phi(x,y) \cdot u'(t) \quad (12)$$

where  $\Phi(x,y)$  is the modeshape (shape of the structural motion),  $\Phi'(x,y)$  are the slopes of the modeshape,  $u(t)$  is the motion, and  $u'(t)$  is the rate-of-change of this motion. In the CAP-TSD code, for example, there are additional terms included in Equation (12) that account for the thickness of the wing. These terms are clearly not a function of time (shape

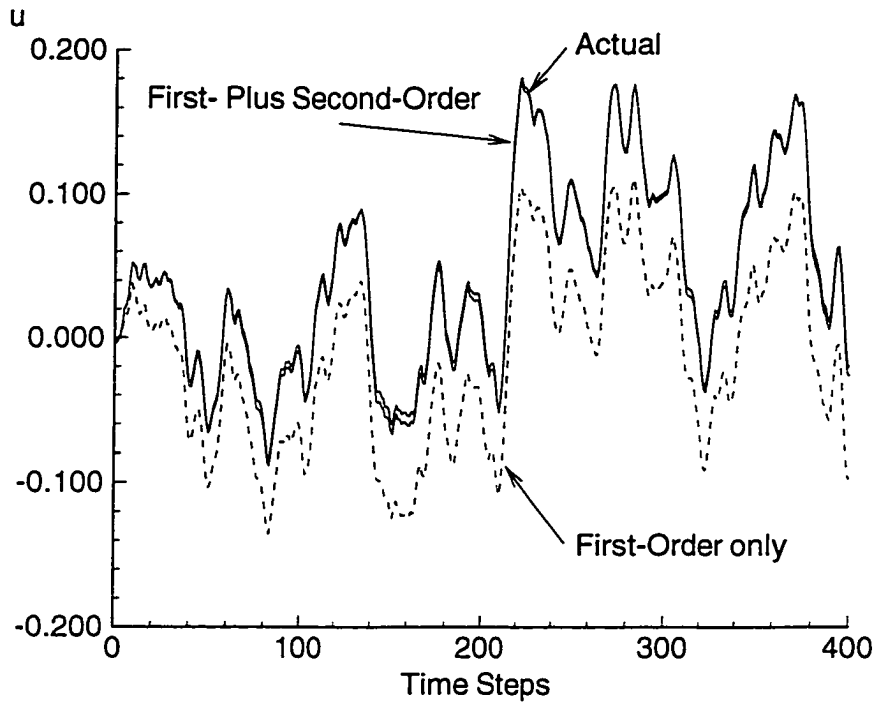


Figure 27 Comparison of high-amplitude, quasi-random responses including actual, first-order, and first- plus second-order responses for viscous Burger's equation problem.

of the wing is constant) and only impact the nonlinear, mean value of the response. For the linear solution, airfoil thickness is not included in the boundary conditions (downwash functions) to simulate a flat plate. The present discussion will be limited, temporarily, to the linear case for illustrative purposes.

The current method for the locally-linear excitation of aeroelastic modes within a CFD code involves the definition of a “smooth” pulse function defined as

$$\mathbf{u}(t) = D_0 \exp(-w(t-t_0)^2) \quad (13)$$

and its derivative

$$\mathbf{u}'(t) = -2w(t-t_0) \mathbf{u}(t) \quad (14)$$

where  $D_0$  is the maximum pulse amplitude desired,  $w$  is the width of the pulse, and  $t_0$  is the time at which the maximum amplitude is reached. This curve (Equation (13)) is referred to as the exponential pulse function and an example of an exponential pulse,  $u(t)$ , and its derivative,  $u'(t)$ , is shown in Figure 28. This exponential pulse is input to each of the modes of the system, via Equation (12), with a “small”  $D_0$ . The downwash equation (Eq. (12)) is then input to the aerodynamic flow solver to obtain small perturbation responses, about a nonlinear steady state solution<sup>67,68</sup>. These responses are then transformed to the frequency domain for use in standard linear analyses techniques. Equations (13) and (14) can be used to define some arbitrary motion and the rate-of-change of that motion which is then passed on to the flow solver via Eq. (12).

This exponential pulse function should not be confused with the unit pulse response mentioned throughout this dissertation. Whereas the unit pulse input (Eq. (1)) excites all the frequencies for a given mode, the exponential pulse input will excite only the particular range of frequencies defined by the width of the exponential pulse and its corresponding derivative. This can be explained using Eq. (12) as follows.

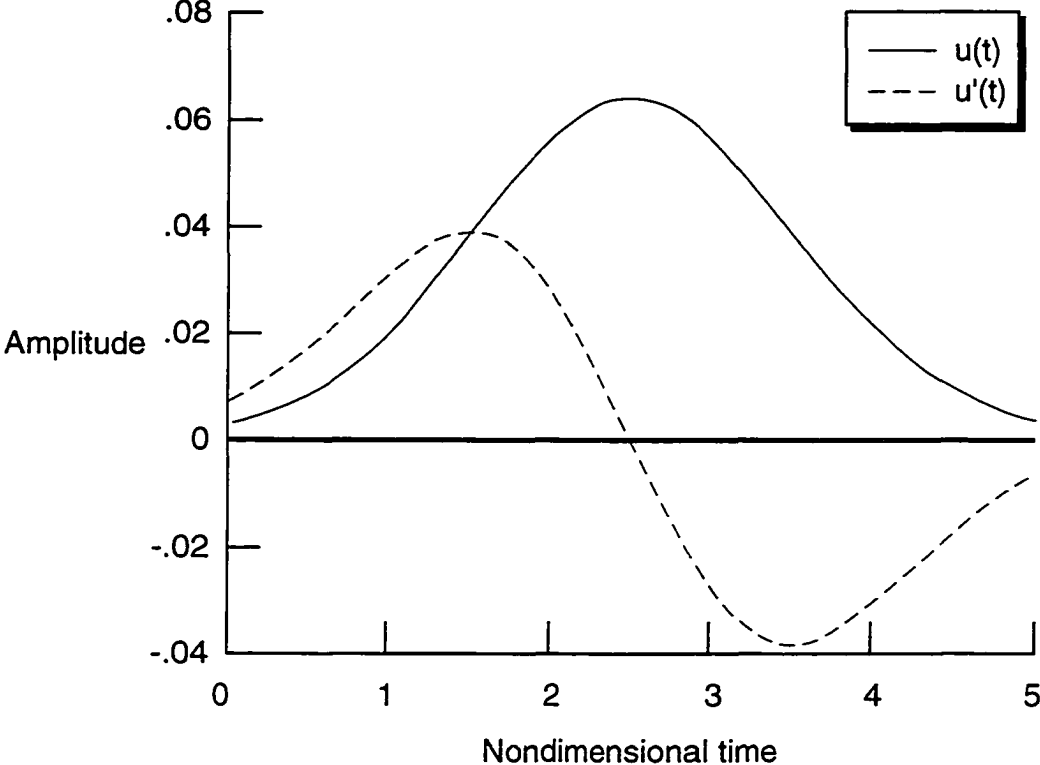


Figure 28 Example of an arbitrary plunge motion,  $u(t)$ , and corresponding rate-of-change of motion,  $u'(t)$ .

The downwash equation consists of the first term which multiplies  $u(t)$  (Eq. (13)) by the slopes of the modeshape. This term is then added to the second term which is the mode multiplied by  $u'(t)$  (Eq. (14)). When the shape of  $u(t)$  is narrowed, the derivative term,  $u'(t)$ , gets bigger and changes more rapidly than it does for a wider pulse. Therefore, a narrow  $u(t)$  will yield a large  $u'(t)$  and the input function (Eq. (12)) will be dominated by the  $u'(t)$  term. Because this  $u'(t)$  term will be large and will change quickly, the combined input to the flow solver (Eq. (12)) will excite primarily higher frequencies. Figure 29 shows a narrow  $u(t)$  and its derivative  $u'(t)$ . Shape optimization may, therefore, have to be performed in order to obtain the desired frequency range of interest. Typically, a “wide” pulse is recommended, forcing the  $u'(t)$  term to be small, resulting in a combined input that will excite primarily lower frequencies. The lower frequency range is usually the range of interest for aeroelastic analyses. This is particularly true for nonlinear aeroelastic analyses since the lower frequencies typically induce greater nonlinearities in the response.

A potential drawback, however, is that the exponential pulse is sometimes perceived as a single input. That is, the fast Fourier Transform (FFT) of the output response is divided by the FFT of the perceived single input,  $u(t)$ , to obtain the linearized frequency response function for that particular mode, or motion. But inspection of Eq. (12) clearly shows that the downwash function is, mathematically speaking, a two-input function since it is a summation of two distinct terms. The user defines  $u(t)$ , Eq. (13), but the quantity that is input to the flow solver is Eq. (12), which also includes the effect of  $u'(t)$  (Eq. (14)). Because this derivative is computed analytically within the code, it is invisible to the user, giving the impression that  $u(t)$  is the only input to the system. But it is clear from Eq. (12) that the  $u'(t)$  term is a contributor to the combined mathematical function that is input to the flow solver.

Equation (12) for a plunge (vertical translation) mode reveals that the first term is identically zero because the slopes of a plunge mode are zero. Therefore, the only temporal function that is actually input to the flow solver is  $u'(t)$ . For a plunge mode, the

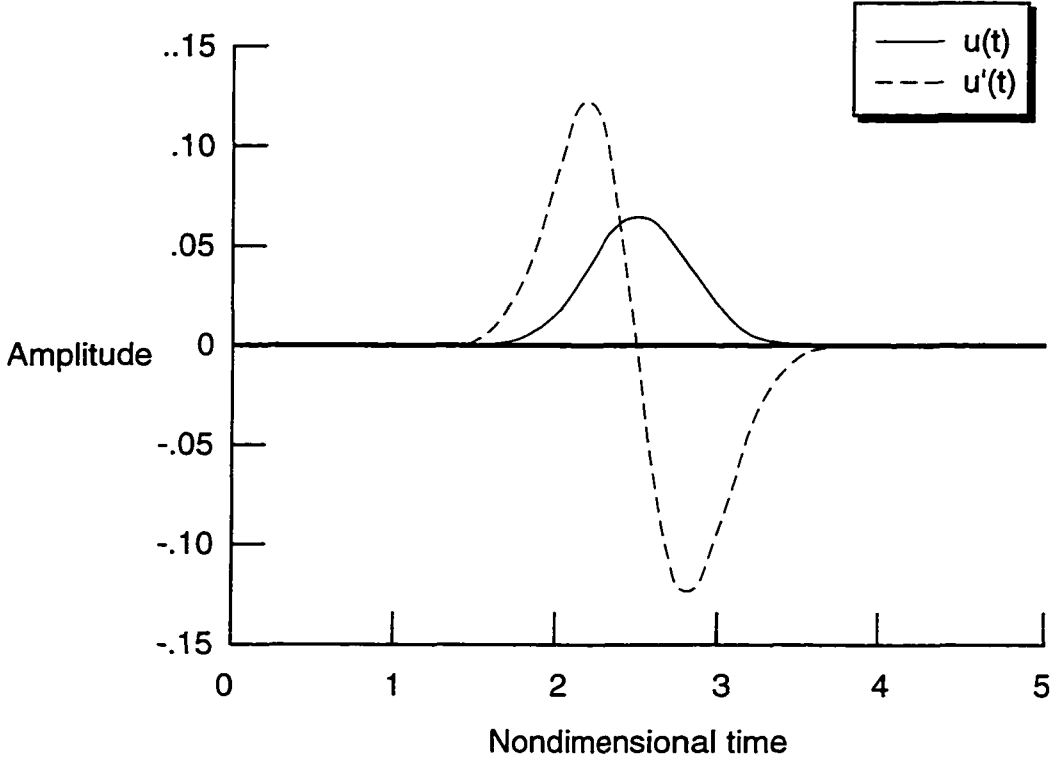


Figure 29 Example of a narrower arbitrary plunge motion,  $u(t)$ , and corresponding rate-of-change of motion,  $u'(t)$ .

computation of the frequency response function should use the FFT of  $u'(t)$  as the denominator, not the FFT of  $u(t)$ . This will be demonstrated using convolution with examples from CAP-TSD and CFL3D in a subsequent section of this dissertation.

The reason for the success of the technique to date is that for most modes, a very wide  $u(t)$  term results in a very small  $u'(t)$  term, thereby exciting, predominantly, the lower frequency range. For most aeroelastic analyses, the lower frequency range is, typically, the frequency range of interest. If an accurate determination of the entire frequency range of a mode is desired, however, then the second term of the downwash function must be included in the FFT analysis. In terms of computational efficiency, the exponential pulse response does not possess any of the mathematical properties of the unit sample response nor can it be formally extended to the analysis of nonlinear systems. The exponential pulse response method is, nonetheless, a standard approach for computing locally-linear responses from modern CFD aeroelastic codes.

The perception of the downwash as a single input can lead to the false conclusion that impulse (or unit pulse) and step inputs cannot be applied to a CFD code because these inputs will result in numerical difficulties. The reasoning being that the application of a unit pulse, or unit step, input as  $u(t)$  would lead to a very large, if not infinite, derivative term,  $u'(t)$ . So typically, a step input is modified, or made “smoother”, so that the  $u'(t)$  does not cause numerical problems. These “smoother” responses, however, are not mathematically consistent with the strict definition of unit pulses or unit step inputs and so will yield inaccuracies when used in convolution. The unit pulse and unit step functions have a very precise mathematical description which allows for convolution to be applied. Any deviation from this precise definition will reduce, or possibly eliminate, the accuracy of the convolution.

Mathematically, the downwash equation (for a given mode) is clearly a two-channel input: the first “channel” is  $u(t)$  and the second “channel” is  $u'(t)$ . For the linear case, each term of the downwash equation can, and should, be treated as a separate input channel.



The correct excitation input, for the linear case, should be the application of a unit sample input to each temporal function ( $u(t)$  and  $u'(t)$ ) of the downwash equation, one at a time. It is important to temporarily ignore the relationship between  $u(t)$  and  $u'(t)$  as one of a function and its derivative. This physical relationship will be reinstated when convolution is applied, as will be seen. Instead, each temporal function should be viewed as an input “channel” that merits its own excitation input, and, thus, its own impulse (or unit sample) response. Based on this reasoning, the unit pulse inputs were defined as

$$u(t) = 1.0 @ t=t_0 \text{ with } u'(t) = 0.0 \text{ for all } t$$

which yields the unit sample response for the  $u(t)$  term, or the first “channel”. The unit sample response for the second “channel” is identified by setting

$$u'(t) = 1.0 @ t=t_0 \text{ with } u(t) = 0.0 \text{ for all } t$$

which yields the unit sample response for the  $u'(t)$  term. These two unit sample responses can then be used to predict the response of the system to an arbitrary temporal variation of this particular mode. An arbitrary  $u(t)$  is convolved with the unit sample response identified for the first “channel”. The corresponding  $u'(t)$  for that arbitrary motion is convolved with the unit sample response for the second “channel”. These two convolutions are then added to obtain the complete response of the linear system to that input motion. This separation of input “channels” and subsequent superposition of convolution responses is certainly appropriate for the linear responses. Application of this concept using the linear equations within the CAP-TSD code are presented in a subsequent section of this dissertation.

For the nonlinear case, the response due to the sum of the terms of the downwash will not, in general, be equal to the sum of the separate responses due to each term of the

downwash. The inputs, however, still need to be treated as independent inputs. At first it might appear that the addition of the  $u(t)$  function with the  $u'(t)$  function would yield the correct input. This, however, is not correct due to the fact that each one of these functions is multiplied (or scaled) by the spatial functions in Eq. (12). Therefore, a different approach had to be developed as follows:

The unit sample response for each term of Eq.(12) was computed separately for the linear case as described above. The total linear response due to some arbitrary input consisting of  $u(t)$  and  $u'(t)$  was then computed, also as described above. A combined unit sample response for the linear equations, that consists of a unit sample input applied to each of the two inputs simultaneously, was then computed. Since the linear response has been computed and the linear combined unit sample response has also been computed, a simple deconvolution technique yields the necessary single, temporal input function. This single, temporal input function replaces  $u(t)$  and  $u'(t)$ . Therefore, when the combined linear unit sample response is convolved with this single input function, the result is the linear response.

A combined unit sample response is then computed for the nonlinear case. The net combined motion of the system, due to the combined inputs of the downwash, must obviously be the same for the linear and nonlinear cases. That is, the linear and nonlinear system of equations “see” the same input as it is being applied in time. Therefore, the nonlinear response to this motion can be computed by convolving the single, temporal input motion (obtained from the linear deconvolution) with the nonlinear, combined unit sample response. The effectiveness of this method will be presented in the final section of this dissertation.

## CHAPTER 6

### RESULTS USING THE CAP-TSD CODE

The CAP-TSD (Computational Aeroelasticity Program - Transonic Small Disturbance) code is a finite-difference program that solves the general-frequency modified TSD potential equation

$$M_{\infty}^2 (\phi_t + 2\phi_x)_t = [(1 - M_{\infty}^2)\phi_x + F\phi_x^2 + G\phi_y^2]_x + (\phi_y + H\phi_x\phi_y)_y + (\phi_z)_z$$

where  $M_{\infty}$  is the freestream Mach number,  $\phi$  is the disturbance velocity potential, and the subscripts represent partial derivatives. Details regarding the coefficients F, G, and H and discretization of this equation in the CAP-TSD code can be found in Reference 36. An application of this inviscid code to the prediction of the aeroelastic stability of a complex, full-span wind-tunnel model is presented in Reference 69. A viscous version of this code, based on an interacted boundary layer method, has recently been developed<sup>70</sup>.

The linear CAP-TSD results that follow were computed using the linear potential equation available within the code by setting the F, G, and H coefficients to zero.

#### *Linear CAP-TSD - Plunge*

The linear equations within the CAP-TSD code were used for comparisons of unit sample and step responses. The computational model is a rectangular wing with an aspect ratio of two. The wing is treated as a flat plate (no thickness) and the linear potential equation is invoked in order to obtain the linear solution. The wing has plunge and pitch degrees of freedom. All results presented are for nondimensional, normal aerodynamic force coefficient, at a Mach number of 0.9, and a time step of 0.001. Shown in Figure 30

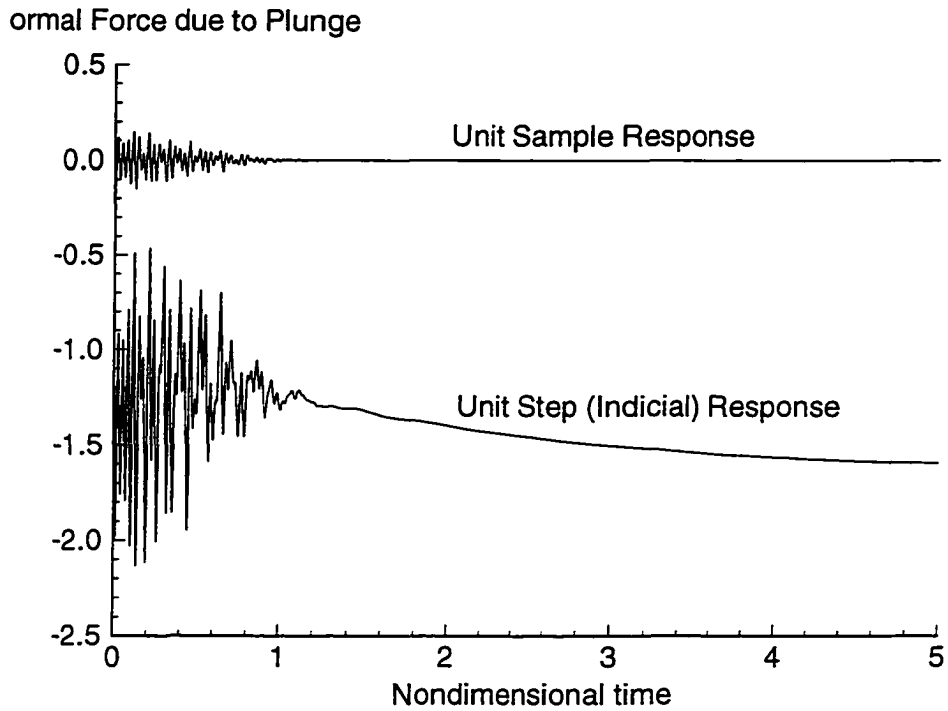


Figure 30 Comparison of plunge unit sample response and plunge unit step response, linear CAP-TSD,  $M=0.9$ ,  $DT=0.001$ .

is a comparison of the plunge unit sample response and the plunge unit step response. Convolution of the unit sample response with a unit step yields the unit step response, as shown in Figure 31. But, clearly, it is computationally more efficient to compute the unit sample response rather than the unit step response since the unit sample response reaches its steady state much faster than the step response. Both of these responses contain physical as well as numerical frequencies. Convolution with physically realistic motions, however, filters out the high-frequency content, as will be seen.

An arbitrary input consisting of  $u(t)$  (Eq. (13)) and the corresponding  $u'(t)$  (Eq. (14)) is applied to the plunge motion via Eq. (12). But as previously discussed, a plunging motion only affects the  $u'(t)$  term of the downwash input function, Eq. (12). Therefore, convolution of the plunge unit sample response with the input shown in Figure 32a,  $u'(t)$ , yields the exact, CAP-TSD-generated result, also shown in Figure 32a. Convolution of the plunge unit sample response with  $u'(t)$ , instead of  $u(t)$ , yields the correct result, consistent with the discussion regarding Equation (12) in a previous section. Comparison with a different (longer) arbitrary plunge motion is presented in Figure 32b, again showing excellent comparison. The same unit sample response can be used to predict the plunge response to an arbitrary plunge motion; any frequency, any amplitude, any time length.

The plunge step response is used to predict the response to the input  $u'(t)$  using Equation (4). The result is presented in Figure 33, along with the actual response, for an excellent comparison. Consistent with the discussion regarding Equation (4), the input used in the convolution with the step response is the *derivative* of  $u'(t)$ , also shown in Figure 33. For this case, it is important to include the first term of Equation (4) in order to correctly predict the actual response since the initial value of the input ( $u''(0)$ ) is non-zero.

The computational costs associated with the computation of ten of these types of responses, for the linear case, are presented in Table 1. Although linear solutions are not computationally intensive, it is important to demonstrate the effectiveness of this technique to linear systems before applying it to nonlinear systems. More importantly, the plunge

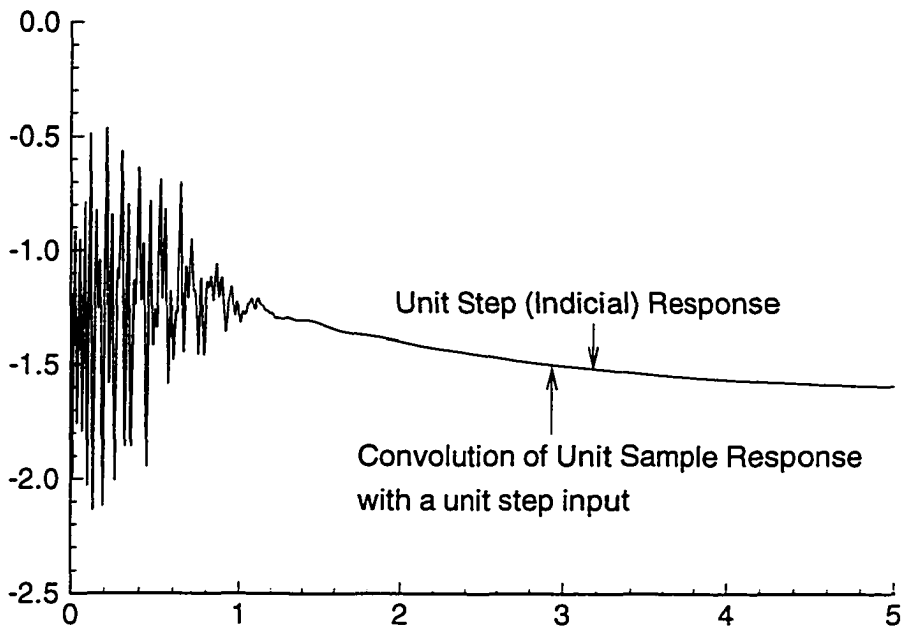


Figure 31 Step response computed via convolution of unit sample response with a unit step input, linear CAP-TSD.

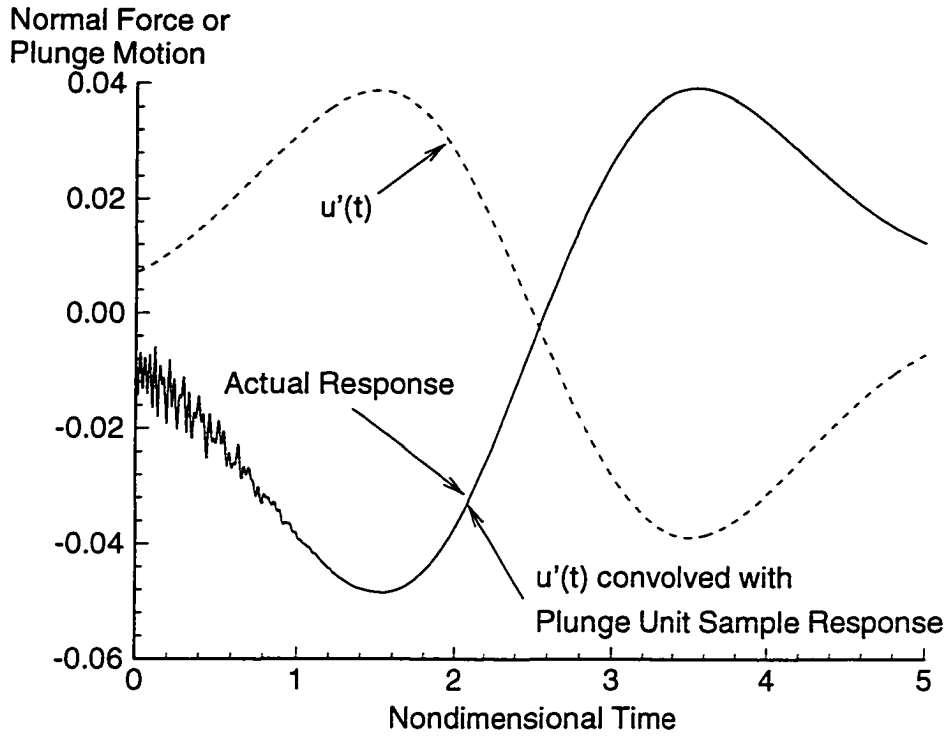


Figure 32a Comparison of Actual and Convolved Plunge Response, Linear CAP-TSD,  $M=0.9$ ,  $DT=0.001$ .

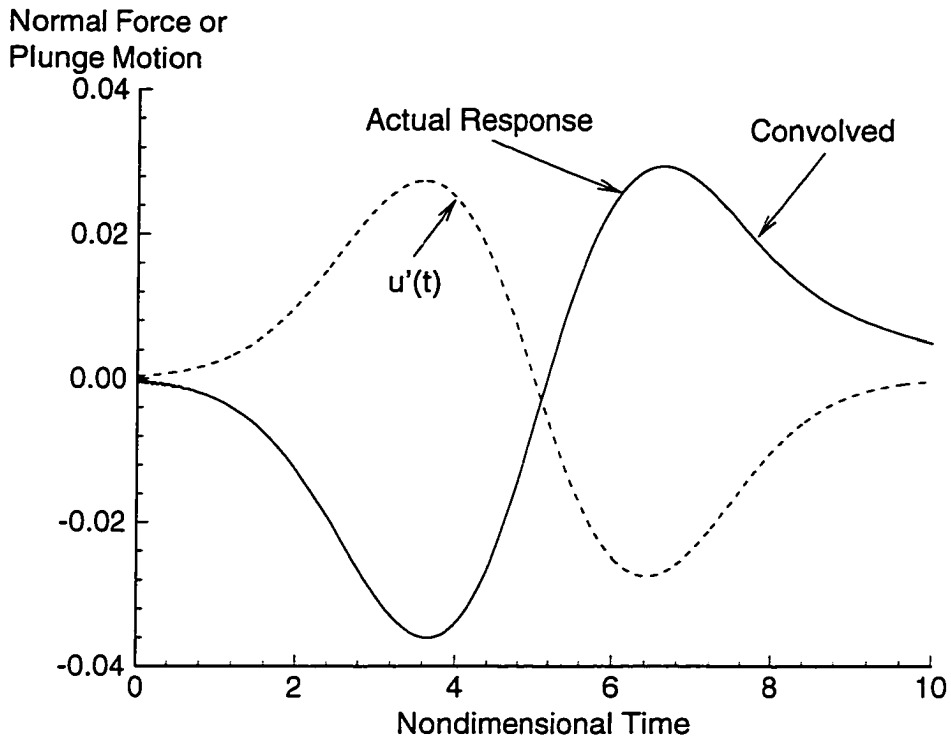


Figure 32b Comparison of Actual and Convolved Responses for lower frequency (longer timelength) arbitrary plunge motion, linear CAP-TSD,  $M=0.9$ ,  $DT=0.001$ .



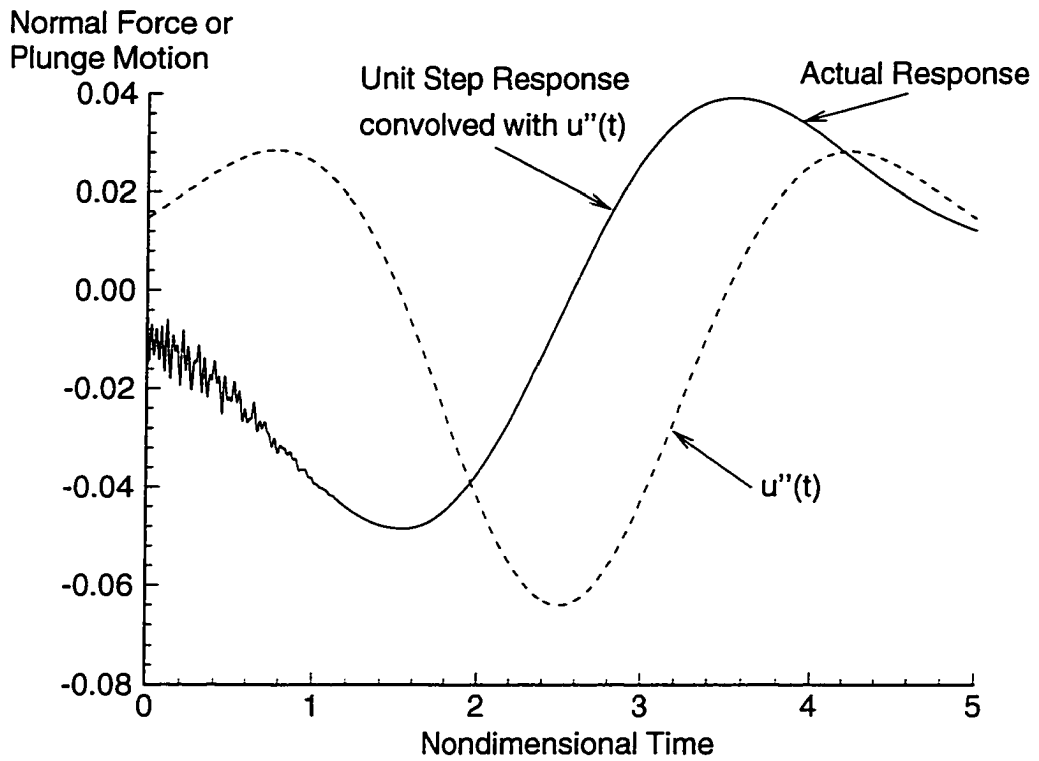


Figure 33 Comparison of Actual and Unit Step Response convolved with  $u''(t)$ , Linear CAP-TSD,  $M=0.9$ ,  $DT=0.001$ .

TABLE 1

COMPUTATIONAL COST COMPARISONS: LINEAR RESPONSES

<u>CAP-TSD</u>			<u>UNIT SAMPLE RESPONSE</u>		
<u>Run #</u>	<u>Cost</u>		<u>Run #</u>	<u>Cost</u>	
	<u>CPU s</u>	<u>Turnaround</u>		<u>CPU s</u>	<u>Turnaround</u>
1	3800	1.5hr - 1 day	ID <i>i</i>	1000	0.5hr - 1 day
2	3800	1.5hr - 1 day	ID <i>ii</i>	1000	0.5hr - 1 day
3	"	"	1	15	15 secs
4	"	"	2	"	"
...			...		

For 10 runs, total costs are:

38,000	15hrs (mininum)	2150	1.04hrs (min)
	10 days (max)		2 days, 150s(max)

unit sample response can now be used to predict the linear response in plunge due to any arbitrary plunging motion, from steady to random motions, without re-execution of the CFD code.

#### *Linear CAP-TSD - Pitch*

The responses due to a pitching (rotation) motion about the wing mid-chord, where both terms of Equation (12) are involved, are now presented. Presented in Figure 34 is the unit sample response in pitch due to the first term of Equation (12). Figure 35 is the unit sample response in pitch due to the second term of Equation (12). The arbitrary pitching motion, shown in Figure 36, was input to the CAP-TSD code (via Eq. (12)) and is referred to as the actual response. The first unit sample response (Fig. 34) is convolved with  $u(t)$  (Fig. 36) and the second unit sample response (Fig. 35) is convolved with  $u'(t)$  (Fig. 36). These two convolutions are then added to obtain the total convolved response. This response is plotted in Figure 37 along with the actual response, showing exact agreement. Additional verification of this method is demonstrated using a different arbitrary input, shown in Figure 38. Once again, the (same) first unit sample response is convolved with  $u(t)$  of Figure 38, the (same) second unit sample response is convolved with  $u'(t)$  of Figure 38, and these two convolutions are added. This response is compared to the actual result from the CAP-TSD code in Figure 39, showing identical agreement.

A different type of input consisting of a sinusoidal pitching motion was then applied. Figure 40 is a comparison of an actual CAP-TSD linear response and a convolved response. The same unit sample responses (Figures 34 and 35) were used for the convolutions. Again, the comparisons are identical. It is particularly interesting to “zoom” in on the first few time steps of the responses shown in Figure 40. As can be seen in Figure 41, the “zoom” comparison between the two responses is identical even for the initial time transients. This is not surprising since this transient is, in fact, the result of the initial part of the convolution of the unit sample responses.

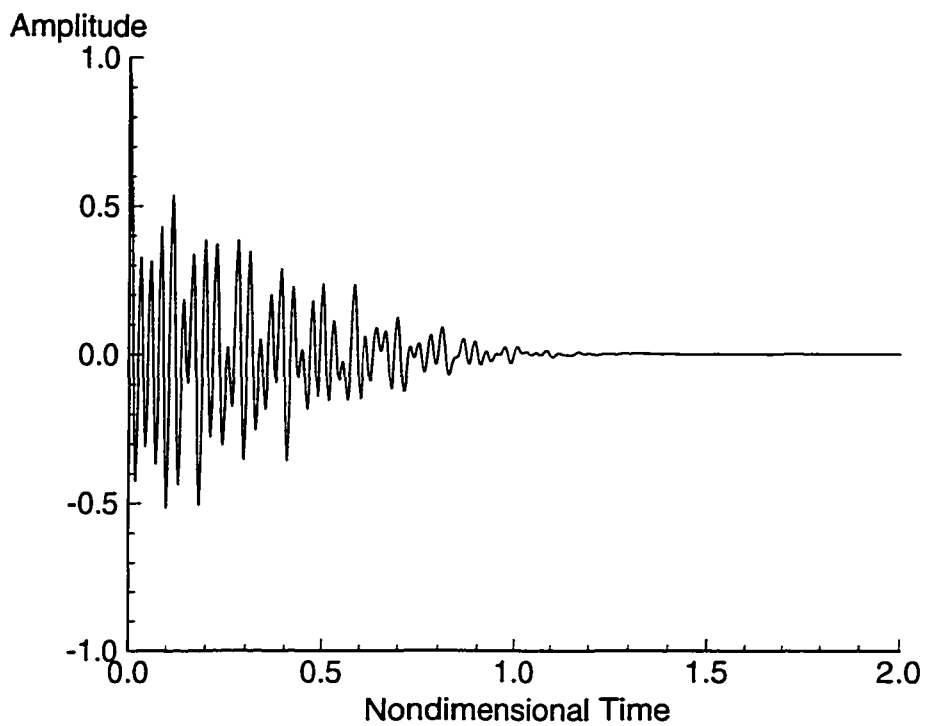


Figure 34 Linear unit sample response due to unit pulse applied to the motion "input channel" of the downwash equation.

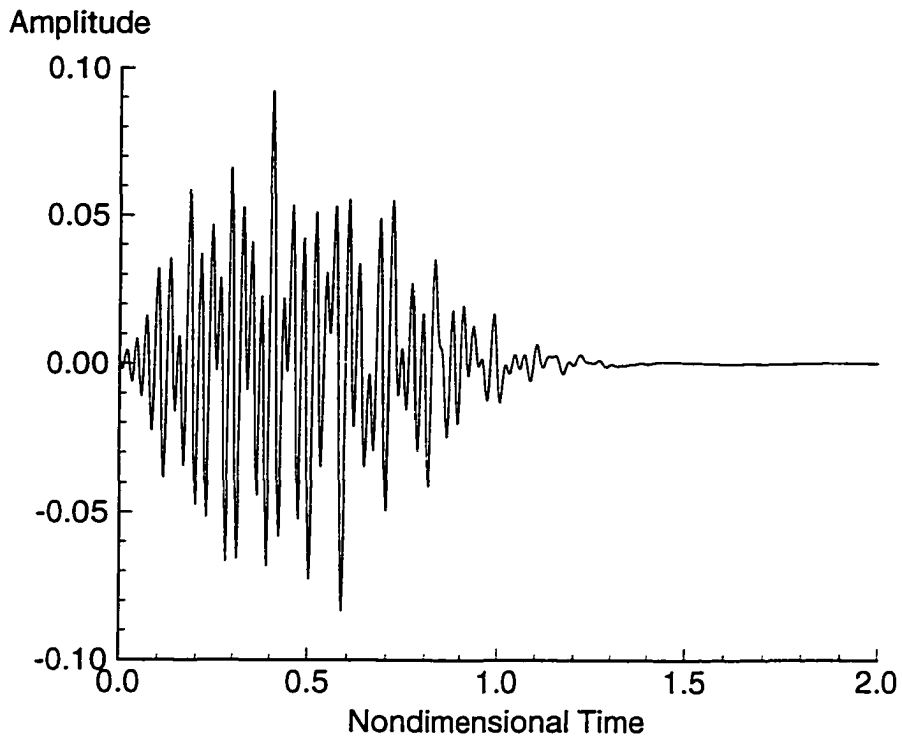


Figure 35 Linear unit sample response due to unit pulse applied to rate-of-change of motion "input channel" of the downwash equation.

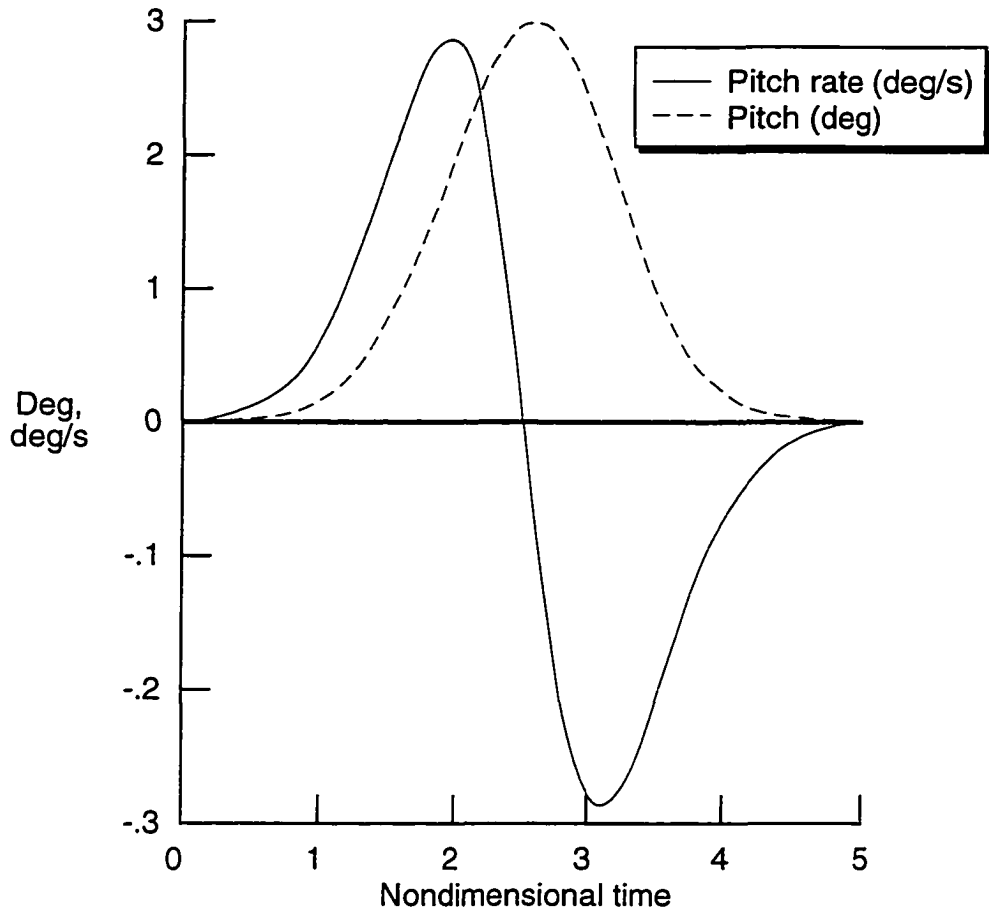


Figure 36 Arbitrary pitching motion, low frequency.

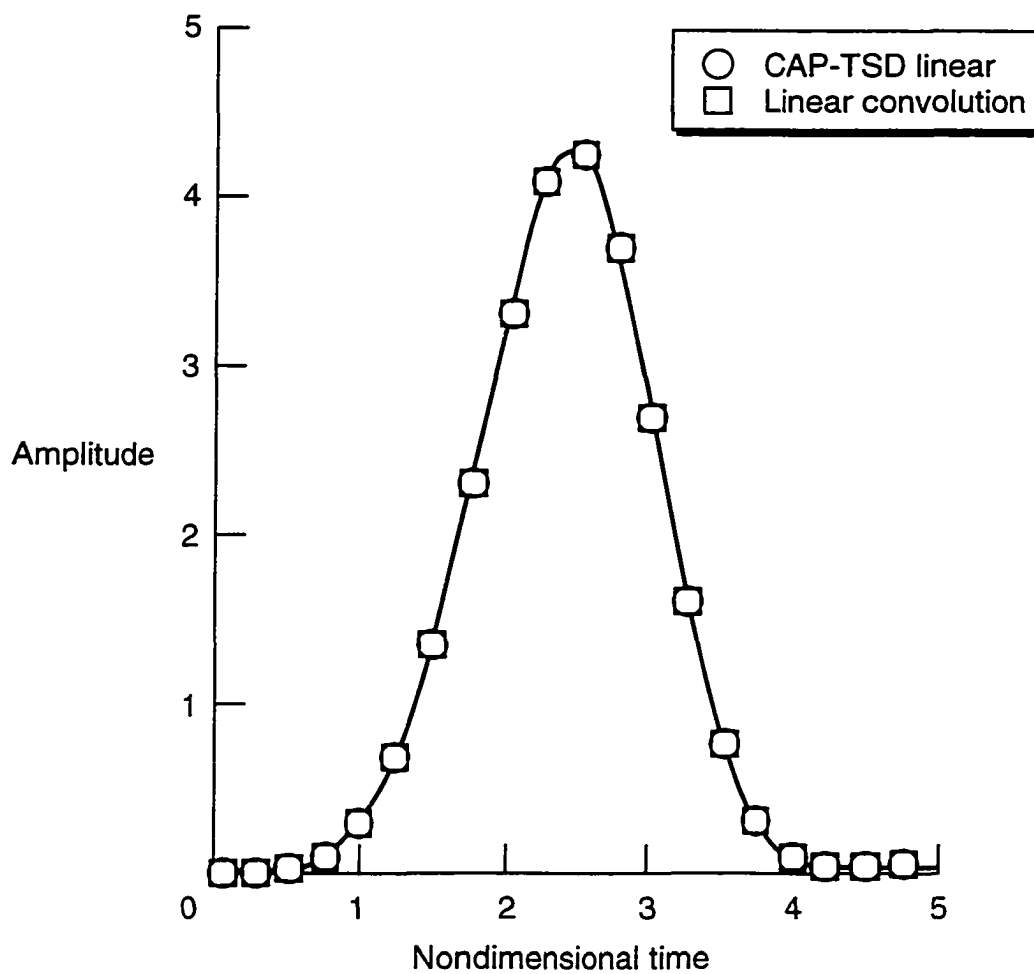


Figure 37 Comparison of actual and convolved plunge responses due to arbitrary pitch motion of Fig. 36, linear CAP-TSD,  $M=0.8$ ,  $DT=0.001$ .

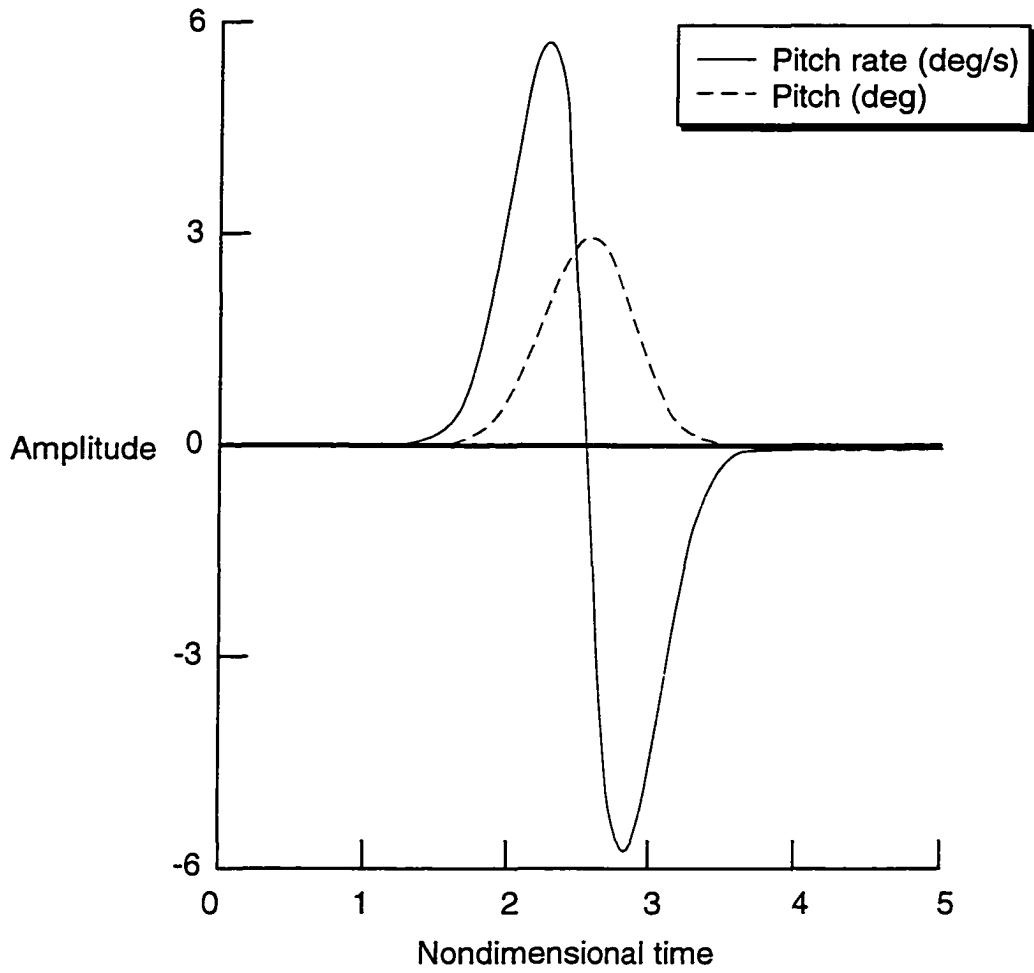


Figure 38 Arbitrary pitching motion, high frequency.



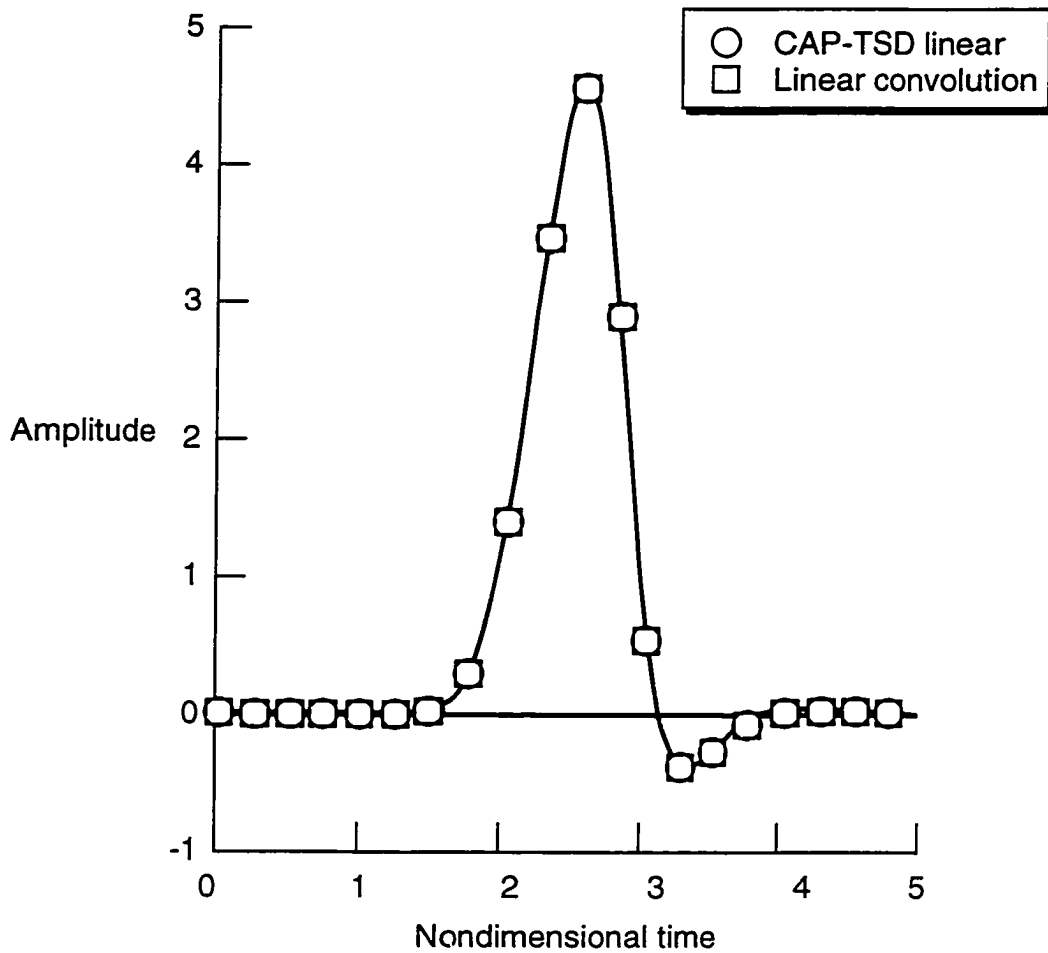


Figure 39 Comparison of actual and convolved plunge responses due to arbitrary pitch motion of Fig. 38, linear CAP-TSD,  $M=0.8$ ,  $DT=0.001$ .

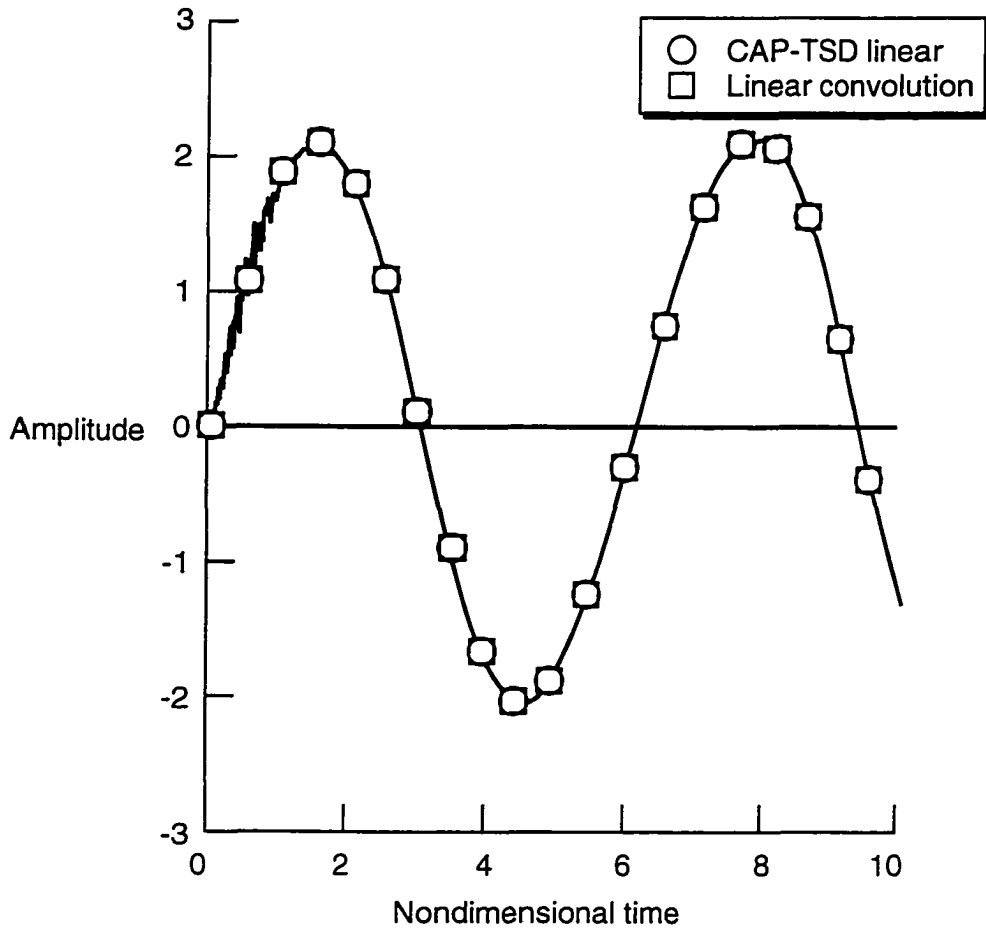


Figure 40 Comparison of actual and convolved plunge responses due to a sinusoidal pitch motion (1.5 degrees amplitude).

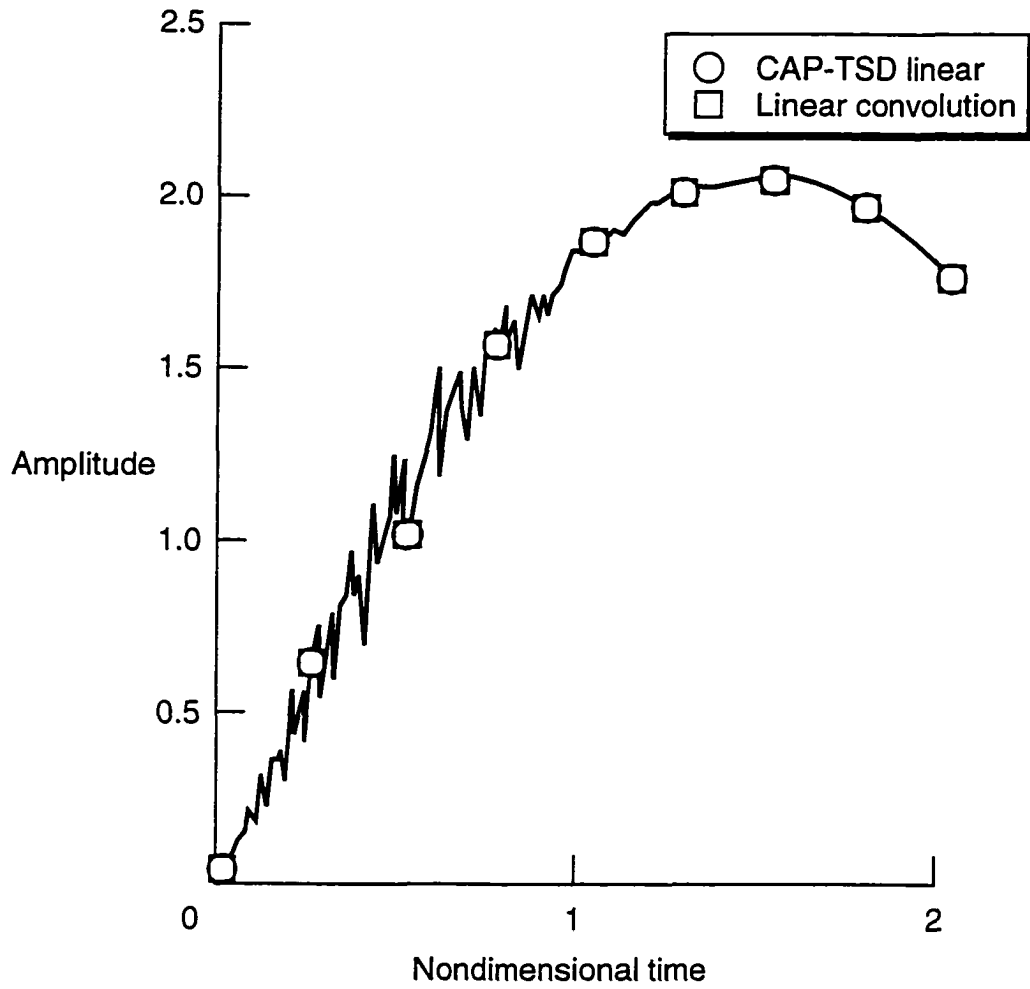


Figure 41 Enlarged view of initial portion of Figure 40.

### *Summary for Linear CAP-TSD Results*

These results demonstrate the relationship between a unit sample response and a unit step response for a linear unsteady aerodynamic system and the correct application of these functions. Also, it is important to realize that the unit sample response, when convolved with a step input results in the steady-state solution. Therefore, unit sample responses can be used for predicting the linear steady and unsteady responses of a system.

These results also demonstrate the validity of the concept of an aerodynamic impulse response and the correct numerical identification and implementation of this function for a linear aerodynamic system. The pitch results validate the interpretation of the downwash function as a two-input function. If only one convolution had been performed with the unit sample response due to the  $u(t)$  term (the single-input perspective), it would not have matched the CAP-TSD results. These results apply to the nonlinear case as well where the savings in computational cost and time are of greater significance and value, as is discussed in the next section.

### *Nonlinear CAP-TSD - Plunge*

The nonlinear TSD equation is solved for the same rectangular wing used for the linear analyses but now with a NACA0012 airfoil section (symmetric airfoil thickness). Results were computed for a Mach number of 0.9 and using a time step of 0.001. At zero degrees angle of attack, this symmetric airfoil induces a zero net normal force. Therefore, for this case, the first term of the Volterra series, the  $h_0$  term, is zero.

Figure 42 is the first-order kernel for this configuration in plunge. Comparison with the linear kernel (Fig. 30) shows only slight differences. These slight differences, however, are sufficient to differentiate between the purely linear response and the “linearized” portion of the nonlinear response. Figure 43 is a comparison of nonlinear CAP-TSD plunge responses, due to exponential pulse inputs at three different amplitudes, with the convolved results of the first-order kernel with those three inputs. The three amplitudes, normalized

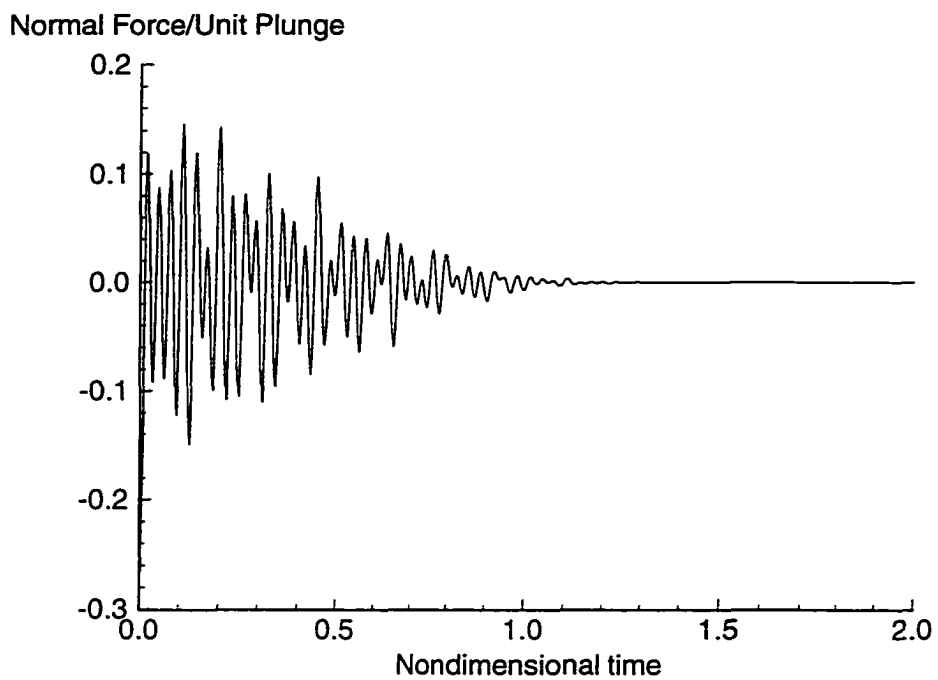


Figure 42 First-order kernel in plunge, nonlinear CAP-TSD.

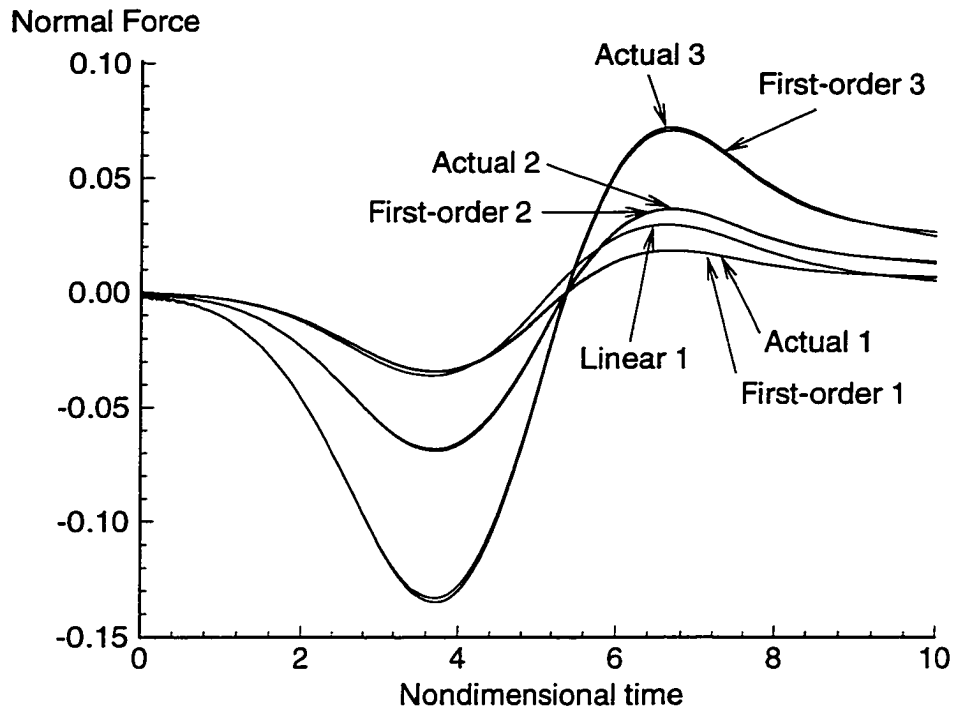


Figure 43 Comparison of actual nonlinear and first-order convolved responses for three different plunge motions; linear response for first is also presented.

to the airfoil chord length, are  $D_0 = 0.064$ ,  $0.128$ , and  $0.25$ . The linear CAP-TSD result for the first, and smallest, amplitude ( $D_0 = 0.064$ ) is also shown for comparison. At this amplitude there is a noticeable difference between the linear and nonlinear CAP-TSD solutions. Notice, however, that the first-order kernel accurately predicts the nonlinear plunge responses with a slight deterioration as amplitude is increased.

A comparison of the computational costs associated with ten of these types of responses is presented in Table 2. Most of the cost of the first-order convolution is the initial identification part of the process since each convolution itself took only 75 seconds on a workstation. As the need for the response of the system to arbitrary inputs (motions) increases, the cost of the method decreases because once the unit sample responses are obtained, the CFD code need not be re-executed.

The five components of the second-order kernel for the plunge mode are presented in Figure 44. Their relatively small size is an indication that for this configuration, for plunge motions at this condition, the first-order kernel is sufficient to adequately predict the nonlinear plunge responses for the amplitudes investigated. This is consistent with the results of Figure 43.

Figure 45 is the combined first-order kernel for pitch due to the combined input. This combined first-order kernel was computed as described in the previous chapter. It is a well-behaved kernel and its computation posed no numerical difficulties. Figure 46 is a comparison of the actual linear and nonlinear CAP-TSD solutions for the same wing undergoing an arbitrary pitching motion; the single, temporal response (from deconvolution); the response obtained by the convolution of the combined linear kernel with the single, temporal input; and the response obtained by the convolution of the combined first-order kernel with the single, temporal input. The single, temporal input was obtained using a linear deconvolution technique described in an earlier section of this dissertation. The comparison for the linear solutions is exact, as expected. The comparison for the nonlinear case is reasonable, but for this mode at this amplitude, the

TABLE 2

## COMPUTATIONAL COST COMPARISONS: FIRST-ORDER RESPONSES

<u>CAP-TSD</u>			<u>FIRST-ORDER RESPONSE</u>		
<u>Run #</u>	<u>Cost</u>		<u>Run #</u>	<u>Cost</u>	
	<u>CPU s</u>	<u>Turnaround</u>		<u>CPU s</u>	<u>Turnaround</u>
1	3800	1.5hr - 1 day	ID <i>i</i>	1000	0.5hr - 1 day
2	3800	1.5hr - 1 day	ID <i>ii</i>	1000	0.5hr - 1 day
3	"	"	ID <i>iii</i>	1000	0.5hr - 1 day
4	"	"	ID <i>iv</i>	1000	0.5hr - 1 day
5	"	"	1	15	15 sec
...			...		

For 10 runs, total costs are:

38,000	15hrs (mininum)	4150	2.04hrs (min)
	10 days (max)		4 days,150s(max)



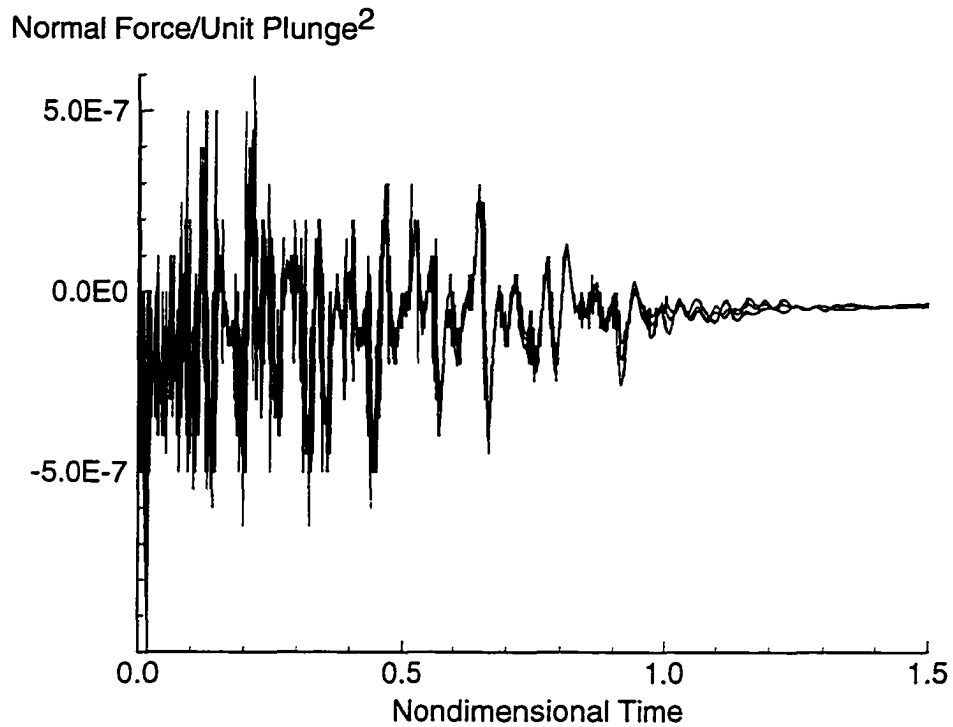


Figure 44 Four components of the plunge second-order kernel, nonlinear CAP-TSD,  $M=0.9$ ,  $DT=0.001$ .

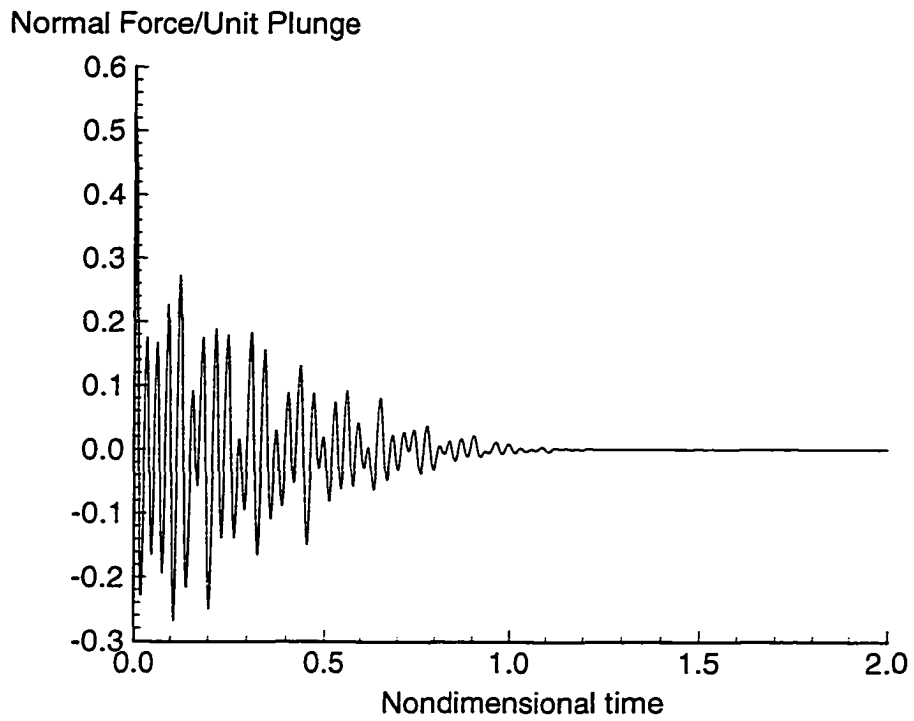


Figure 45 Combined pitch first-order kernel, nonlinear CAP-TSD.

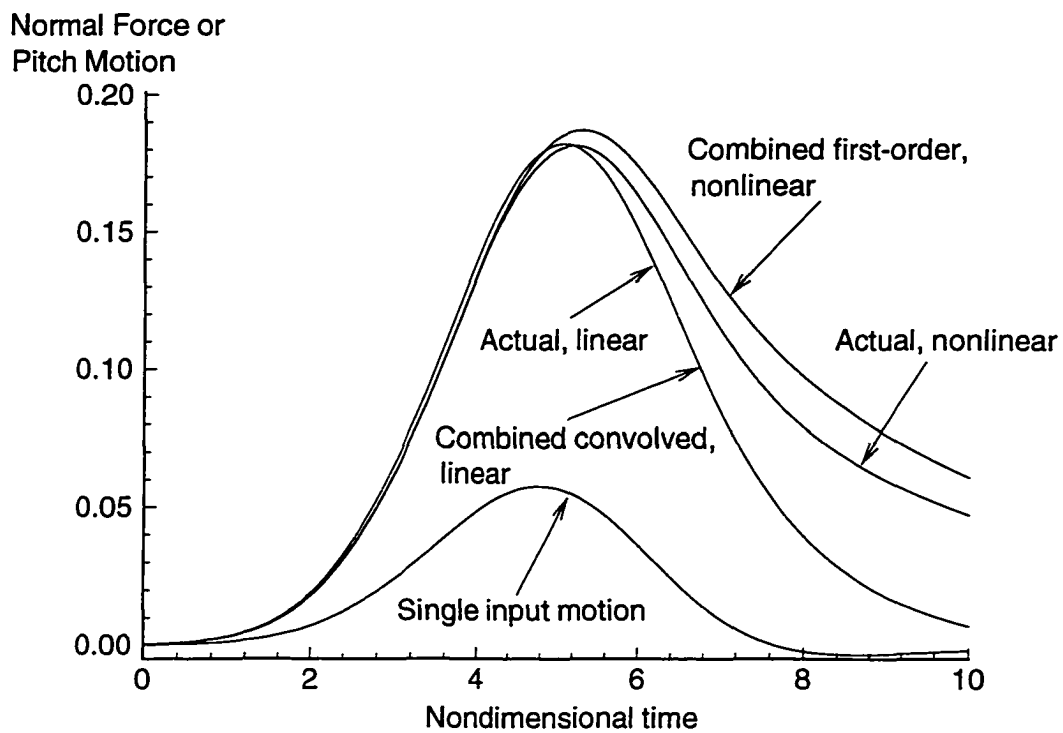


Figure 46 Single pitching motion (deconvolution) and comparison of linear and nonlinear, actual and convolved responses.

second-order components are needed. The computational efficiency, however, has been significantly improved. The reason being that instead of computing two responses per mode (one for each term of the downwash function, Eq. (12)), only one response per mode is needed. In addition, the identification technique, as applied to the downwash function, is now mathematically correct for nonlinear responses.

A selected number of components of the second-order kernel for pitch are presented in Figure 47. These are clearly larger than any of the second-order kernels presented thus far, an indication of the greater nonlinearity induced by this motion.

Normal Force/Unit Pitch<sup>2</sup>

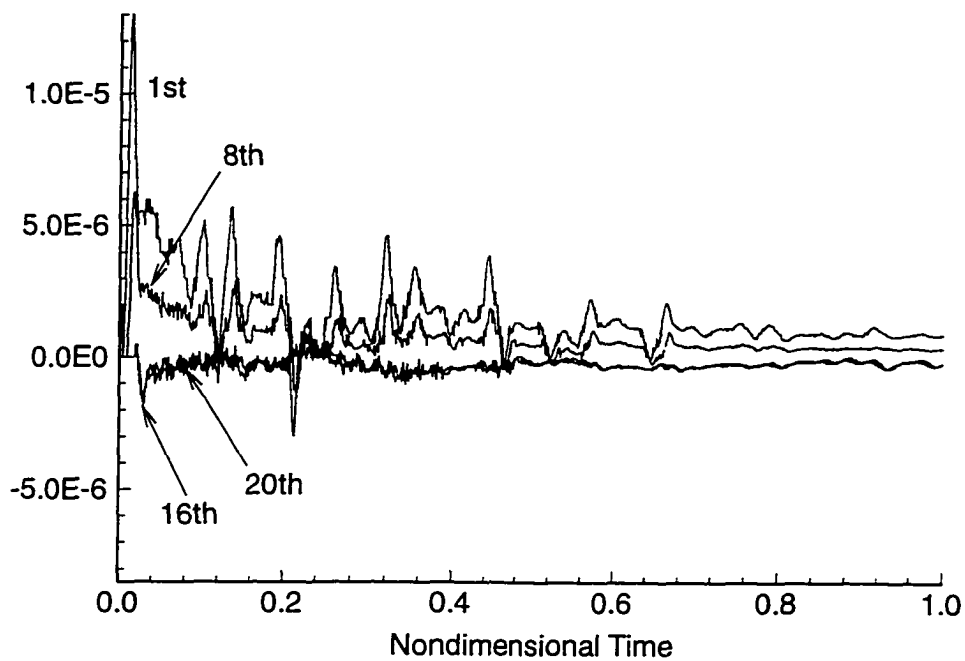


Figure 47 Four selected components of the second-order kernel for the combined pitch motion, nonlinear CAP-TSD,  $M=0.9$ ,  $DT=0.001$ .

## CHAPTER 7

### RESULTS USING THE CFL3D CODE

The CFL3D code<sup>71</sup> solves the time-dependent, Reynolds-averaged Navier-Stokes equations in conservation law form. Upwind-biasing is used for the pressure and convective terms, central differencing is used for the shear stress and heat transfer terms, and the spatial discretization is based on a semi-discrete finite-volume concept. Accelerated convergence can be achieved using multigrid and mesh sequencing capabilities and implicit time-stepping is used. The code provides several turbulence models, including the Spalart-Allmaras turbulence model used in the subsequent analyses.

#### *Results for RAE Airfoil*

Navier-Stokes results (CFL3D version 5.0) for a dense-grid RAE airfoil<sup>71</sup> (Figure 48) with the Spalart-Allmaras turbulence model undergoing plunge at  $M=0.75$  and a zero degree angle of attack were computed at a time step of 0.001. At this Mach number and zero degrees angle of attack, this non-symmetric airfoil induces a net normal force coefficient of 0.2953. When generating the first- and second-order kernels for this system, this “DC offset” has to be subtracted from the kernel computations. The response to a particular input is computed using the convolution procedures and then the  $h_0$  ( $= 0.2953$ ) of the Volterra series is added back to obtain the total response.

This code has several computational options, depending on the type of analysis desired. Accelerated convergence can be obtained using the sub-iteration and multigrid capabilities<sup>72</sup>. In addition, a method is available that diagonalizes the governing matrices (diagonally dominant) based on the spectral radius. Experimentation with these techniques revealed the numerical method that resulted in the most accurate Volterra kernels.

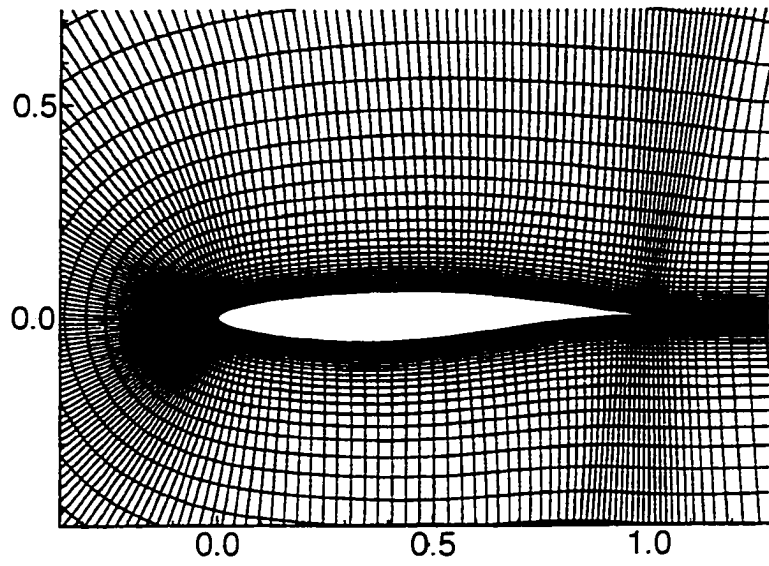


Figure 48 RAE 2822 airfoil grid, from Ref. 71.

Figure 49 is a comparison of the first-order kernel, with and without diagonalization, using the first-order, time-accurate option. As can be seen, both kernels go to zero very quickly, in less than 30 time steps. Both kernels exhibit the square-integrable nature that is characteristic of impulse responses but the diagonalized kernel appears somewhat attenuated compared to the non-diagonalized kernel. Diagonalization is a clear advantage when accelerated convergence to steady state is desired. However, recall that the function that needs to be identified is a memory function that contains the entire frequency range of the system. The diagonalized kernel appears to be a function that is optimized for steady-state results. This is consistent with a warning in the User's Manual regarding the use of this option for unsteady analyses. Therefore, at least for results similar to those presented in this chapter, it is recommended that the full matrix solution (non-diagonalization) be used when identifying Volterra kernels with this CFD code.

Figure 50 is a comparison of the first-order kernel without diagonalization, with and without multigrid capability. The nature of a multigrid scheme is to accelerate convergence by filtering out high- and low-frequency numerical error by using grids of varying coarseness. For the cases investigated in this chapter, this filtering tended to attenuate the memory of the system, similar to the diagonalization scheme. This effect is clear in Figure 50 where the multigrid result very quickly converges on the steady state solution. But, again, since the goal in identifying Volterra kernels is to excite as much of the system's memory as possible, it is recommended that kernels be identified without multigrid. A method might exist that uses multigrid to optimize the frequency content of a Volterra kernel. That is, this optimal Volterra kernel would contain mostly physical frequencies and very little or no numerical frequencies. But the computational cost associated with that method may not justify its application. As will be seen, the Volterra kernel identified without multigrid, for the RAE airfoil model, is highly accurate and computed directly at a minimal CPU cost and a fast turnaround time.

Figure 51 is a comparison of the non-diagonalized, no multigrid first-order kernel



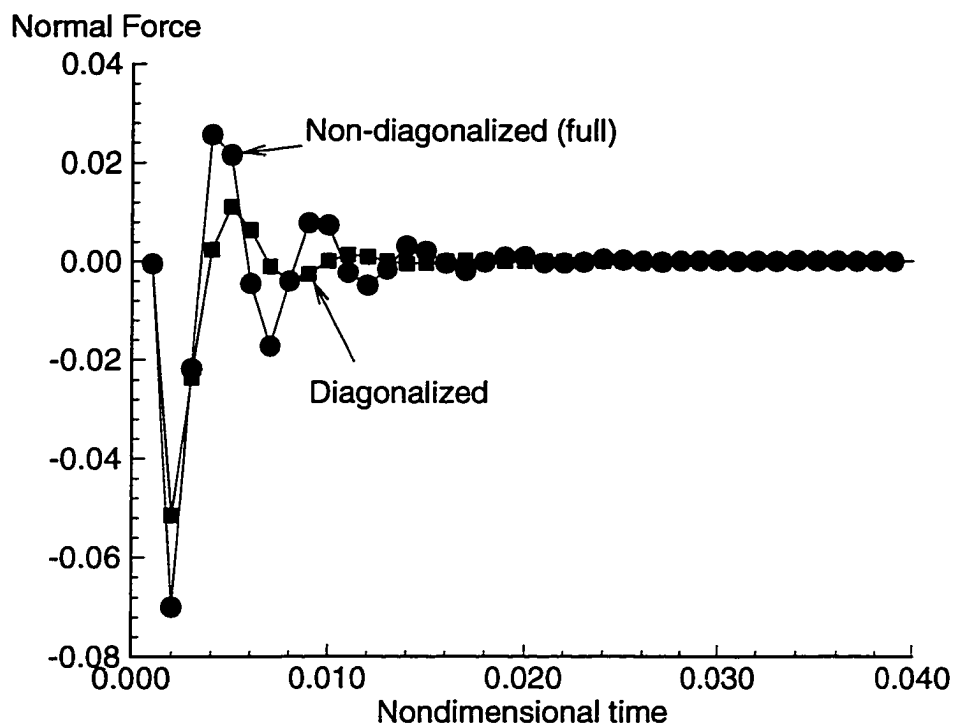


Figure 49 First-order kernel for RAE airfoil in plunge, first-order accurate in time, with and without diagonalization;  $M=0.75$ ,  $\alpha=0.0$ .

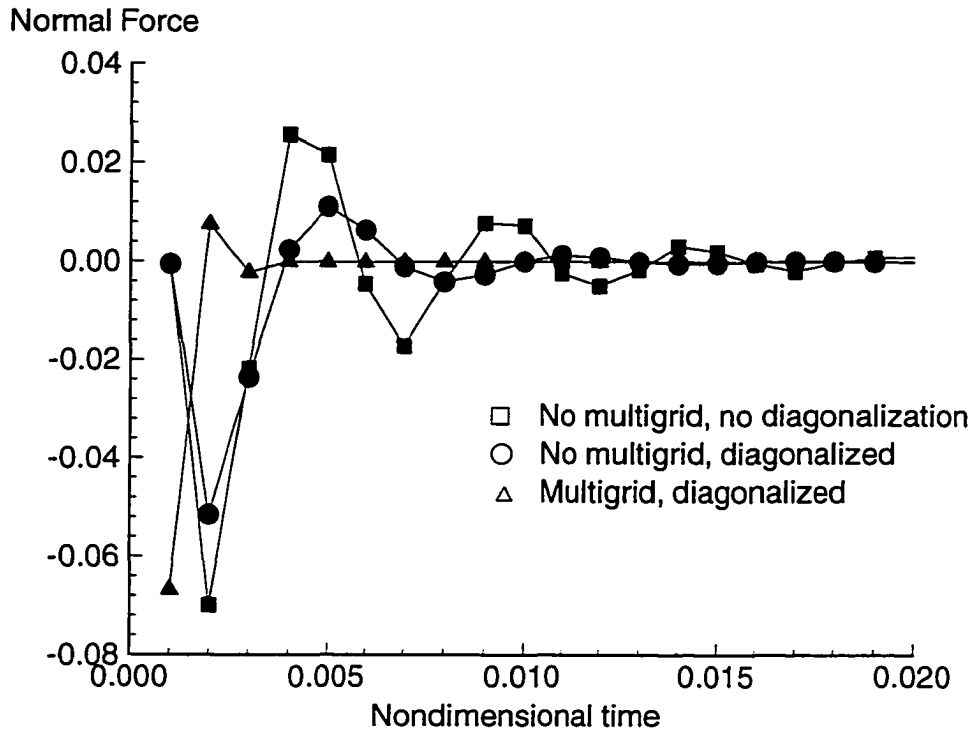


Figure 50 First-order kernel for RAE airfoil in plunge, first-order accurate in time, with and without diagonalization, with and without multigrid;  $M=0.75$ ,  $\alpha=0.0$ .

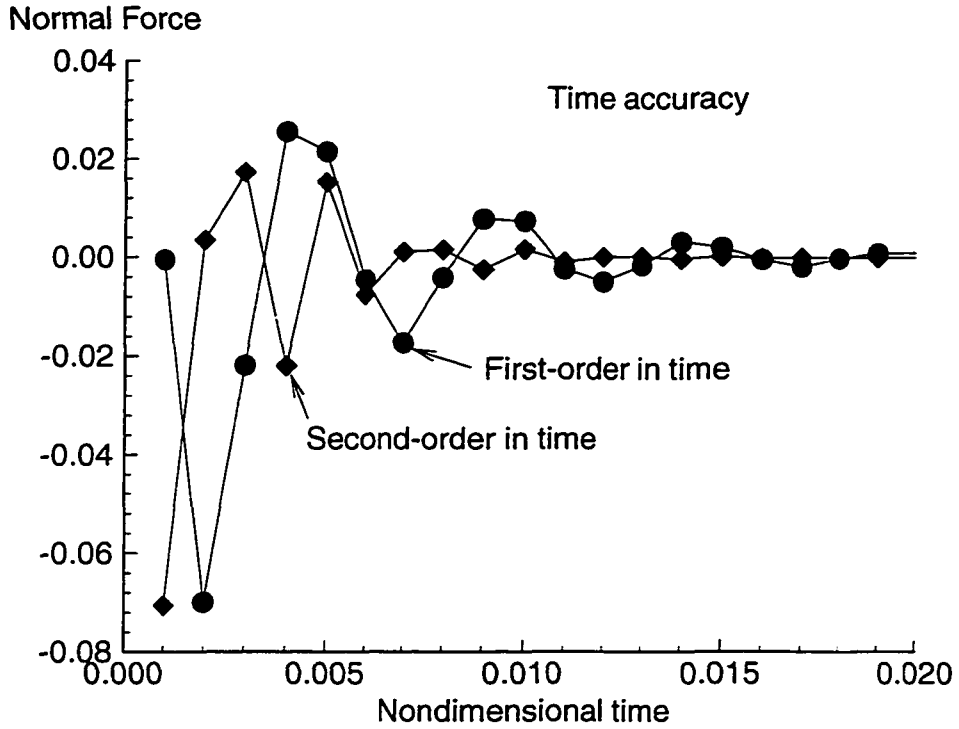


Figure 51 First-order kernel for RAE airfoil in plunge, non-diagonalized, no multigrid,  $M=0.75$ ,  $\alpha=0.0$ .

computed using first-order time accuracy and second-order time accuracy. This first- and second-order accuracy refers to the error associated with different time-integration schemes, not to the order of the kernels. There exist clear differences between these two kernels, an indication that second-order accuracy should be used in order to keep numerical error down to a minimum.

Finally, Figure 52 is a comparison of non-diagonalized, no-multigrid, second-order accurate-in-time first-order kernels for two different identification input amplitudes. Recall that the first-order kernel is identified using a response due to a primary amplitude (1.0, for example) and a second response due to double that amplitude (2.0, correspondingly). This is evident in Equation (10). An important question is “What is the effect of varying these amplitudes on the identification of the kernels and on their predictive capability?” The small-amplitude kernel of Figure 52 was identified using the primary input amplitude of 0.01 and a corresponding amplitude of 0.02. The first-order convolved response, using this kernel, was multiplied by 100 to compensate for the primary input amplitude of 0.01, yielding the final response for this kernel. This input excitation was also used for the kernels in the previous figures. The large-amplitude kernel shown in Figure 52 was identified using the primary input amplitude of 0.1 and a corresponding amplitude of 0.2. The first-order convolved response, due to this kernel, was multiplied by 10 to compensate for the primary input amplitude of 0.1, yielding the final response for this kernel.

The correlation between these two kernels is not exactly linear. That is, one kernel is not exactly ten times the other, indicating a deviation from linearity or some measure of nonlinearity. In order to evaluate the accuracy of each of these kernels, several sinusoidal plunging motions at different amplitudes were computed using CFL3D and used for comparison with convolved results using each kernel. The three amplitudes, as a fraction of chord length, are 0.002, 0.005, and 0.01. Figure 53 is a comparison of these plunging motions with the convolved results using the small-amplitude first-order kernel. As can be seen, the accuracy of this particular kernel diminishes as amplitude is increased. Figure 54

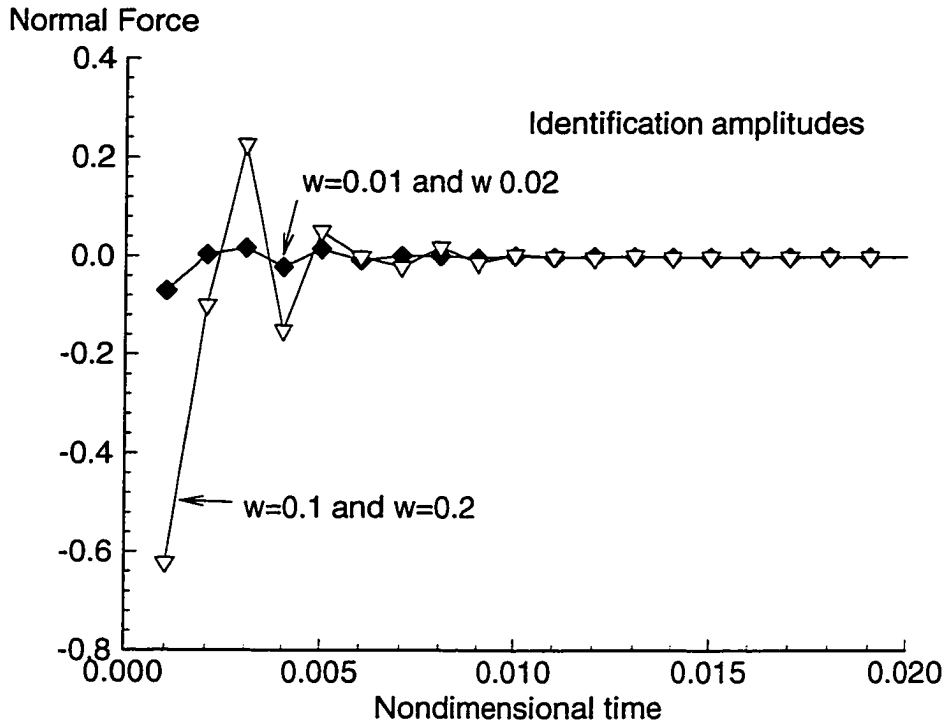


Figure 52 First-order kernel for RAE airfoil in plunge, non-diagonalized, no multigrid, effect of ID amplitudes.

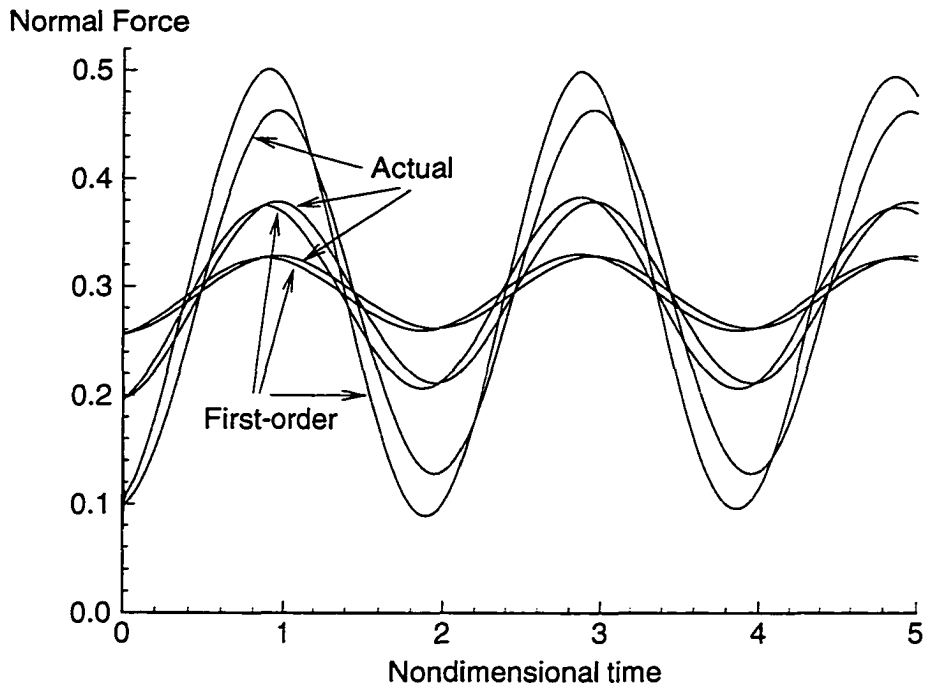


Figure 53 Comparison of actual nonlinear responses and first-order convolved responses (small amplitude, 1st-order in time) for three different plunge motions.

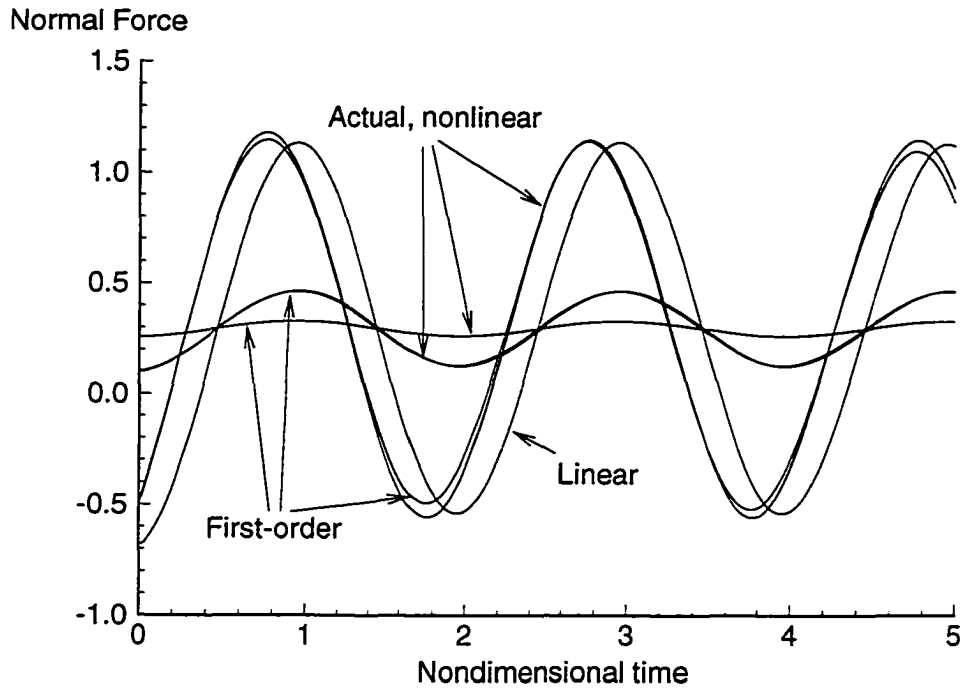


Figure 54 Comparison of actual nonlinear and first-order (2nd-order accuracy, large amp.) responses for three different plunge motions and a linear response for the largest plunge motion.

is a comparison of two nonlinear sinusoidal plunge responses from CFL3D (actual, nonlinear), one linear plunge response, and the convolved responses using the large-amplitude first-order kernel. The smaller, nonlinear actual response corresponds to a plunge amplitude of 0.01. This response is the largest of the three responses in Figure 53. The larger, nonlinear actual response corresponds to a plunge amplitude of 0.05. The linear result shown in Figure 54 is the linear response due to a plunge amplitude of 0.05. Since the CFL3D code cannot be used directly to compute a linear response, the linear response of Figure 54 was computed by multiplying the smaller nonlinear response (due to plunge amplitude of 0.01) by 5.0.

Clearly, Figure 54 shows improved accuracy of the large-amplitude first-order kernel over that of the small-amplitude first-order kernel (Figure 53), even for a larger range of amplitudes. These results indicate that improved accuracy can be obtained over a larger amplitude range if the input amplitude used to identify the first-order kernel is chosen appropriately. One possible approach for determining this identification amplitude is to base it on 1) physical considerations and 2) code execution limitations. If the CFD code executes properly for the largest input amplitude of interest (a sinusoidal input, for example) and the input amplitude is physically realistic, then the accuracy and effectiveness of the first- and second-order kernels, identified within this amplitude range, will be improved.

The first five components of the second-order kernel for this airfoil in plunge are presented in Figure 55. The input amplitude used to identify these components of the second-order kernel was 0.10, consistent with the large-amplitude first-order kernel of Figure 54. Even so, the first component of the second-order kernel is an order of magnitude smaller than the large-amplitude first-order kernel (Figure 54). The remaining components approach zero rather quickly, an indication that, for this condition and for this motion (plunge), the first-order kernel may be sufficient for predicting nonlinear plunge responses.



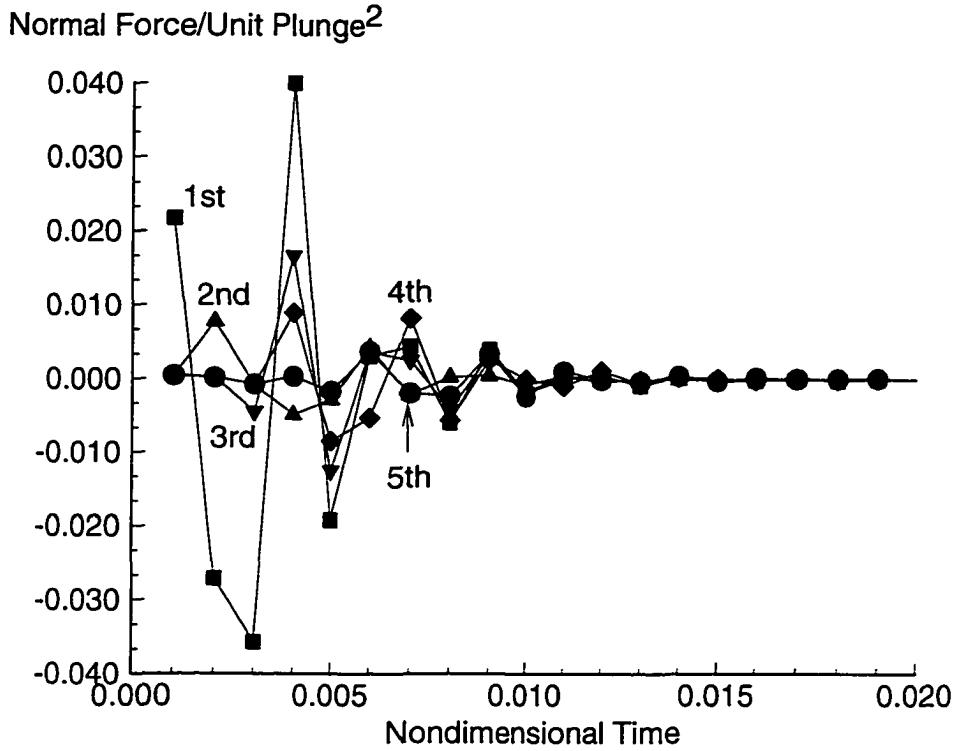


Figure 55 First five components of the second-order kernel for the RAE airfoil in plunge, non-diagonalized, no multigrid, second-order accurate in time, largest ID amplitudes, CFL3D,  $M=0.75$ ,  $DT=0.001$ .

It is also interesting to note that the components shown in Figure 55 go to zero in less than 15 time steps. Because both the first- and second-order kernels for this CFD model go to zero very quickly, computation of these kernels is obtained extremely fast. In fact, the author was able to completely avoid the high turnaround time on a supercomputer by submitting these jobs on the DEBUG queue. The DEBUG queue is for the execution of small to large CPU memory jobs but constrained to a very small amount of execution time (time steps) for the purposes of code debugging. The average turnaround time on a standard queue can be as high as a day to a day-and-a-half whereas the DEBUG queue executes almost immediately. As a result, CFL3D jobs submitted to the DEBUG queue, for kernel identification, executed within minutes or even seconds.

The computational turnaround time associated with a CFD code consists of time spent waiting for the job to execute (time in the queue) in addition to the execution time itself.

It is also interesting to discuss the differences between the first-order kernels obtained using the CAP-TSD code and those obtained using the CFL3D code. Although the results are for different configurations at different conditions, the time constant associated with each is indicative of the numerical algorithm and equation level. Whereas the CAP-TSD results take longer to “die out”, the CFL3D results go to zero very quickly. This could be an indication of the dissipative nature of each of the codes. Additional research in this area could be of significant interest to CFD code developers.

The preferred identification technique for the first- and second-order kernels using the CFL3D code, therefore, consists of using second-order accuracy (in addition to the small time step), no multigrid, no diagonalization, and a large kernel identification amplitude.

These results demonstrate the applicability of discrete-time, nonlinear, unit sample responses at the NS equation level, as discussed in the beginning of the dissertation. A clear understanding of time-invariant impulse responses and time-invariant convolution, as presented in this dissertation and Appendix, provides additional verification of the time-invariant nature of the NS equations. That is, if the NS equations were time varying, the

convolved results of Figures 53 and 54 would not have been possible.

### *Computational Efficiency*

The cost of each sinusoidal plunge CFL3D response was about 2,000 CPU seconds. These responses were for a particular frequency of motion that required a particular length of time for a certain number of cycles. The DEBUG queue, obviously, could not be used for these analyses due to its strict time limitations. Instead, the standard job submittal queue had to be used, resulting in large turnaround times. The current procedure for using CFD codes, such as CFL3D, results in large turnaround times due to: 1) the time spent waiting for job execution in the queue and 2) the time spent in actual execution.

On the other hand, results from this dissertation show that the application of the Volterra theory to CFD codes reduces computational turnaround time significantly. The actual execution time (CPU) is reduced because repeated execution of the CFD code is reduced or eliminated. The time spent waiting in the queue, for execution of kernel identification analyses, is also significantly reduced from days to seconds due to the nature of the Volterra kernels and the identification technique that is used.

In terms of actual costs for the RAE airfoil using the CFL3D code, the cost of the first-order kernel identification was 400 CPU seconds; 200 for each of the two required responses. Because the kernel goes to zero in less than 100 time steps, execution of these jobs was performed in the DEBUG queue with a turnaround time of seconds. The cost of each convolution, for the plunge motions investigated, was 30 seconds on a workstation. Identification of the first five components of the second-order kernel was performed on the DEBUG queue as well. As a result, these five components were completely identified within minutes.

A concise mathematical model, consisting of a first-order and a second-order discrete-time Volterra kernel, has been identified. This model can be used to accurately predict the nonlinear plunge response of the CFL3D/RAE airfoil model, due to any arbitrary plunge

motion, over a wide range of plunge amplitudes. The range of valid plunge amplitudes for this model is greater than the range associated with “small”, or linear, responses. Most importantly, these nonlinear responses can be computed on a workstation, completely sidestepping the costly (time and CPU) re-execution of the CFD code<sup>73</sup>.

## CONCLUSIONS

The mathematically-correct and numerically-accurate identification of linear and nonlinear, discrete-time aerodynamic impulse responses, based on the Volterra theory of nonlinear systems, was presented. Important differences between continuous-time and discrete-time concepts, critical to the successful identification of these aerodynamic functions, were described.

For the linear case, the aerodynamic impulse response functions were used to reproduce exactly the responses of a linearized three-dimensional aeroelastic CFD model, to arbitrary aeroelastic input motions, at a fraction of the computational cost and time. It was shown that the aerodynamic response to step (steady), sinusoidal, and arbitrary motions can all be computed from an aerodynamic impulse response. This establishes the aerodynamic impulse response function as the most fundamental aerodynamic function that can be extracted from a discrete-time, aerodynamic system.

For the nonlinear case, the existence, identification, and application of nonlinear, discrete-time, aerodynamic impulse responses was presented. Applications of the discrete-time Volterra theory to the nonlinear viscous Burger's equation revealed the existence of well-behaved first- and second-order impulse response functions. The method was then applied to nonlinear aeroelastic CFD models using the CAP-TSD (TSD) and CFL3D (Navier-Stokes) codes. Results demonstrate the existence of these functions for complex, two- and three-dimensional CFD models. Applications based on predicting the nonlinear responses of the CFD models demonstrate the accuracy and significant computational efficiency of these functions. Computational turnaround time for the range of nonlinear responses investigated was reduced from days to minutes. The method sidesteps the costly and time-consuming re-execution of the CFD code as inputs are varied.

These results represent a new perspective on linear and nonlinear, steady and unsteady computational aerodynamics. Modern textbooks on aeroelasticity and unsteady aerodynamics do not adequately address discrete-time aerodynamic impulse responses. The work presented in this dissertation will, hopefully, have an impact on our understanding of fundamental computational aerodynamic principles, the teaching of these ideas in appropriate courses, and, most importantly, on the efficient use of CFD codes in analyses where the information from these codes is needed.

## AREAS OF FUTURE RESEARCH

Additional research, related to the research presented in this dissertation, is needed in the following areas:

- CFD/Aerodynamics/Aeroelasticity

- Evaluation of the aerodynamic Volterra kernels as numerical diagnostic tools to address dissipation and dispersion issues
  - Effect of various levels of physical modeling on the aerodynamic Volterra kernels (such as viscosity, shocks, and different turbulence models)
  - Additional investigations regarding multigrid
  - Efficient computation of nonlinear, steady and unsteady stability derivatives using aerodynamic Volterra kernels
  - Identification of higher-order kernels (third-order, and so on)
  - Determination of the equilibrium points for a given Navier-Stokes CFD model
  - Experimental identification of aerodynamic Volterra kernels
  - Frequency-domain Volterra theory related to nonlinear aerodynamics
  - Couple aerodynamic kernels with structural model to obtain aeroelastic transients
  - Apply Volterra theory to the modeling of nonlinear structures for use in aeroelasticity
- Discrete-time Systems and Control
- Bilinear aerodynamic state-space models from Volterra kernels
  - Application of method to other nonlinear systems
  - Nonlinear aeroservoelasticity
  - Application of Volterra theory to the determination of nonlinear maximized gust loads and alleviation methods

- Optimization and design using Volterra kernels
- Accelerated neural network training using Volterra kernels
- Effect of discretization on the identification of the Volterra kernels



## APPENDIX

### Fundamental Aspects of the Volterra Theory of Nonlinear Systems

The body of literature that addresses the Volterra theory of nonlinear systems (sometimes referred to as the Volterra-Wiener theory) is quite large. This dissertation and Appendix identify and discuss most of the major references on this topic. Additional references can be found within the cited references and textbooks<sup>25,43,58</sup>. The frequency-domain version of the Volterra series is a significant area of interest that was not addressed in this dissertation. References regarding the frequency-domain theory, however, are provided in the Introduction. Reference 59 is an excellent source of information on this topic.

However, in order to provide the reader with some of the fundamentals of the time-domain theory, this Appendix is included. This Appendix addresses the following areas: 1) Mathematical Classification of Systems, 2) Impulse Response, Convolution, and Memory, 3) Functional Origins and Interpretation of the Volterra Kernels and, 4) Convergence Issues. The figures are meant to be of a qualitative nature in order to enhance the explanation of fundamental concepts.

#### *Mathematical Classification of Systems*

Application of system identification techniques (linear or nonlinear) requires an understanding of the mathematical nature of the system under investigation. For example, the method used for the identification of the impulse response of a linear system, and its subsequent use in an appropriate convolution scheme, varies depending on whether the

system is time invariant or time varying. Likewise, the proper identification of the Volterra kernels of a nonlinear system, and their subsequent application, depends on whether the nonlinear system is time invariant or time varying. This is discussed in Chapter 4 but is discussed in greater detail in this Appendix.

The mathematical system classifications that are important to the application of the Volterra theory, and some examples of each type of system, are presented in Figure A1. The focus of this dissertation is on time-invariant (TI), linear and nonlinear systems with memory. Note that included in this classification are the Navier-Stokes equations, as discussed in Chapter 5. The Van der Pol equation, which exhibits limit cycle oscillations (LCO), also belongs to this category. For rigorous details, see Khalil<sup>44</sup>. The application of the Volterra series to time-varying (TV) nonlinear systems is discussed in Ref. 46 as well as other references.

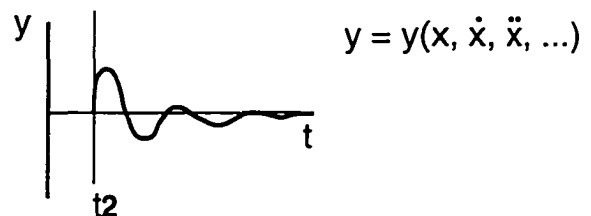
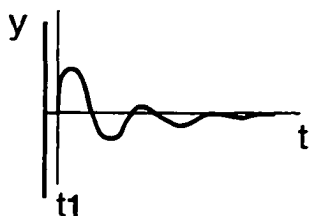
	<b>Time Invariant</b>		<b>Time Varying</b>	
	Linear	Nonlinear	Linear	Nonlinear
<b>Zero Memory</b>	$y = mx + b$	$y=x^2$ , <b>Saturation,</b> <b>Deadband</b>	$y = m(t)x + b$	<b>Saturation,</b> <b>Deadband</b> <b>as f(t)</b>
<b>Memory</b>	$\dot{x} = Ax + Bu$	<b>Van der Pol,</b> <b>Duffing and</b> <b>N-S Eqs</b>	$\dot{x} = A(t)x + B(t)u$	<b>Mathieu</b>

Figure A1 Mathematical system classifications and some examples.

A time-invariant system, also referred to as an autonomous or stationary system, is a system with the characteristic that its response to an input is independent of the time of application of the input. A time-invariant system is therefore a “shift invariant” system. That is, shifting of the input in time yields the same response, only shifted in time.

Inspection of the governing equations of the system provides the necessary information for classifying the system as TI or TV. The governing equations of a time-invariant system are not explicit functions of time. The governing equations of a time-varying system, on the other hand, are explicit functions of time. A time-varying system is also referred to as a non-autonomous or non-stationary system. Figure A2 is a graphical depiction of the difference between a time-invariant and a time-varying system with  $u(t)$  as an input with a time of application that is shifted in time.

- Time Invariant -->  $y(u(t_1)) = y(u(t_2))$  (Shift Invariant)



- Time Varying -->  $y(u(t_1)) \neq y(u(t_2))$

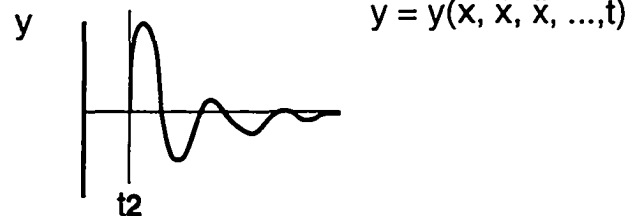
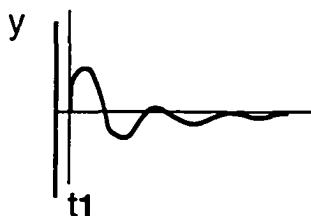


Figure A2 Response characteristics of time-invariant and time-varying systems.

Once the temporal classification of the system is defined (TI or TV), the memory classification of the system (with memory or zero memory) can be determined. Because the concept of the memory of a system is directly related to the impulse response of the system, and, subsequently, to its application in a convolution scheme, the impulse response function and convolution are briefly reviewed. A thorough understanding of the Volterra theory requires a thorough understanding of these concepts. These concepts are described for both continuous-time and discrete-time systems so that similarities and differences can be emphasized. Also, for simplicity, single-input-single-output (SISO) systems are assumed without loss of generality.

### *Impulse Response, Convolution, and Memory*

It is well-known that the unit impulse response of a continuous-time, linear time-invariant (CT-LTI) system can be obtained by applying a unit impulse input to the system. This is shown schematically in Figure A3 with the unit impulse,  $\delta(t)$ , defined as shown.

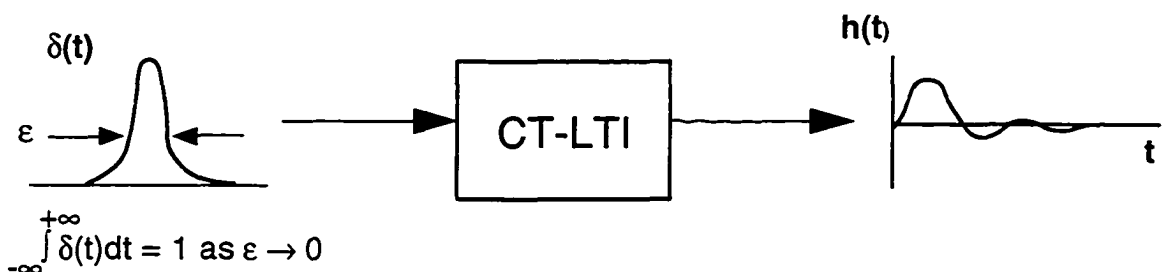


Figure A3 Application of a continuous-time unit impulse function to a continuous-time linear time-invariant system to yield the continuous-time unit impulse response function.

Once the linear unit impulse response function is computed, the response of the linear time-invariant system to any input can be obtained via convolution. Because the system is

time invariant, the impulse response of the system is the same regardless of the time at which the unit impulse is applied. Shifting the time at which the unit impulse is applied simply shifts the (same) unit impulse response by the corresponding time shift. Shifting the time at which the unit impulse is applied to a linear time-varying system, however, yields different (and, therefore, multiple) impulse responses. A linear time-varying system is, therefore, not shift invariant. As a result, the convolution scheme used for a time-invariant system is different from the convolution scheme used for a time-varying system. The focus of this dissertation (and Appendix) is on time-invariant systems and the convolution technique appropriate for time-invariant systems.

The traditional approach to convolution is to “flip” one of the functions involved in the convolution and then perform the convolution. An alternative way to visualize time-invariant convolution is presented in Figure A4. Figure A4 shows how convolution can be viewed as a three-part process: 1) scaling: the entire unit impulse response,  $h(t)$ , is scaled (multiplied) by the value of the input at a particular point in time,  $u(t_0)$ , for example, 2) shifting: as each scaled response is computed, it is shifted so that it corresponds to the point in time when the particular value of the input was applied, and 3) addition: all the scaled and shifted responses are added to yield the total response of the system.

It is clear that the impulse response of a linear system is, in fact, the memory of that system. Convolution simply scales and shifts that memory function, based on some arbitrary input, and combines all the scaled and shifted functions to yield the total response of the system. The shift invariance of the system justifies the use of one and the same memory function for the convolution process described (scaling, shifting, and adding).

The next question is “How can the continuous-time unit impulse, shown in Figure A2,

● Convolution

$$y(t) = \int_0^t h(t - \tau) u(\tau) d\tau$$

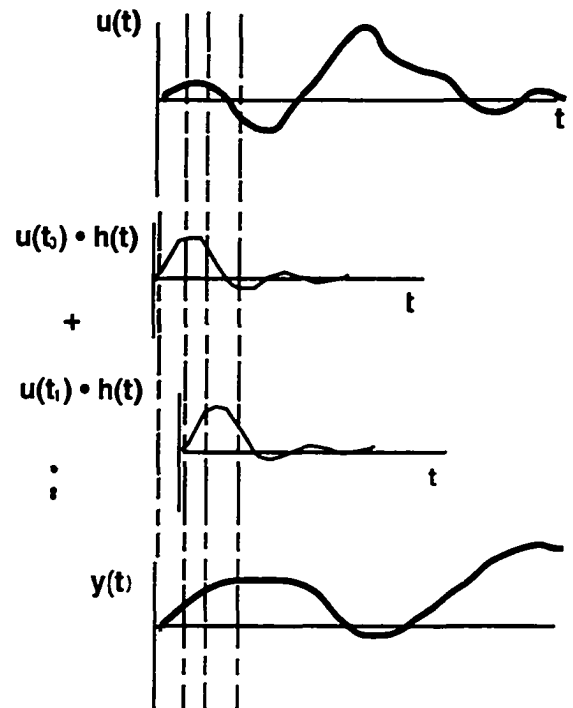


Figure A4 Convolution as a three-part process: scaling, shifting, and summation of memory function (impulse response).

be applied to a problem of computational interest such as a discrete-time aerodynamic system, for example?" According to the literature cited in the Introduction to this dissertation, the answer to this question is mixed, at best. The definition of the continuous-time unit impulse function introduces a certain amount of vagueness when considered for numerical (discrete-time) applications. One of the contributions of this dissertation is the realization that classical linear aerodynamic theories and modern nonlinear computational theories can be viewed from a discrete-time perspective, resulting in significant computational efficiency. The transition from continuous-time to discrete-time is described in the following paragraphs.

Instead of applying a continuous-time function to a discrete-time model, the solution to this problem is to apply the discrete-time unit impulse (unit pulse) to the discrete-time model. The discrete-time unit impulse response, known as the unit sample response in the

fields of digital signal processing and digital filter design, has a simple definition that is suitable for direct application to discrete-time models. Application of the unit pulse to a discrete-time, linear time-invariant (DT-LTI) system, yielding that system's unit sample response, is shown schematically in Figure A5. Also shown in Figure A5 is the equation for discrete-time convolution which involves a straightforward summation.

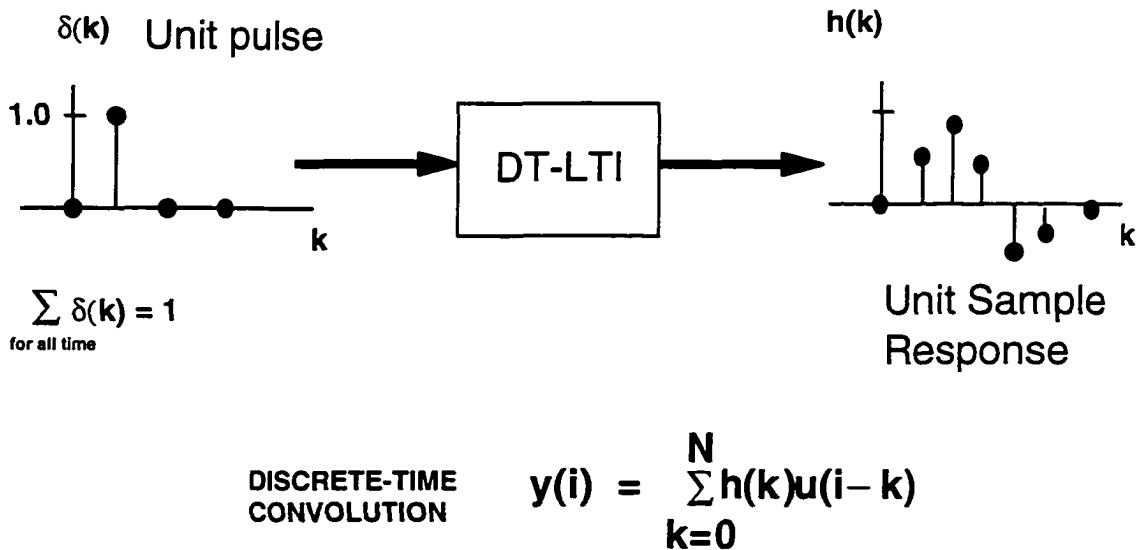


Figure A5 Application of the discrete-time unit pulse to a discrete-time linear time-invariant (DT-LTI) system, yielding the system's unit sample response. The unit sample response is then used in the discrete-time convolution process.

The continuous-time unit impulse response and the discrete-time unit sample response share similar properties as discussed in Chapter 2 and Oppenheim and Schaffer<sup>38</sup>. In the limit, the unit sample response approaches the unit impulse response and so discretization issues need to be understood in the identification and application of the unit sample response. The convolution process for a discrete-time system involves the summation of sequences rather than the integration of functions, a computationally simpler task. Clearly,

for a discrete-time system, such as a CFD code, the unit sample response is the function that needs to be identified and applied in a discrete-time convolution process.

For a nonlinear system, the concepts of memory and convolution can be expanded to include higher-order memory functions and corresponding higher-order convolution processes. This is discussed in the next section.

### *Functional Origins and Interpretation of the Volterra Kernels*

An important question to ask is “Can the concepts of memory and convolution be applied to nonlinear systems?” The answer to this question is yes and this is, in fact, what Volterra<sup>42</sup> and Frechet<sup>74</sup> did in their development of the Volterra theory.

An understanding of the theory begins with a fundamental theorem of mathematics, the Weierstrass Theorem (see, for example Rugh<sup>25</sup>, Dieudonne<sup>75</sup>, Boyd<sup>47</sup>):

“If  $f(t)$  is a continuous, real-valued function on the closed interval  $[t_1, t_2]$ , then given any  $\epsilon > 0$ , there exists a real polynomial  $p(t)$  such that

$$| f(t) - p(t) | < \epsilon \text{ for } t \in [t_1, t_2]$$

A modern embodiment of this theorem, based on topological concepts, is known as the Stone-Weierstrass theorem. In either case, this is the well-known theorem for the polynomial approximation of arbitrary functions, subject to the stated conditions. These approximations, however, are valid only on the interval  $[t_1, t_2]$ . Extension of this concept to the response of a nonlinear system with memory is the fundamental seed of the Volterra theory of nonlinear systems.

The functions  $f(t)$  and  $p(t)$  in the theorem above are, clearly, zero-memory functions since their range (values) depends only on the present value of the input,  $t$ . As it stands, the Weierstrass theorem is directly applicable to zero-memory linear and nonlinear



functions, or systems. The application of a regression technique to obtain the best linear slope for a particular data scatter is a simple example of the identification of a zero-memory linear system. In this case, the polynomial function that approximates the system consists of only the first-order term, a constant slope. If the first-order term does not provide adequate correlation with the data, then additional higher-order terms may be added to improve the approximation. This fundamental concept of polynomial approximations can be applied to systems with memory as well.

Recall that the response of a linear system with memory, to an arbitrary input, is the result of scaled and shifted superpositions (convolution) of its memory function (impulse response). Also, the memory function for this linear system defines the first-order relationship between the output and the input of the system. This is analogous to the regression example with the only difference being that this system is characterized by a first-order memory function instead of a constant slope.

Likewise, for a (particular type of) nonlinear system with memory, the Weierstrass theorem is applied and indicates the existence of a polynomial approximation to the output/input relationship of the system. The polynomial approximation in this case consists of a polynomial expansion of memory functions, including a first-order memory function, a second-order memory function, and so on. This is the basis for the Volterra theory of nonlinear systems where the Volterra series for a TI, continuous-time system is defined as

$$\begin{aligned}
 y(t) = & \mathbf{h}_0 + \int_0^{\infty} \mathbf{h}_1(t - \tau) \mathbf{u}(\tau) d\tau + \\
 & \int_0^{\infty} \int_0^{\infty} \mathbf{h}_2(t - \tau_1, t - \tau_2) \mathbf{u}(\tau_1) \mathbf{u}(\tau_2) d\tau_1 d\tau_2 + \dots \\
 & + \int_0^{\infty} \dots \int_0^{\infty} \mathbf{h}_n(t - \tau_1, \dots, t - \tau_n) \mathbf{u}(\tau_1) \dots \mathbf{u}(\tau_n) d\tau_1 \dots d\tau_n + \dots
 \end{aligned} \tag{A1}$$

with  $y(t)$  the response of the nonlinear system,  $u(t)$  the input to the system, and the  $h_1$ ,  $h_2$ , and  $h_n$  are the first-order, second-order, and  $n$ th order kernels (memory functions) respectively. An important point to be made is that the Volterra series is not limited to a particular interval  $[t_1, t_2]$  as are the functions defined in the Weierstrass theorem. This is due to the fact that memory functions are now involved in the approximation process. Due to the convolution process, these memory functions can be scaled and shifted accordingly to follow an arbitrary input of arbitrary length. This is a significant improvement for the applicability of the Volterra series for practical problems (see Boyd<sup>47</sup>). This discussion is continued in the last section of this Appendix.

Physical interpretation of the Volterra kernels begins with a simplification of Equation (A1) as

$$y(t) = h_0 + y_1 + y_2 + y_3 + \dots \quad (\text{A2})$$

where the interpretation of  $y_1$ ,  $y_2$ , and subsequent  $y_i$ 's is shown in Figure A6. The  $h_0$  term is typically a constant that is included to account for a non-zero steady-state value. For illustrative purposes, it can be assumed to be zero without loss of generality.

It can be seen in Figure A6 that each term of the series ( $y_1$ ,  $y_2$ , and subsequent  $y_i$ 's) corresponds to a memory function and a corresponding convolution at a particular order (i.e., first-order, second-order, and so on). The higher-order kernels (second-order and above) are in fact the memory functions that capture the input's effect on the output for that particular order. This is analogous to determining the coefficients of a polynomial fit for a zero-memory nonlinear function. For the case of time-invariant nonlinear systems with memory, the coefficients of the polynomial expansion are memory functions involving higher-order convolutions. The appropriate convolution technique is applied to each memory function to yield the first-order response ( $y_1$ ), second-order response ( $y_2$ ), and so

on. The sum total of these responses yields the total response of the system to some arbitrary input.

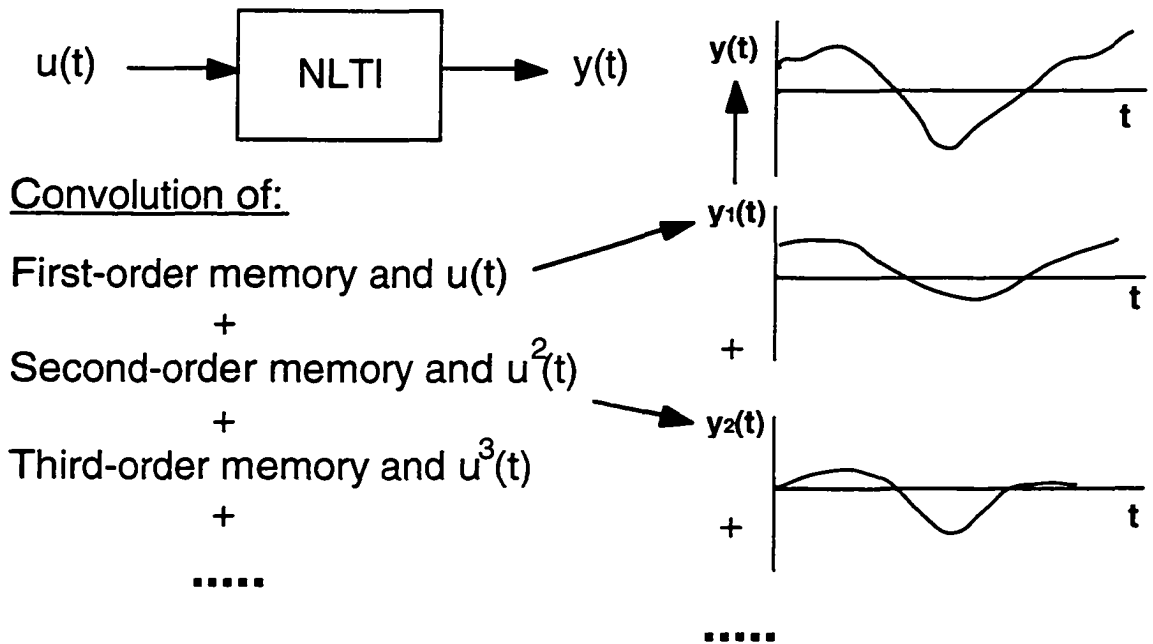


Figure A6 Interpretation of each of the terms of the Volterra series for a nonlinear time-invariant (NLTI) system with input  $u(t)$  and output  $y(t)$ .

Improved understanding of the nature of each of the memory functions (kernels) can be obtained by focusing on one kernel at a time; the second-order kernel, for example. The second-order kernel of a system defines the memory of the system that relates the response of the system to squaring of the input. Therefore, this kernel is composed of impulse responses that correspond to all the possible ways that the input can be squared. This is depicted in Figure A7. The input function can be squared at the same point in time ( $i=j$  component) and it can be squared at different points in time ( $i \neq j$  components). Each one of those squaring operations has a corresponding memory component associated with it. The grouping of all these memory components due to squaring of the input yields the second-

order kernel as described in Chapter 4. Similar interpretations can be made for the other kernels in the series.

The conditions for valid application and convergence of the Volterra series are discussed in the next section.

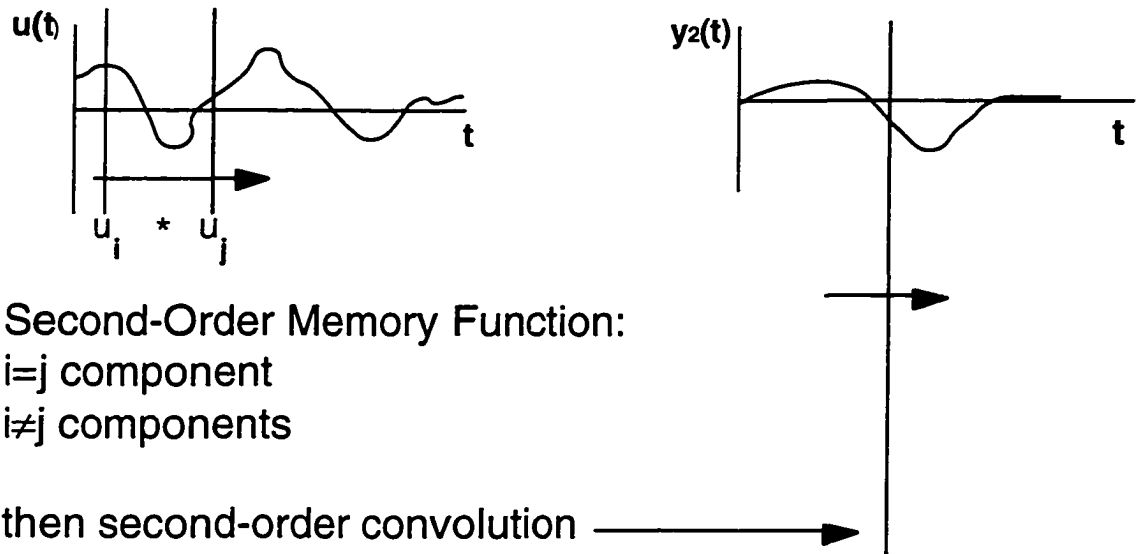


Figure A7 The various components that define the second-order memory function (kernel) and the resultant response ( $y_2(t)$ ) due to a second-order convolution of this second-order memory function with some arbitrary input.

### *Convergence Issues*

Like any infinite series, the Volterra series has convergence issues that need to be understood. A discussion of the similarity between the Volterra series (Eq. (A1)) and Taylor series can be found in Boyd<sup>47</sup>. Sandberg<sup>76</sup> investigates Volterra-like series solutions for nonlinear integral equations and nonlinear differential equations. Additional references of significant interest are Sandberg<sup>77,78</sup>, Barrett<sup>79</sup> and Thapar and Leon<sup>80</sup>.

The Volterra theory is applicable to a particular class of nonlinear systems under certain conditions. The first condition is that the nonlinearities of the system of interest be

analytic. As Boyd<sup>47,54</sup> and Park and Sandberg<sup>65</sup> show, this is related to the concept of fading memory. Volterra [pg. 188] defines fading memory as:

“A first extremely natural postulate is to suppose that the influence of the heredity corresponding to states [input] a long time before the given moment gradually fades out;...”

A fading memory function returns to the system's steady state value after some finite amount of time. Boyd<sup>47</sup> introduces a weighting function and provides a mathematically-formal definition of fading memory. The importance of the fading memory concept is related to three items: 1) fading memory is a slight strengthening of continuity while being an easier concept to investigate than analyticity from an engineering perspective; 2) fading memory removes the limited interval of applicability associated with the Weierstrass theorem; and 3) fading memory is related to a dynamical system's unique steady state, which is important for understanding convergence limitations, as will be seen.

Convergence issues of Volterra series have been studied by several researchers, primarily Ku and Wolf<sup>55</sup> and Barrett<sup>79</sup>. Interesting work regarding methods for approximating the error due to the truncated series is investigated by Thapar and Leon<sup>80</sup>. For the discrete-time case, where the series is truncated at some order (i.e., second-order) and the kernel at that order is truncated as well, the work of Sandberg<sup>81</sup> is appropriate. This “double truncation” of the series is referred to as a doubly finite Volterra series by Sandberg<sup>81</sup> and corresponds to the models developed in this dissertation.

In general terms, a radius of convergence can be associated with a Volterra series in much the same way that a radius of convergence exists for an ordinary power series. The following results, from Ku and Wolf<sup>55</sup>, are presented without proof. See Ku and Wolf<sup>55</sup> for proofs.

**Theorem I:** The  $n$ th-order response of a Volterra series can be defined as

$$y_n(t) = \int_0^\infty \dots \int_0^\infty h_n(\tau_1, \dots, \tau_n) u(t - \tau_1) \dots u(t - \tau_n) d\tau_1 \dots d\tau_n$$

with  $u(t)$  as the input function. Then, for a bounded forcing function  $u(t)$ , that is, there exists a constant  $M > 0$  such that

$$|u(t)| \leq M \quad \text{for all } t,$$

then

$$\left\| \sum_{n=1}^{\infty} y_n(t) \right\| \leq \sum_{n=1}^{\infty} a_n M^n$$

with

$$a_n \equiv \int_0^\infty \dots \int_0^\infty |h_n(\tau_1, \dots, \tau_n)| d\tau_1 \dots d\tau_n$$

Clearly, the maximum amplitude of the input defines the condition for convergence of the series. A direct result of Theorem I is the definition of the radius of convergence of a Volterra series as

$$\rho \equiv (\lim_{n \rightarrow \infty} \sup \|h_n\|^{1/n})^{-1}$$

which is Theorem II of Ku and Wolf<sup>55</sup>. Boyd<sup>47</sup> relates these theorems to the gain bound function and the gain bound theorem.

Limiting the amplitude of the input and the concept of fading memory are necessary conditions for the definition a Volterra series representation of a nonlinear system. More specifically, these conditions help to define the nature of the equilibrium points of the nonlinear system about which a Volterra series representation is admissible. That is, fading memory implies a unique steady state (stable equilibrium point) and limiting the maximum value of the input implies constraining the responses of the system to the region of attraction of the equilibrium point.

For discrete-time systems, the convergence issues defined above apply directly, according to Rugh<sup>25</sup>. For additional details and insight regarding the discrete-time version of the Volterra theory, the reader is referred to Diaz<sup>19</sup>, Park and Sandberg<sup>65</sup>, Sandberg<sup>81</sup>, and Alper<sup>82</sup>.

The definition of the error bound for a truncated Volterra series (Boyd<sup>47</sup>, Thapar and Leon<sup>80</sup>) is valuable and the form from Boyd<sup>45</sup> is presented henceforth.

### *Error Bound for a Truncated Volterra Series*

The truncated Volterra series is defined as

$$y^{(k)}(t) = \sum_{n=1}^k y_n(t) = \sum_{n=1}^k \int_0^{\infty} \dots \int_0^{\infty} h_n(\tau_1, \dots, \tau_n) u(t - \tau_1) \dots u(t - \tau_n) d\tau_1 \dots d\tau_n$$

which satisfies

$$\|y(t) - y^{(k)}(t)\| \leq \sum_{n=k+1}^{\infty} \|h_n\| \|u\|^n$$

which is of order

$$o(\|u\|^k)$$

Therefore, if

$$\sum_{n=k+1}^{\infty} \|h_n\| M^n$$

is small, then the full Volterra series (no truncation),  $y(t)$ , is well modeled by the truncated Volterra series,  $y^{(k)}(t)$ , for inputs whose peaks do not exceed  $M$ .

## BIBLIOGRAPHY

- [1] Edwards, J. W.; and Thomas, J. L. : Computational Methods for Unsteady Transonic Flows, Chapter 5 in Unsteady Transonic Aerodynamics, Edited by David Nixon, Progress in Astronautics and Aeronautics, Volume 120,1989.
- [2] Peele, Elwood L.; and Adams, William M., Jr. : "A Digital Program for Calculating the Interaction Between Flexible Structures, Unsteady Aerodynamics, and Active Controls," NASA TM-800040, January 1979.
- [3] Noll, T. E. ; Blair, M. ; and Cerra, J. : "An Aeroservoelastic Analysis Method for Analog or Digital Systems," *Journal of Aircraft*, November 1986.
- [4] Perry, B. III; Mukhopadhyay, V.; Hoadley, S. T.; Cole, S. R.; Buttrill, C. S.; and Houck, J. A. : "Design, Implementation, Simulation, and Testing of Digital Flutter Suppression Systems for the Active Flexible Wing Wind-Tunnel Model," ICAS Paper Number 90-1.3.2, Presented at the 17th International Council of the Aeronautical Sciences, Stockholm, Sweden, September 9-14, 1990.
- [5] Ide, H. ; and Ominsky, D. : "Simulation of Static and Dynamic Aeroelastic Behavior of a Flexible Wing with Multiple Control Surfaces," AIAA Paper Number 90-1075, Presented at the 31st Structures, Structural Dynamics, and Materials Conference, Long Beach, CA, April 2-4,1990.



[6] Lee, Elizabeth M.; and Batina, J. T. : "Conical Euler Simulation and Active Suppression of Delta Wing Rocking Motion," NASA TM-102683, October 1990.

[7] Jones, Robert T., "The Unsteady Lift of a Wing of Finite Aspect Ratio," NACA dissertation No. 681, 1940.

[8] Giesing, J.P.; Kalman, T.P.; and Rodden, W.P., "Subsonic Unsteady Aerodynamics for General Configurations, Part I. Direct Application of the Nonplanar Doublet Lattice Method. dissertation AFFDL-TR-71-5, Vol. I, November 1971.

[9] Ballhaus, W. F.; and Goorjian, P. M., "Computation of Unsteady Transonic Flows by the Indicial Method," AIAA Journal, Volume 16, No. 2, February 1978, pp. 117-124.

[10] Leishman, J.; and Crouse, G., "A State-Space Model of Unsteady Aerodynamics in a Compressible Flow for Flutter Analyses," AIAA Paper No. 89-0022, 27th Aerospace Sciences Meeting, January 9-12, 1989, Reno, Nevada.

[11] Nixon, D., "Alternative Methods for Modeling Unsteady Transonic Flows, Unsteady Transonic Aerodynamics, Vol. 120 of Progress in Astronautics and Aeronautics, Ed. by D. Nixon, AIAA, 1989.

[12] Reisenthel, P.H., "Development of a Nonlinear Indicial Model for Maneuvering Fighter Aircraft," AIAA Paper No. 96-0896, 34th Aerospace Sciences Meeting & Exhibit, January 15-18, 1996, Reno, Nevada.

- [13] Govind, G.; and Ramamoorthy, P. A. , "Multi-layered Neural Networks and Volterra Series: The Missing Link," IEEE International Conference on Systems Engineering, August 9-11, 1990, Pennsylvania, pp633-636.
- [14] Soloway, D.I. and Bialasiewicz, J.T., "Neural Network Modeling of Nonlinear Systems Based on Volterra Series Extension of a Linear Model", Proceedings IEEE International Symposium on Intelligent Control, Glasgow, Scotland, 1992.
- [15] Marques, F.; and Anderson, J., "Modelling and Identification of Non-Linear Unsteady Aerodynamic Loads by Neural Networks and Genetic Algorithms,"
- [16] Dowell, E.H.; Hall, K. C.; and Romanowski, M. C.: "Eigenmode Analysis in Unsteady Aerodynamics: Reduced Order Models," ASME Applied Mechanics Review, Volume 50, Number 6, June 1997, pp371-386.
- [17] Baker, M.L., "Model Reduction of Large, Sparse, Discrete Time Systems with Application to Unsteady Aerodynamics," PhD Dissertation, University of California at Los Angeles, 1996.
- [18] Seidel, D. A.; Bennett, R. M.; and Whitlow, W. W., "An Exploratory Study of Finite-Difference Grids for Transonic Unsteady Aerodynamics," AIAA Paper No. 83-0503, January 1983.
- [19] Diaz, Hernando, "Modeling of Nonlinear Systems from Input - Output Data," PhD Dissertation, Rensselaer Polytechnic Institute, 1986.

[20] Pitas, I.; and Venetsanopoulos, A.N., Nonlinear Digital Filters: Principles and Applications, Kluwer Academic Publishers, 1990.

[21] Ueda, T.; and Dowell, E.H.: "Flutter Analysis Using Nonlinear Aerodynamic Forces," Presented at the 23rd AIAA/ASME/ASCE/AHS Structures, Structural Dynamics, and Materials Conference, New Orleans, LA, May 10-12, 1982.

[22] Tobak, Murray ; and Pearson, Walter E. : "A Study of Nonlinear Longitudinal Dynamic Stability," NASA Technical dissertation R-209, September 1964.

[23] Jenkins, J. E.: "Relationships Among Nonlinear Aerodynamic Indicial Response Models, Oscillatory Motion Data, and Stability Derivatives," Paper No. CP-89-3351, Presented at the AIAA Atmospheric Flight Mechanics Conference, Boston, Massachusetts, August 14-16, 1989.

[24] Stalford, H.; Baumann, W. T. ; Garrett, F. E. ; and Herdman, T. L. : "Accurate Modeling of Nonlinear Systems Using Volterra Series Submodels," Presented at the 1987 American Control Conference, Minneapolis, MN, June 10-12, 1987.

[25] Rugh, Wilson J. : Nonlinear System Theory, The Volterra-Wiener Approach, The Johns Hopkins University Press, 1981.

[26] Clancy, S. J.; and Rugh, W. J.: "A Note on the Identification of Discrete-Time Polynomial Systems," IEEE Transactions on Automatic Control, Volume AC-24, Number 6, December 1979.

[27] Schetzen, M.: "Measurement of the Kernels of a Nonlinear System of Finite Order," *International Journal of Control*, Volume 1(3), pp.251-263, March 1965; Corrigendum, Vol. 2(4),p.408, October, 1965.

[28] Boyd, Stephen ; Tang, Y. S. ; and Chua, Leon A. : "Measuring Volterra Kernels," *IEEE Transactions on Circuits and Systems*, Volume CAS-30, Number 8, August 1983.

[29] Tromp, J. C.; and Jenkins, J. E.: "A Volterra Kernel Identification Scheme Applied to Aerodynamic Reactions," AIAA Paper No. 90-2803, Presented at the AIAA Atmospheric Flight Mechanics Conference, Portland, Oregon, August 20-22, 1990.

[30] Rodriguez, E.A., "Linear and Nonlinear Discrete-Time State-Space Modeling of Dynamic Systems for Control Applications," PhD Dissertation, Purdue University, December 1993.

[31] Silva, W.A., "Application of Nonlinear Systems Theory to Transonic Unsteady Aerodynamic Responses," *Journal of Aircraft*, Volume 30, Number 5, September-October 1993, pp. 660-668.

[32] Silva, W.A., "Extension of a Nonlinear Systems Theory to General-Frequency Unsteady Transonic Aerodynamic Responses," AIAA Paper No. 93-1590, Presented at the 34th Structures, Structural Dynamics, and Materials Conference, La Jolla, California, April 19-21, 1993.

[33] Fung, Y.C., An Introduction to the Theory of Aeroelasticity, Dover Publications, Inc., New York, 1969.

- [34] Dowell, E.H., et al, A Modern Course in Aeroelasticity, Sijthoff & Noordhoff, The Netherlands, 1980.
- [35] Bisplinghoff, R. L.; and Ashley, H., Principles of Aeroelasticity, Dover Publications, Inc., New York, 1975.
- [36] Batina, J.T., "A Finite-Difference Approximate-Factorization Algorithm for Solution of the Unsteady Transonic Small-Disturbance Equation," NASA Technical Paper 3129, January 1992.
- [37] Rumsey, C. L.; Biedron, R. T.; and Thomas, J. L., "CFL3D: Its History and Some Recent Applications," NASA TM 112861, May 1997.
- [38] Oppenheim, A.V.; and Schafer, R.W., Discrete-Time Signal Processing, Prentice Hall Signal Processing Series, A. V. Oppenheim, series editor, Englewood Cliffs, NJ, 1989.
- [39] Wylie, C.R., Jr., Advanced Engineering Mathematics, Second Edition, McGraw-Hill Book Company, Inc., 1960.
- [40] Edwards, J.W., "Applications of Laplace Transform Methods to Airfoil Motion and Stability Calculations," AIAA/ASME/ASCE/ AHS 20th Structures, Structural Dynamics, and Materials Conference, April 4-6, 1979, St. Louis, MO., pp465-481.
- [41] Juang, J.-N. ; and Pappa, R.S., "An Eigensystem Realization Algorithm for Modal Parameter Identification and Model Reduction," *Journal of Guidance, Control, and Dynamics*, Vol. 8, No. 5, September-October 1985, pp.620-627.

[42] Volterra, V.: Theory of Functionals and of Integral and Integro-Differential Equations, Dover Publications, Inc., New York, 1959.

[43] Schetzen, Martin : The Volterra and Wiener Theories of Nonlinear Systems, John Wiley & Sons, 1980.

[44] Khalil, H.K., Nonlinear Systems, Macmillan Publishing Company, New York, 1992.

[45] Blair, Max, "A Compilation of the Mathematics Leading to the Doublet-Lattice Method," WL-TR-95-3022 (supersedes WL-TR-92-3028), November 1994, Air Force Wright Laboratories.

[46] Ku, Y. H.; and Su, C. C.: "Volterra Functional Analysis of Nonlinear Time-Varying Systems," *Journal of the Franklin Institute*, Volume 204, Number 6, December 1967.

[47] Boyd, S.P.: "Volterra Series: Engineering Fundamentals," PhD Dissertation, University of California, Berkeley, 1985.

[48] Wiener, N.: "Response of a Nonlinear Device to Noise," dissertation No. 129, Radiation Laboratory, M.I.T., Cambridge, Massachusetts, April 1942. (Also published as U.S. Department of Commerce Publications PB-58087.)

[49] Lee, Y.W.; and Schetzen, M.: "Measurement of the Wiener Kernels of a Non-linear System by Crosscorrelation," *International Journal of Control*, Volume 2(3), pp. 237-254, September 1965.

[50] Flake, R. H., "Volterra Series Representation of Nonlinear Systems," Transactions of the American Institute of Electrical Engineers, Volume 81, 1962, Part II: Applications and Industry.

[51] Ibrahim, R. A., "Response Analysis of Nonlinear Systems Using Functional-Perturbational Type Approach," 6th International Modal Analysis Conference, February 1-4, 1988, Kissimmee, FL.

[52] Boyd, S. ; Chua, L. O. ; and Desoer, C. A. : Analytical Foundations of Volterra Series, *IMA Journal of Mathematical Control & Information*, 1984, Volume 1, pp. 243-282.

[53] Brilliant, M. B.: "Theory of the Analysis of Nonlinear Systems," Technical dissertation 345, M.I.T. Research Laboratory of Electronics, March 1958.

[54] Boyd, S. P.; and Chua, L. O.: "Fading Memory and the Problem of Approximating Nonlinear Operators with Volterra Series" *IEEE Transactions on Circuits and Systems*, Volume CAS-32, Number 11, November 1985.

[55] Ku, Y. H.; and Wolf, A. A.: "Volterra-Wiener Functionals for the Analysis of Nonlinear Systems," *Journal of the Franklin Institute*, Volume 281, Number 1, January 1966.

[56] Bedrosian, E.; and Rice, S. O.: "The Output Properties of Volterra Systems (Nonlinear Systems with Memory) Driven by Harmonic and Gaussian Inputs," *Proceedings of the IEEE*, Volume 59, Number 12, December 1971.

- [57] Sandberg, I. W.: "Nonlinear Input-Output Maps and Approximate Representations," AT&T Technical Journal, Volume 64, Number 8, October 1985, pp. 1967-1983.
- [58] Bendat, J. S., Nonlinear System Analysis & Identification from Random Data, A Wiley-Interscience Publication, 1990.
- [59] Tryon, P. V., "The Bispectrum and Higher-Order Spectra: A Bibliography," National Bureau of Standards Technical Note 1036, April 1981.
- [60] Nikias, C. L.; and Petropulu, A. P., Higher-Order Spectra Analysis: A Nonlinear Signal Processing Framework, Prentice-Hall Signal Processing Series, Alan V. Oppenheim, Series Editor, 1993.
- [61] Ritz, C. P.; and Powers, E. J., "Estimation of Nonlinear Transfer Functions for Fully Developed Turbulence," *Physica D 'Nonlinear Phenomena'*, May 1986, pp320-334.
- [62] Roberts, J. B., "Nonlinear Analysis of Slow Drift Oscillations of Moored Vessels in Random Seas," *Journal of Ship Research*, Volume 25, Number 2, June 1981, pp. 130-140.
- [63] Yates, E. C., "Unsteady Transonic Flows - Introduction, Current Trends, Applications," Lecture by Dr. Yates, NASA Langley Research Center,
- [64] Temam, R., Navier-Stokes Equations and Nonlinear Functional Analysis, CBMS-NSF Regional Conference Series in Applied Mathematics, Society for Industrial and Applied Mathematics, Philadelphia, Pennsylvania, 1995.



[65] Park, J.; and Sandberg, I.W., "Criteria for the Approximation of Nonlinear Systems," *IEEE Transactions on Circuits and Systems I: Fundamental Theory and Applications*, Volume 39, No. 8, August 1992, pp673-676.

[66] Anderson, D.A.; Tannehill, J.C.; and Pletcher, R.H., Computational Fluid Mechanics and Heat Transfer, Series in computational methods in mechanics and thermal sciences, Hemisphere Publishing Corporation, McGraw-Hill Book Company, 1984.

[67] Seidel, D.A.; Bennett, R.M.; and Ricketts, R.H., "Some Recent Applications of XTRAN3S," AIAA Paper No. 83-1811, July 1983.

[68] Lee-Rausch, E. M., and Batina, J. T.: "Wing Flutter Computations Using an Aerodynamic Model Based on the Navier-Stokes Equations," *Journal of Aircraft*, Vol. 33, no. 6, pp.1139-1148, Nov-Dec 1996. (Also AIAA Paper 93-3476, Aug. 1993).

[69] Silva, W.A., and Bennett, R.M., "Application of Transonic Small Disturbance Theory to the Active Flexible Wing Model," *Journal of Aircraft*, Vol. 32, No. 1, January-February 1995.

[70] Edwards, J.W., "Transonic Shock Oscillations and Wing Flutter Calculated with an Interactive Boundary Layer Coupling Method," *EUROMECH-Colloquium 349, Simulation of Fluid-Structure Interaction in Aeronautics*, Gottingen, Germany, September 16-18, 1996.

[71] Krist, S.L.; Biedron, R.T.; and Rumsey, C.L., "CFL3D User's Manual (Version 5.0)," November 1996, First Edition.

[72] Rumsey, C. L.; Sanetrik, M. D.; Biedron, R. T.; Melson, N. D.; and Parlette, E. B., "Efficiency and Accuracy of Time-Accurate Turbulent Navier-Stokes Computations," AIAA Paper No. 95-1835, Presented at the 13th AIAA Applied Aerodynamics Conference, June 19-22, 1995, San Diego, CA.

[73] Silva, W.A., "Identification of Linear and Nonlinear Aerodynamic Impulse Responses Using Digital Filter Techniques," AIAA Paper No. 97-3712, Presented at the AIAA Atmospheric Flight Mechanics Conference, August 11-13, 1997, New Orleans, LA.

[74] Frechet, M., "Sur les Fonctionelles Continues," *Annales de l'Ecole Normale Sup.*, volume 27, 1910.

[75] Dieudonne, J., Foundations of Modern Analysis, Academic Press, New York, 1969.

[76] Sandberg, I.W., "Volterra-like Expansions for Solutions of Nonlinear Integral Equations and Nonlinear Differential Equations," *IEEE Transactions of Circuits Syst.*, Volume CAS-30, Number 2, pp. 68-77, February 1983.

[77] Sandberg, I.W., "Series Expansions for Nonlinear Systems," *Circuits, Systems, and Signal Processing*, Volume 2, Number 1, pp. 77-87, 1983.

[78] Sandberg, I.W., "The Mathematical Foundations of Associated Expansions for Mildly Nonlinear Systems," *IEEE Trans. Circuits Syst.*, Volume CAS-30, pp. 441-455, July 1983.

[79] Barrett, J.F., "The Use of Functionals in the Analysis of Nonlinear Physical Systems," *International Journal of Electronic Control*, Volume 15, pp. 567-615, 1963.

[80] Thapar, H.K., and Leon, B.J., "Lumped Nonlinear System Analysis with Volterra Series," Rome Air Development Center (RADC) TR-80-140, 1980.

[81] Sandber, I.W., "Uniform Approximation with Doubly Finite Volterra Series," *IEEE Transactions on Signal Processing*, Volume 40, Number 6, pp. 1438-1442, June 1992.

[82] Alper, P., "A Consideration of the Discrete Volterra Series," *IEEE Transactions on Automatic Control*, AC-10, pp. 322-327, July 1965.

## VITA

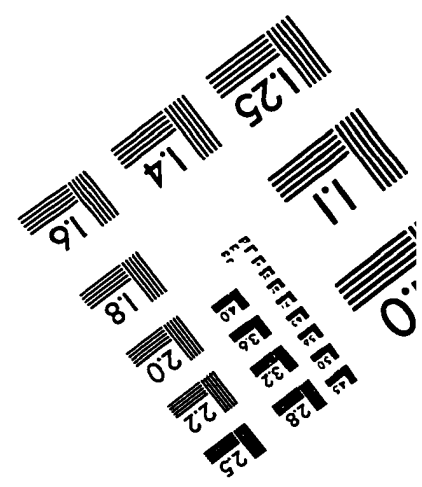
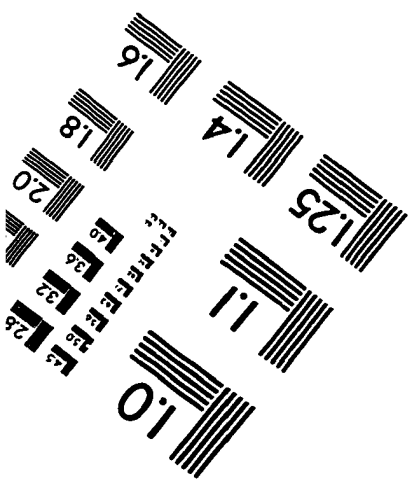
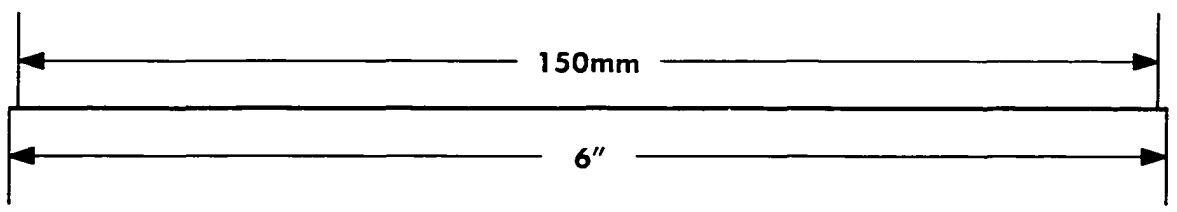
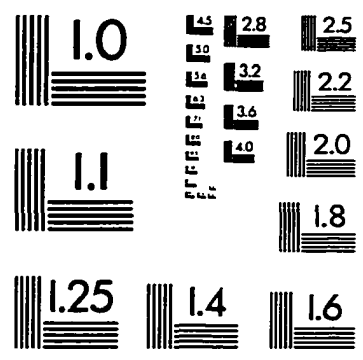
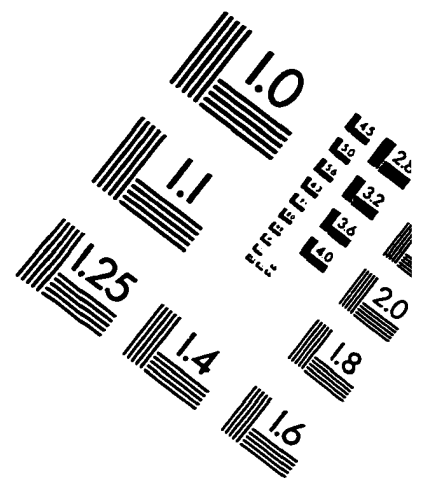
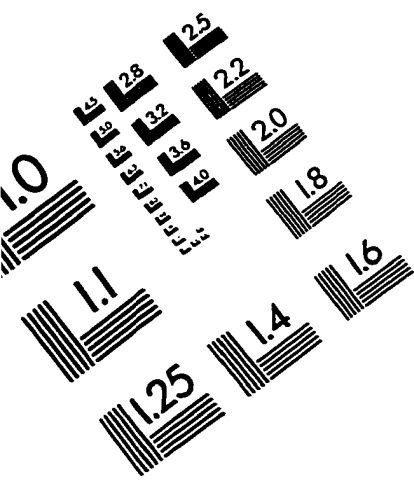
Walter Arturo Silva is currently a research engineer at the Aeroelasticity Branch at NASA Langley Research Center. Mr. Silva was born in Bogota, Colombia, South America on September 30, 1960. He came to the U.S. in 1965.

He received his undergraduate degree from Boston University in Aerospace Engineering, where he assisted Prof. Luigi Morino in research involving computational aerodynamics, primarily subsonic/supersonic panel methods. He worked for Grumman Aerospace for four years in the areas of Propulsion Integration, Development of Experimental Methods for Boundary Layer Control, Computational modeling of offset diffusers using VSAERO (with a rapid, interactive panel generation program for VSAERO), Mission sizing and Preliminary Design, Flight Controls (EA-6B Spin Modeling and Simulation), Loads and Aeroelasticity (JVX empennage and Shuttle trainer aircraft flutter analyses), and the Advance Tactical Fighter (ATF) program. He had the opportunity to work with these groups as a recipient of the Grumman Aerospace Corporation's Master's Fellowship Program, through which he received his Master's degree in Aerospace Engineering from the Polytechnic Institute of NY.

In 1986, he accepted a position as a contractor in the Aeroservoelasticity Branch (now the Aeroelasticity Branch), headed by Dr. Tom Noll. He performed aeroelastic and aeroservoelastic analyses of the X-Wing aircraft in cooperation with Sikorsky Aircraft and Northrop Corporation. In 1990, he accepted an offer from NASA LaRC to work for the Unsteady Aerodynamics Branch (UAB, now part of Aeroelasticity Branch) for Dr. John Malone. While at the UAB, he performed aeroelastic and flutter analyses for the Active Flexible Wing (AFW) wind-tunnel model using the CAP-TSD code. After a reorganization, he was Group Leader for the Active Controls Group in a new branch, Aeroelastic Analysis and Optimization Branch (Dr. Woodrow Whitlow, Branch Head), part of which was combined with the current Aeroelasticity Branch.

More recently, he was Project Engineer for the High Speed Research (HSR) Flexible Semi-span Model (FSM) wind-tunnel test, conducted in April-May of 1996, to acquire high-quality steady, unsteady, and flutter data for code validation.

# IMAGE EVALUATION TEST TARGET (QA-3)



**APPLIED IMAGE, Inc**  
 1653 East Main Street  
 Rochester, NY 14609 USA  
 Phone: 716/482-0300  
 Fax: 716/288-5989

© 1993, Applied Image, Inc., All Rights Reserved